Development of a dynamic hip joint simulation model

Niel Pieterse

Development of a dynamic hip joint simulation model

by

Niel Pieterse

A dissertation submitted in partial fulfillment
of the requirements for the degree

Master of Engineering (Chemical Engineering)

in the

Faculty of Engineering, the Built Environment and Information Technology

University of Pretoria
Pretoria

24th February 2006

Development of a dynamic hip joint simulation model

Author:	Niel Pieterse
Supervisor:	Prof PL de Vaal
Department:	Department of Chemical Engineering University of Pretoria
Degree:	Master of Engineering (Chemical Engineering)

Synopsis

Synovial joints, like the hip joint, has unique characteristics. In order to study these characteristics by making use of mathematical techniques, it is necessary to develop a model simulating the dynamic forces and joint movements during joint operation. Once this is available, the effect of the synovial fluid lubricant properties can be added by describing its behaviour as a component of the hip joint simulation model. This was the ultimate aim of this research effort.

With this work a model based on fundamental principles, like the equations of mass and motion, was developed and validated experimentally with a hip joint simulator. It is also shown that the effect of the lubricant properties can be studied by adding the relevant rheological equations. These fluid properties can have a significant effect on the joint under typical joint operations like dynamic loading and movement. To develop a model with relative complexity, certain simplifying assumptions have to be made. In this study, the fluid was assumed to have no boundary interactions with the articulating surfaces. It is known that complex rheological interaction exists in these systems. Although certain assumptions were made during development, model results are promising and a firm basis was established for subsequent research.

In future, the model needs to be extended to simulate the continuous, multi-cycle operation of a human joint, with accurate geometrical descriptions of articulating surfaces and known components of synovial joints like articular cartilage. The model could then contain lubrication mechanisms known to prevail in synovial joints, with accurate rheological models of synovial fluid which will play an increasing role under typical joint operations.

Keywords: modelling, synovial fluid, hip joint, rheology, biotribology

Acknowledgements

I would like to acknowledge the guidance of professor Philip de Vaal, the programming support supplied by Mr Carl Sandrock and the help of Mr Adrain Hols during experimental design and data gathering.

The financial assistance of the National Research Foundation (NRF) towards this study is hereby acknowledged. Opinions expressed and conclusions arrived at, are those of the author and are not necessarily to be attributed to the NRF.

CONTENTS

LIST OF FIGURES

LIST OF TABLES

NOMENCLATURE

A	Area	m^2
b	Maxwell parameter	-
F	Force	N
F_f	Frictional resistance force	N
g	Gravitational acceleration	m/s^2
k	Wear coefficient	$mm^3/N.mm$
L	Sliding distance	mm
$l_{i'i}$	The direction cosine matrix	-
M	Torque	Nm
P	Fluid pressure	Pa
r	Radial distance in spherical coordinates as defined in section 4.1	m
R_1	The radius of the femoral ball	m
R_2	The radius of the acetabular cup	m
R_a	Surface roughness	m
$R_{(\theta,\varepsilon)}$	Radius defined in figure 4.5	m
t	Time	s
t_{touch}	Time it takes for articulating surfaces to deplete the hydrodynamic film and solid-solid contact occurs	s

V	Volume	m^3
v	Linear velocity	m/s
V_r	Volume of material removed	mm^3
W	Weight	N
x	Cartesian coordinate	m
Y	Distance	m
y	Cartesian coordinate	m
z	Cartesian coordinate	m

Subscripts

θ,ϕ,r	In the direction of θ, ϕ or r	-
x,y,z	In the direction of x, y or z	-
yx	In the x-direction on a fluid surface at constant y	-

Greek

χ	Angle defined in figure 4.5	m
δ	Distance from the ball surface to the axis of rotation	m
η	Non-Newtonian viscosity	Pa.s
η_0	Maxwell and Oldroyd parameter	Pa.s
γ	Shear rate or $-(\mathrm{d}v_x/\mathrm{d}y)$	s^{-1}
λ	Maxwell parameter	s
λ_1	Oldroyd parameter	s
λ_2	Oldroyd parameter	s
μ	Coefficient of friction	-
μ	Fluid viscosity	Pa.s
μ_0	Oldroyd parameter	s
μ_{app}	Apparent fluid viscosity	Pa.s

ω	Angular velocity	rad/s
ϕ	Angle in spherical coordinates as defined in section 4.1	rad
ρ	Fluid density	kg/m^3
σ	The normal stress	N/m^2
τ	Shear stress	N/m^2
θ	Angle in spherical coordinates as defined in section 4.1	rad
υ	Linear velocity scalar	m/s
ε	Distance between the center of the femoral ball and the center of the acetabular cup	m

CHAPTER 1

Introduction

1.1 Background

A synovial joint can be viewed as a complex joint system where processes like mechanics, secretion, permeability and lubrication are combined to provide a fine example of how nature engineers amazing systems. For many years, studies into the nature and function of synovial joints were driven by investigators attempting to duplicate the working of these joints. This is primarily because of the growing number of artificial joint implant procedures performed annually. The ability to asses the tribological performance of artificial joint replacements is playing an increasing role in understanding the wear characteristics of joint prostheses.

1.2 Problem statement

Due to the complex nature of synovial joints, there exists a need to understand and learn more about these sophisticated biological systems and their tribological behaviour. The application of the laws of nature coupled with mathematical techniques provide a means to study these complex systems. The tribology associated with artificial joints can likewise be studied. Knowledge obtained in this manner can contribute toward the development of prostheses that will ensure sustained operation and reduce the need for revision surgery. Simulation models also contribute towards reduction of the cost of in-situ experimentation of biotribological systems, as well as overcoming difficulties with ethical and practical problems related to in-situ testing.

1.3 Research objectives

The purpose of this research was to:

- Develop a general understanding of synovial joints, specifically the hip joint and the components that make up this unique system.
- Review the biotribology of hip joints and the different proposed lubrication mechanisms
- Research artificial joint replacements and simulative testing of such prostheses
- Conduct a literature study on simulative tribological modelling of synovial joints in general
- Develop a dynamic hip joint model from first principles to obtain a means with which the effect of physical properties, like rheology and density, on the tribological performance of the hip joint model can be investigated
- Gather experimental data from a hip joint simulator to confirm the validity of the proposed joint model

CHAPTER 2

Literature background

This section provides a basic overview of the tribology of synovial joints. Included in this section is a short overview of synovial joints, their components, structure and function. Synovial fluid is discussed in detail. This chapter looks at artificial joint replacements and the simulative testing of these replacements. A summary of proposed joint lubrication mechanisms is presented followed by some of the developments in the science of biotribological modelling. A look at lubricant flow equations are also included.

2.1 Human joint design and materials

There exists a strong relationship between joint design and function. Function may be said to determine structure while structure in turn determines function. Joints are used to connect one component of a structure to one or more other components. The main function of the joint could be to provide stability and static support or to provide mobility. Human joints vary from simple to complex. The more simple joints serve primarily for mobility, but most human joints have to serve both for the purpose of mobility and stability. This dual function makes them somewhat more complex. (Norkin & Levangie, 1988: 63–64)

The living materials found in human joints include connective tissue in the form of cartilage, joint capsules, ligaments, tendons, disks, plates, menisci, and bones. (Norkin & Levangie, 1988: 66)

The structure of connective tissue is characterised by large amounts of intercellular substance and a wide dispersion of cells. The composition and form of the intercellular substance determine the basis of classification of connective tissue into a range of different types, including loose fibrous tissue, dense fibrous tissue, bone and cartilage. (Norkin

& Levangie, 1988: 66) The general property of all connective tissues is viscoelasticity. (Norkin & Levangie, 1988: 68) This means these tissues are able to resist deformation due to shearing (viscosity) and return to their original form after deformation (elasticity). (Walker, 1977: 118) Connective tissue can be subjected to creep. (Norkin & Levangie, 1988: 69) This implies that the tissue keeps on deforming under constant compressive force or sudden tensile load. (Walker, 1977: 118) Connective tissue can enter a plastic range, if it is subjected to sudden, prolonged or excessive forces. In this range the tissue undergoes permanent deformation, and failure can occur. Figure 2.1 is a simplified graphical representation of a hip joint and all the structures that make up this synovial joint. These components and structures are discussed in subsequent sections.

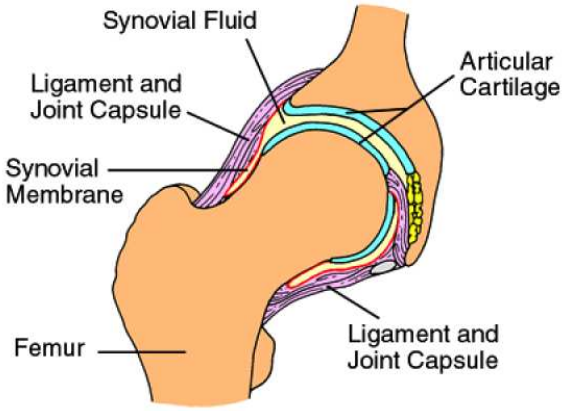

Figure 2.1: The synovial hip joint. (Wausau Hospital Medical Library, 2004)

2.1.1 Dense fibrous tissue

Ligaments are used to connect bone to bone, and tendons are used to connect muscle to bone. Both of these connective tissue structures are composed of dense fibrous tissue. The intercellular structure of dense fibrous tissue consists mainly of collagen. Collagen is a protein that has a tensile strength in order of magnitude of that of steel. These fibers can be arranged in many different ways and vary in shapes and sizes. Although collagen is non-elastic, certain structural arrangements of collagen allow for a small amount of elastic behaviour. Elastin is the yellow fibrous component of the intercellular structure of connective tissue. They have elastic properties that allow the fibers to deform under applied loads and return to their original state after applied load. Collagen and elastin are mixed in different ratios in different connective tissue. The ratio depends on whether the tissue's primary function is mobility or stability. (Norkin & Levangie, 1988: 66–67)

2.1.2 Cartilage

Cartilage is a solid type of connective tissue. It is relatively elastic. Two types of cartilage are found in the human joint, fibrocartilage and hyaline or articular cartilage. Fibrocartilage consists primarily of collagen. This makes the cartilage stronger and denser than fibrous connective tissue. (Norkin & Levangie, 1988: 67) Articular cartilage is discussed in the section below.

On initial inspection, cartilage can appear to have a smooth surface finish. On closer inspection, irregular arrangements of humps, ripples and hollows are clearly observed. This is shown in figure 2.2. Sokoloff (1978: 454–455) debates whether these ripples are inherent to cartilage surfaces or whether they are wear scars, consequent of rubbing surfaces in contact. Measured surface roughnesses revealed peaks of up to 2 μm in young human cartilage and 15 μm in arthritic cartilage. (Sokoloff, 1978: 453)

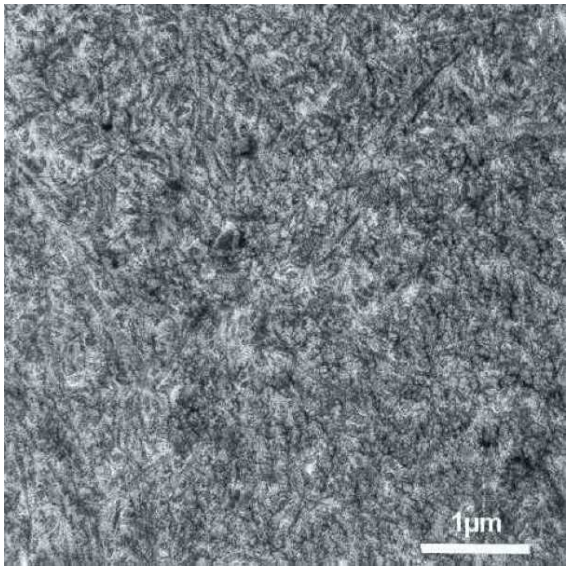

Figure 2.2: The roughened cartilage surface observed under an electron microscope. (University of Bern- Institute of Anatomy, 2005)

Articular cartilage

Articular cartilage consists mainly of collagen, protein-polysaccharides and water. This high content of fibers, fibrils and filaments make the articular cartilage truly inhomogeneous. (Sokoloff, 1978: 106) Three distinct layers of articular cartilage are found on the ends of bony components of mobility joints. The outermost layer has collagen fibres that are arranged parallel to the surface while in the middle layer they are coiled and form an open lattice network. The deepest layer consists of closely packed collagen fibers that lie perpendicular to the cartilage surface, and are embedded in calcified cartilage. The junction between this uncalcified and calcified cartilage is called the tidemark. The tide mark is an important area when it comes to growth, healing and ageing. (Norkin &

Levangie, 1988: 67) The main function of the smooth outer layer of cartilage is to reduce friction, while the inner loose-coiled fibre layer absorbs the impact forces and permit some deformation.

During joint motion or when the cartilage is compressed, fluid content of the cartilage flows through the outermost layer of cartilage. The fluid flows back the moment the motion or compression is ceased. The moving fluid reduces friction and nourishes the blood vessel and cartilage. (Norkin & Levangie, 1988: 68)

One of the main functions of articular cartilage is the transmission of loads through joints. Sometimes load can exceed 4–7 times that of the body weight. Hence, the mechanical properties of the cartilage has been the topics of several researchers. (Hori & Mockros, 1976) (Saxena et al., 1991)

2.1.3 Bones

Bones consist of fibrous connective tissue embedded in a solid matrix containing minerals, calcium and phosphorous. This makes bones the hardest of all connective tissue found in the human body. Bone functions as a support system for the body while protecting the body organs. This is only possible due to the unique qualities of bone. Bone possesses both rigid and elastic properties, and is capable of modelling and remodelling in response to the stresses it is subjected to. Bone, unlike cartilage, receives nourishment from a direct blood supply located within the bone. (Norkin & Levangie, 1988: 68)

The highly calcified collaginous intercellular substance in bones differ in form and structure at different parts of the bone. The innermost layer of bone is called cancellous (spongy) bone. Here the calcified tissue forms thin plates called trabeculae. These trabeculae are laid down in response to stresses placed in the bone. The cancellous bone is covered by a thin layer of compact bone called cortical bone. This layer is laid down in concentric circles which makes it very dense. The cortical bone is covered by a tough fibrous membrane called the periosteum. This part of the bone is responsible for bone repair, growth and nourishment. It is well vascularised and contains many capillaries. (Norkin & Levangie, 1988: 68)

2.1.4 Synovial membrane

The synovial membrane or synovium is a complex membrane that lines the bearing surfaces of the synovial joint. The joint cavity between the load bearing surfaces which is covered with articular cartilage is filled with a liquid called synovial fluid. The synovial membrane is found around this cavity.

The synovial membrane aids in the production of synovial fluid. This is achieved by addition of a small amount of a lubricating macromolecular protein called hyaluronic

acid during the diffusion process of fluid through the membrane. (Momberger et al., 2005) (Hlaváček, 1993a) Synovial fluid is discussed in detail in the following section.

2.2 Synovial fluid and its function in human joints

Synovial fluid is defined as a dialysate of blood plasma to which hyaluronic acid has been added. (Momberger et al., 2005) Synovial fluid forms an interface with the articular cartilage in synovial joints. (Hlaváček, 1993a) The main function of the synovial fluid is to lubricate and nourish the joint tissue. As lubricant, synovial fluid has good load bearing and shock absorption characteristics. (Sokoloff, 1978: 407) (Hlaváček, 1993a)

2.2.1 Composition of synovial fluid

The main constituents of synovial fluid are cells, electrolytes, proteins and hyaluronic acid. (Fujimura et al., 2005) In order to determine the origin and composition of synovial fluid, initial studies showed that electrolytes were distributed between blood and synovial fluid and that they act in some measure as nutrients for synovial joints. (Sokoloff, 1978: 410) (Walker, 1977: 136)

It is now excepted that all but a few proteins are derived directly from plasma and that the relative proportions of the individual constituents are dependent on the protein molecular weight and the permeability of the synovial capillaries. (Sokoloff, 1978: 410) Walker (1977: 136) reports that synovial fluid protein content is in the range of 1.3 to 2.8% compared to 7.4% in blood. The protein is mainly albumin and some γ-globulin, with no other protein with molecular weight exceeding 10^5 g/mole present in normal fluids. (Fujimura et al., 2005)

The cells present in synovial fluid appear to be derived largely from blood. In normal joints, mononuclear cells predominate, and the total white blood cell count is below 100 cells/μl. A much higher count is observed in rheumatoid fluids. (Pascual & Jovan, 2005) The main purpose of the cells is to remove small debris particles derived from the various joint surfaces. (Walker, 1977) (Sugiuchi et al., 2005)

Hyaluronic acid

Hyaluronic acid or hyaluronan is a polysaccharide that is present in synovial fluid. It is a linear non-sulfated polysaccharide composed largely of 2-acetamino-2-deoxy-3-*o*-β-D-glucopyranosyluronic acid-D-glucose linked by 1,4-β-glycosidic linkages. (Sokoloff, 1978: 412) Figure 2.3 shows the straight-chain repeating disaccharides of glucuronic acid and N-acetyl-glucosamine known as hyaluronic acid. (Afify et al., 2005) The molecular weight of this repeat unit is 394 g/mole.

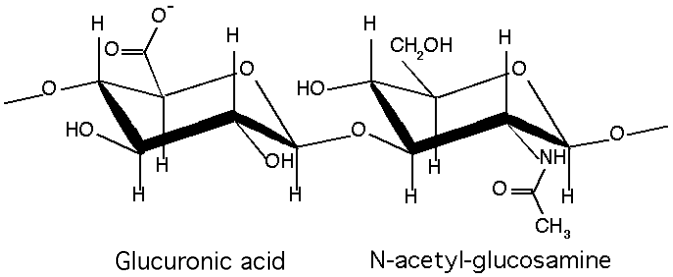

Figure 2.3: The repeating disaccharide unit of hyaluronic acid as presented by MadSci Network (2001).

Hyaluronic acid is not confined to synovial fluid, it is also found in connective tissue and in the synovial membrane. The main functions of this chemical substance include: (Praest et al., 1997)

- Regulating oxidative damage
- Forming high molecular weight aggregates
- Lubrication and viscoelastic properties in joints

Investigations show that hyaluronic acid molecules in solution occur as solvated spheres and that the polysaccharide chains have a slightly stiff but random molecular conformation, that are arranged in an orderly manner. (Sokoloff, 1978: 413) In these extended shapes, the molecules occupy a solvent domain much larger than the polymer chain itself. (Hlaváček, 1993a) Walker (1977: 136) reports spherical molecules with a diameter of 0.28 μm.

Studies done, show that the actual length of the hyaluronic polysaccharide chain in human synovial fluid corresponds to a molecular weight of about 10^6 g/mole, (Walker, 1977: 136) which corresponds to a about 2500 of the disaccharide repeat units shown in figure 2.3. (Sokoloff, 1978: 415) More resent work by Praest et al. (1997), shows that hyaluronic acid is found in highest concentrations in connective tissue, with molecular weights ranging from 4×10^3 to 8×10^6 g/mole. Fraser et al. (1997) report that normal concentrations of hyaluronic acid in human synovial fluid ranges between 4100–3600 μg/g. At these normal concentrations, the hyaluronic acid molecules form a transient cross-linked macromolecular network. These networks give synovial fluid its unique non-Newtonian rheological properties like the shear-thinning and viscoelastic effects. (Hlaváček, 1993a) According to Praest et al. (1997), high molecular weight hyaluronan ($6 - 10 \times 10^6$) shows excellent lubricating and viscoelastic properties. Walker (1977: 136) explains these rheological phenomena by defining a concentrated dilution where the hyaluronan starts showing significant non-Newtonian characteristics. This concentration is well below 0.1 mg/ml. (Walker, 1977: 136) Authors Lai et al. (1978) and Cooke et al. (1978) report on detailed rheological studies of synovial fluid.

The absolute viscosity of synovial fluid ranges from about 0.1 – 1 Pa.s for normal fluids and 0.01 – 0.1 Pa.s for rheumatic fluids. (Walker, 1977: 138) The decrease in the viscosity of isolated synovial fluid samples may be due to the change in the degree of polymerisation and a decrease in interaction between the macromolecule and other neighbouring molecules. The decrease in the viscosity observed with rheumatic fluids may reflect a change in the orderly structure of the polysaccharide chains observed by previous investigators. (Sokoloff, 1978: 415) Osteoarthritis can be improved by treating patients with hyaluronic acid, administrated into the affected joint cavities. (Nonaka et al., 1999) To summarise, the absolute viscosity of synovial fluid depends on the following major hyaluronic acid properties: (Sokoloff, 1978: 415) (Walker, 1977: 138)

- The length or molecular weight of the polysaccharide chain
- The conformations of these chains
- The interactions and entanglements between adjacent chains and other molecules
- The hyaluronic acid concentration

Scott et al. (2000) studied the effect that hyaluronan concentration has on fluid drainage from the joint cavity. Under conditions of intra-articular pressure, synovial fluid is drained from the joint cavity. The presence of hyaluronic acid greatly opposes this fluid drainage, even with large pressure increments. (Scott et al., 2000)

Lubricating Glycoproteins

Synovial fluid contains a protein component. This protein component is essential for lubrication. The length of the polysaccharide chain has very little effect on the lubricity of the fluid. (Sokoloff, 1978: 416)

Different fractionation methods for isolating glycoproteins and experimentally determined compositions are reported by Sokoloff (1978: 417–419). The lubricating protein can be divided into two major fractions called lubricating glycoprotein-1 (LGP-1) and LGP-2. Analysis of pure LGP-1 shows that it consists of equimolar parts of amino acids and carbohydrate constituents and that it has a molar weight of approximately 2.275×10^6. Threonine, glutamic acid, proline and lysine account for 75% of the amino acids. Galactoseamine, galactose and N-acetylneuraminic acid account for 98% of the carbohydrate residue. (Sokoloff, 1978: 420–423) The LGP-2 molecule has an apparent molecular weight of 7×10^4. It has a high content of aspartic acid, glutamic acid and leucine. Its amino acid composition and electrophoretic characteristics are similar to glycoproteins found in the articular cartilage. (Sokoloff, 1978: 423)

LGP-1 is actually a 50% (w/w) glycosylated with O-linked β-(1-3)-Gal-GalNAc oligosaccharides capped with NeuAc. This glycoprotein is also known as lubricin and it appears to be a semi-rigid rod shaped structure of approximately 800 amino acids. (Jay

et al., 2001) Lubricin is a glycoprotein responsible for boundary lubrication of the articulating surfaces in synovial joints by adsorbing on these surfaces. Authors Jay et al. (2001) later identified the genes that are responsible for the origin of lubricin in the synovial cavity.

2.2.2 The role of synovial fluid

The different constituents found in synovial fluid each has a unique function that is achieved by its specialised molecular structure.

Lubrication of soft tissue

Previous studies concluded that synovial fluid lubricates the tissue by a boundary mechanism. (Jay et al., 2001) This gave rise to new questions about the exact role the different synovial fluid constituents played in joint lubrication. Samples of rheumatoid synovial fluid, where the hyaluronic acids were purified, were chemically analysed. The authors investigated the intrinsic viscosity, which is the ratio of the solution's specific viscosity to the concentration of the solute. The specific viscosity is a dimensionless ratio of the viscosity of the solution to the viscosity of the pure solvent at the same temperature. Tests confirmed the fact that lubricating activity was not only dependent on the measured intrinsic viscosity of the fluid, but also on the structures of the hyaluronic acid. The lubricating activity was related to the intrinsic viscosity of the hyaluronic acid and not the kinematic viscosity of the solutions. This implies a relationship between lubricity and the structure, organisation and the length of the hyaluronic acid polysaccharide chains. But the length of the hyaluronic acid chain is not the only important factor. Macromolecular hyaluronic acid with high intrinsic viscosity has either particular conformations or organised structures of polysaccharide chains that is required for lubrication. These interactions are dependent on the degree of purification of the hyaluronic acid samples. High purification means little proteins are left to stabilise the chain conformations and a decrease in specific viscosity. All these observations confirm that the hyaluronic acid in synovial fluid has a specific structure that allows it to interact with soft tissue surfaces by adsorption and act as boundary lubricant. (Sokoloff, 1978: 425–427)

Authors Praest et al. (1997) did a study on the synovial fluid of 29 patients with degenerative joint diseases. They studied the viscosity, hyaluronan concentration and molecular weight. They found that the molecular weight of the hyaluronic acid of the samples ranged between 1.09×10^6 g/mol for acute-inflammatory joint disease to 1.91×10^6 g/mol for degenerative joint disease. They found a good correlation between the viscosity of the synovial fluid and the hyaluronan concentration and no correlation between the viscosity and the hyaluronan molecular weight. These results suggest that hyaluronic acid concentration could be a future marker to evaluate different kinds and the extent

of the joint disease. This parameter gives a more reliable diagnostic than viscosity. Mabuchi et al. (1999) confirmed these results published by Praest et al. (1997). They also observed a decrease in the friction coefficient after treating contacting joint surfaces with a 1% hyaluronic acid solution. They also concluded that the lubricating ability of hyaluronan is independent of molecular mass.

Mazzucco et al. (2002) studied the rheology of joint fluids of patients that underwent total knee arthroplasty (TKA). They investigated joint fluid samples to determine whether any alterations of the properties of the fluid, like viscosity would result from TKA. The same properties were also evaluated for commercially available sodium hyaluronate and bovine serum. Samples were from 35 arthritis patients undergoing TKA, 14 patients undergoing revision TKA and 2 patients with joint effusion after TKA. Results given in figure 2.4 show that joint fluid samples displayed shear-thinning behaviour except for the bovine serum which remained Newtonian.

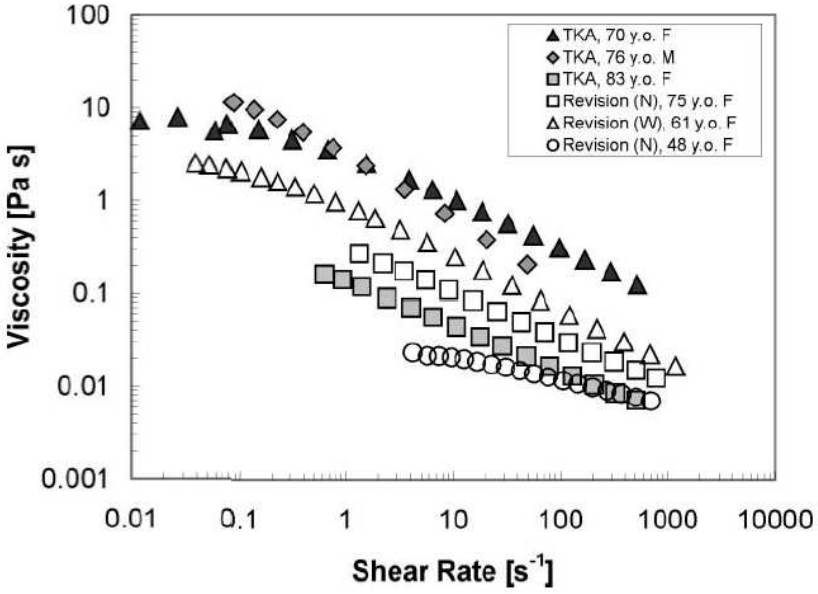

Figure 2.4: Rheogram showing the viscosity shear rate dependency of joint fluid from patients undergoing TKA and revision TKA as published by Mazzucco et al. (2002).

From these results the authors concluded that the rheological properties of the fluids that were investigated showed a reduction in viscosity between index TKA and revision TKA. Mazzucco et al. (2002) report that bovine serum showed different rheological properties than that of the joint samples which led to the conclusion that it is not an adequate and representative artificial joint lubricant, yet it is still used by several investigators as test lubricant. (Walker, 1977: 399–404) (Wang et al., 1998) The sodium hyaluronate samples showed rheological behaviour closer to that of the synovial fluid samples that were investigated, and should be considered for use as artificial lubricant.

Opperman (2005) evaluated the lubricity and viscosity of synovial fluid samples re-

trieved from patients receiving primary and revision surgery. The lubricity and viscosity of the samples were evaluated at three different temperature namely 38℃, 50℃ and 60℃. Lubricity was evaluated with an SRV machine, taking into consideration the failure load and the friction coefficient as monitoring parameters. They found a decrease in lubricity with increase in temperature. By monitoring the viscosity at the same temperatures, they found that the change in viscosity was not only temperature-dependent but also a function of the shear rate. Viscosity increased with increasing temperature and at low shear rates, a bigger change was observed than at higher shear rates.

Lubrication of articular cartilage

The protein constituent of synovial fluid is responsible for the lubrication of the articular cartilage. These proteins interact with the surface of the articular cartilage and act as a boundary lubricant by adsorbing on the articulating surfaces and forming a protective boundary layer. The excess of these constituents replenishes the boundary film as the film is worn away by the continuous joint movement. (Sokoloff, 1978: 428)

After some investigation into protein lubrication, investigators found that the lubricating protein of synovial fluid alone had 50% of the synovial fluid's lubrication activity. Other constituents in the synovial fluid may influence the lubricating ability of these lubricating proteins. The presence of receptors on the articular cartilage and the specific structure of the lubricant is very important in the role synovial fluid plays as boundary lubricant. The bi-functional lubricating protein molecule, interacts with the articular cartilage, while the long asymmetrical hydrophilic end maintains stable layers of water molecules in between the moving surfaces. (Sokoloff, 1978: 428–430)

Several authors worked on the role of phospholipid proteins as boundary lubricant. (Saikko & Ahlroos, 1997) (Sarma et al., 2001) First Saikko & Ahlroos (1997) isolated different proteins and confirmed that they are effective boundary lubricants. Then Sarma et al. (2001) did a complete chemical analysis of the boundary lubricants that adsorb to the articulating surfaces of bovine joints. They successfully identified the compositions of the different phospholipids of the adsorbed layer. They also identified the most abundant fatty acid in all three lipid types as oleic acid. The authors recommend more work to be done on the interaction of the phospholipid molecules on the cartilage surfaces hoping to unveil the lubrication and friction mechanisms of synovial joints. Important topics include protein interaction, molecular modelling and packing and orientation estimation. Sarma et al. (2001) also studied the phospholipid content on the surface of bovine articular cartilage. This was done to determine which proteins adsorb to the cartilage surface to act as boundary lubricant.

2.3 Joint tribology history

After a firm establishment of tribology as a scientific discipline with work from Tower and Reynolds, came a shift in interest and the controversial subject of joint lubrication or biotribology was born. This led to investigations into the mechanisms of joint lubrication. Mechanisms proposed by previous investigators include hydrodynamic, mixed, boundary, weeping, floating, elastohydrodynamic, osmotic, synovial gel, squeeze film, boosted, lipid and electrostatic lubrication. (Sokoloff, 1978: 444)

Interesting findings by several investigators reported by Sokoloff (1978: 446–447) that forms the skeletal history of joint lubrication include:

- Synovial fluid lubricates better than water at almost zero speed, showing that its advantages cannot result from a hydrodynamic mechanism
- Due to the small average pore diameters of cartilage, it has a very low permeability for high molecular weight molecules. This shows that synovial fluid lubrication cannot depend on the supply of high molecular weight molecules from within the cartilage
- Synovial fluid lubrication depends strongly on the presence of high molecular weight molecules
- Surfaces soaked in synovial fluid suggested that some form of adsorption took place, resulting in a boundary lubrication mechanism
- By reacting synovial fluid with certain enzymes, no change in viscosity is noted, but all lubricity is lost. This shows evidence against hydrodynamic lubrication
- Conflicting results that hyaluronic acid plays a part in joint lubrication.

2.3.1 Proposed lubrication mechanisms

This section gives a short overview of different lubrication mechanisms found in synovial joints, as is proposed by several authors. The lubrication regime that is predominant in a system is dependent on the system's prevailing conditions like viscosity (μ), relative velocity (v) and the applied load (P). Figure 2.5 shows the relationship between the dimensionless Sommerfeld number, $\mu \times v/P$ and the friction coefficient. The lubrication regimes are discussed in the following sections.

Hydrodynamic lubrication

Hydrodynamic lubrication or fluid-film lubrication is achieved when a viscous fluid film of sufficient thickness is compressed between two surfaces and a sufficient hydrodynamic

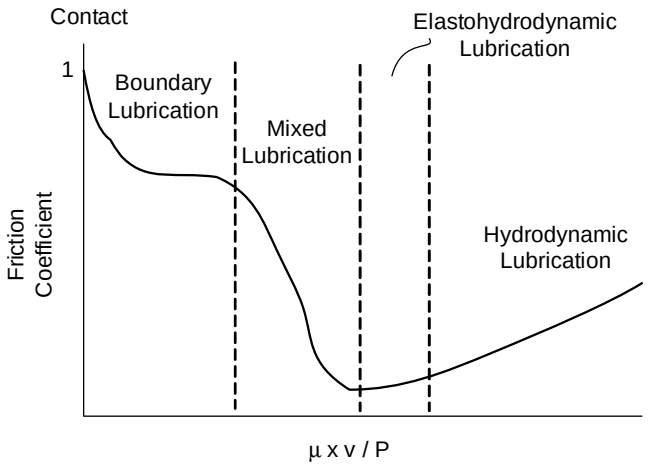

Figure 2.5: The Stribeck curve.

pressure is generated to support the load and prevent the two surfaces from touching. (Bhushan, 2002: 425–426)

Clinical trails showed that the viscosity of synovial fluid in arthritic joints was abnormally low. This shows that viscosity is an essential property of joint lubrication and that subnormal viscosities cause arthritis by allowing the cartilage surfaces to rub against each other. This proved that some form of hydrodynamic lubrication is observed in synovial joints. (Mazzuccoa et al., 2004) Synovial fluid samples are elastic due to the unique molecular shape of its constituents. Under high shearing the molecules flatten out and orientate in the direction of the movement, and if shearing stops completely, it recoils. In full hydrodynamic lubrication, the friction coefficient changes very little with a change in viscosity. (Sokoloff, 1978: 448–453)

Boundary lubrication

Boundary lubrication is found when solid surfaces are so close to each other that surface interactions take place between lubricant molecules and solid asperity contact prevails. (Bhushan, 2002: 428)

Boundary lubrication is found in natural and artificial joints. Effective boundary lubrication depends on the adsorption of lubricating components on the articulating surfaces. Potential boundary lubricants include phospholipids, proteins and lubricin, all found in synovial fluid. These components bind to the articular cartilage and provide a protective boundary between moving surfaces. Unsworth (1995) reports on work done to evaluate the importance of boundary lubrication in joints under steady state loading. By observing the tribological properties when synovial fluid was stripped of all protein components, it was confirmed that the proteins in synovial fluid act as boundary lubricants. (Mazzuccoa et al., 2004). Sokoloff (1978: 452–453) reports that previous investigators found similar friction coefficients for different viscosity synovial fluids indicating boundary lubrication.

The physical properties of boundary lubricants, like shear strengths and hardness, play an important role to minimise wear. (Bhushan, 2002)

Elastohydrodynamic lubrication

In the elastohydrodynamic lubrication (EHL) regime, the elastic deformation of the solid surfaces in contact play an increasing role in the lubrication mechanism. (Bhushan, 2002: 427)

Preliminary studies into joint tribology led to believe that synovial joints operate in the EHL regime. Sokoloff (1978: 449–455) debates that for human joints to be in the elastohydrodynamic region, the cartilage surface has to be rather smooth with viscosity playing a minor role. After careful investigation of the rough cartilage surface, he excludes the mechanism of elastohydrodynamic lubrication. This is supported by the argument that the thin elastohydrodynamic film thickness reported by various authors can not keep the large cartilage asperities from touching.

This is certainly not the case in modern biotribological studies. It has since been shown by Dowson & Jin (1986) that the cartilage roughness can be largely smoothed out due to micro-elastohydrodynamic action. Several other authors express the importance of EHL in modern artificial joint prosthesis. (Jalali-Vahid et al., 2001) (Jalali-Vahid et al., 2000) (Dowson, 1995b) (Mabuchi et al., 2004) According to Bhushan (2002: 427), EHL is commonly found in highly loaded oscillating bearing surfaces like ball bearings, which is the case with artificial hip joints.

Mixed lubrication

In the mixed lubrication regime, a combination of boundary, hydrodynamic and elastohydrodynamic lubrication is observed. Solid contact occurs frequently, while parts of the solid surface is supported by lubricant film. (Bhushan, 2002: 427) Studies performed on dog ankle joints under oscillating motion and constant heavy loading indicated the presence of mixed lubrication. (Unsworth, 1995)

Synovial fluid filtration by cartilage

Previous investigators investigated a so-called biphasic mixture theory for cartilage. This theory looks at a number of basic compressive situations in the cartilage and the effect of fluid flow. (Unsworth, 1995) The mechanism is based on the principle of fluid flowing into the cartilage in the central contact regions, boosting the lubrication.

Hlaváček presents his mathematical model of the role that synovial fluid filtration by cartilage plays on joint lubrication in a multi-part paper.

In the first part, Hlaváček (1993a) considers synovial fluid as a mixture of two incompressible fluids and carries out a squeeze film analysis for the axially symmetric synovial

film. In the second part, Hlaváček (1993b) reports on the numerically analysed biphasic synovial fluid model. A hyaluronic acid equilibrium concentration of 50 mg/ml results in a stable lubricating film with thickness 0.1 μm

Weeping lubrication

Sokoloff (1978: 444) explains the mechanism of weeping lubrication by referring to cartilage as permeable and soaked in synovial fluid. Applying a load to the non-rigid cartilage pressurises the liquid within. This causes liquid to flow to the cartilage surface, still pressurised, carrying the load and reducing the friction coefficient.

Experimental work showed that by pressing against a soaked cartilage, the fluid squeezed is the actual fluid absorbed in the cartilage and not fluid obtained from damaged cartilage. During constant rubbing, the cartilage deformation and friction coefficient rise with time. This is due to the actual thinning of the cartilage as absorbed fluid in load-bearing regions slowly leaked out of the cartilage and contacting surfaces. This lowers the pressure of the fluid at the surface, causing load to be carried by solid-solid contact and therefore increasing friction. Further investigation confirmed that the lubricating liquid came from the cartilage and was not a trapped squeeze film. Cartilage is constantly replenished by soaking up free synovial fluid. In joints, weeping lubrication carries most of the load by hydrostatic pressure leaving gentle solid-solid contact which can be effectively lubricated by synovial fluid.(Sokoloff, 1978: 444–446)

Squeeze film lubrication

Unsworth (1995) reports on several investigations into squeeze film lubrication. With viscous synovial fluid, the film thickness can increase due to the squeeze film mechanism and unlike the elastohydrodynamic mechanism, keep cartilage surfaces from contacting. It was found that the squeeze film could carry the high loads imposed on joints during walking, thus making this lubrication mechanism even more attractive.

Work done by Unsworth (1995) proved the feasibility of squeeze film lubrication in normal joints. A simple pendulum experiment was conducted. The difference between the friction coefficient with a steady state load and a suddenly applied load were investigated. He found that:

- Under steady state loading the results yielded almost constant friction coefficients throughout the whole experiment
- Sudden loading revealed lower friction coefficient at first which increased with time

This increasing friction coefficient characteristic can be explained in terms of the squeeze film lubrication mechanism. When the femoral head first encountered the acetabular socket a thick film of fluid separated the two surfaces. Since friction is inversely related

to film thickness, friction at this point is low. As the film squeezed down under the effect of the heavy loading, the friction increased.

2.3.2 Human joint lubrication mechanism

In summary of the previous section, joint lubrication mechanism are not easily restricted to only one specific lubrication mechanism. They are highly dependent on the operation conditions of the joints. Figure 2.6 shows the typical loads imposed on a hip joint during a single walking cycle.

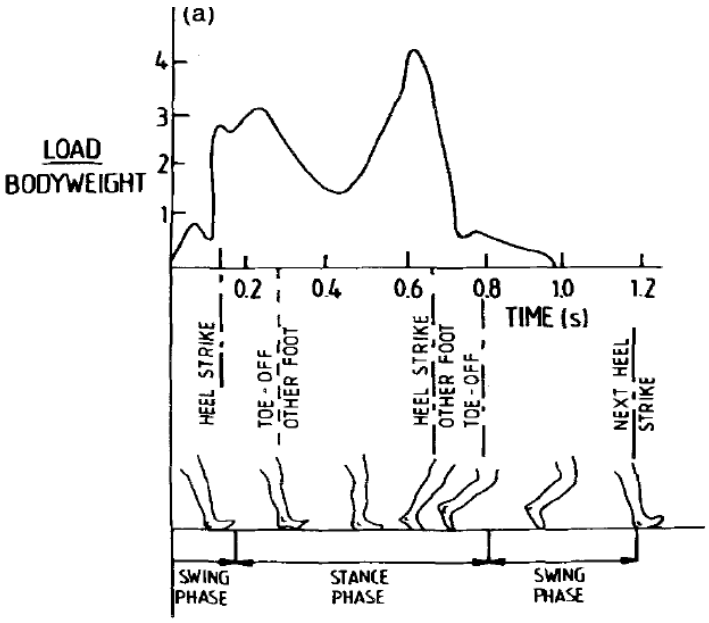

Figure 2.6: Vertical loads on a hip joint during a single walking cycle as presented by Unsworth (1995).

During the swing phase, the loading on the joint is very low and the entrainment velocity high. This induces a thick film of fluid between the cartilage surfaces. During the swing phase, small loads in the order of 20 N generate thick films. At heel strike, the load rises dramatically to well over 2 kN while the entrainment velocity is very low. The thick film is then reduced and the lubrication mechanism is squeeze film. The stance phase has lower loads and higher entrainment velocities. Here again, some form of fluid film lubrication mechanism is observed. (Unsworth, 1995)

In the case of artificial joints, it is a known fact that even the most technologically advanced joint prosthesis is subject to wear. Current researchers estimate that the life-time for artificial joints is between 15 and 20 years. (College of Engineering, University of California, 2005) New technological research aims to prolong the in-situ life of joint replacement by optimising or minimising wear rates and frictional resistance. It can therefore safely be said that hip joint prostheses operate in the boundary or mixed lubrication regimes.

2.4 Artificial joints

Joint arthroplasty or the surgical reconstruction or replacement of a malformed or degenerated joint is one of the most successful surgical procedures carried out today. The increase in joint implants in patients place great demands on the lifetime and performance of these prostheses. Material performance, friction reduction and wear minimisation include some of the tribological topics that are studied to meet these demands. This section focuses on the tribological aspects of joint replacements.

2.4.1 Joint diseases

Osteoarthritis or degenerative joint disease, is a common disorder that affects diarthrodial joints. It is characterised by the deterioration, degradation, and abrasion of the articular cartilage as well as the formation of new bone at the articular cartilage surface. (Hori & Mockros, 1976) If the damage to the articulating surfaces is severe a partial joint replacement or total joint replacement is performed on the patient. Over a million hip implants are performed each year worldwide (Affatato et al., 2005)

Gamlin & Brostoff (1997) studied the connection between food sensitivity and rheumatoid arthritis. They found that 30-40% of patients suffering form this disease can improve physically by undergoing an elimination diet. These results could last for up to 12 years or more.

2.4.2 Artificial joint replacements

Artificial joint replacements have been around for some time now. Material combinations that are relevant in artificial joints are metal-on-metal, metal-on-polymer, ceramic-on-polymer and ceramic-on-ceramic. Numerous investigators researched the tribological behaviour of these pairs like friction and wear. These two tribological parameters play an important part in improving joint prostheses in order to achieve better in vivo lifetimes.

Friction

Friction, is known as the resistance force to the sliding or rolling motion of two solid bodies in contact. (Bhushan, 2002: 207) The coefficient of friction, μ, is the ratio of the frictional resistance, F_f, due to the load, W, of two contacting solid bodies. In mathematical terms, it can be expressed as

$$\mu = \frac{F_f}{W} \tag{2.1}$$

Normal polymers like polyethelene or nylon rubbing against a smooth surface of a hard material like metal or glass, a fairly low friction coefficient of between 0,1 and

0,4. (Walker, 1977: 371) PTFE is an exception of this rule, with extremely low friction coefficients. Lubricants are usually not used with polymer. This is due to the comparable shear strengths of the polymer interface and that of typical lubricants. Frictional properties of materials are evaluated with typical pin-on-disk machines. (Fisher & Dowson, 1991) (Walker, 1977: 371)

Wear

Wear, as defined by Bhushan (2002: 331), is the surface damage or removal of material from one or both of two solid surfaces in a sliding, rolling or impact motion relative to one another. If the nature of wear is not very severe, it usually is (Walker, 1977: 373)

- Independent of the apparent area of contact
- Proportional to the load
- Proportional to the sliding distance

The volume of material, V_r removed during wear is related to the wear coefficient or the wear factor, k, the load and the sliding distance L by the following widely used equation. (Walker, 1977: 373)

$$V_r = k.W.L \tag{2.2}$$

The wear coefficient is very useful when comparing the wear characteristics of different materials. Wear can also be described by defining the wear rate. This is usually the depth of the wear scar per unit sliding distance. It is always important to denote the experimental conditions, like temperatures and pressures, when reporting wear rates of materials. This is due to the sensitivity of this parameter to any experimental condition changes.

The different types of wear mechanisms include:

1. **Adhesive wear**

   Adhesive wear occurs when the asperities of two sliding bodies which are in contact, undergo shearing. This can lead to the detachment of fragments from one surface to form wear debris, or the attachment to the other surface. (Bhushan, 2002: 332) Figure 2.7 shows signs of adhesive wear found in a metal-on-metal prosthesis.

2. **Abrasive wear**

   Bhushan (2002) states that abrasive wear occurs when detached asperities of a hard surface or hard particles slide on a softer surface. This sliding damage the interface by plastic deformation or fracture. The entrapment of methyl methacrylate cement

in an artificial joint is a practical example of abrasive wear. (Walker, 1977: 375) An example of abrasive wear is shown in figure 2.8.

3. **Fatigue wear**

   This wear mechanism is observed when to surfaces are in repeated sliding and rolling contact. The repeated or cyclic loading may cause subsurface or surface cracks or faults, which in time can break off the surface and form large fragments. The signs of this wear mechanism is large pits that form on the surface. (Bhushan, 2002: 360) The continuous cyclic loading on artificial joints make it very susceptible to fatigue wear.

4. **Fretting**

   Fretting occurs where low amplitude oscillatory motion takes place between two surfaces which are normally at rest. It is a form of adhesive and abrasive wear, where normal load cause adhesion and the vibratory movement causes rupture resulting in wear debris (Bhushan, 2002: 383)

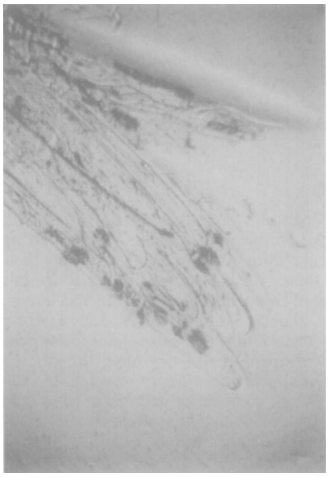

Figure 2.7: Adhesive wear found in a metal-on-metal joint.(Unsworth, 1995)

Wear of artificial joint bearing surfaces and cytotoxic effects associated with wear particles play a significant role in the failure of artificial joint prostheses Infection of surrounding tissue and loosening of prostheses can result from the presence of wear particles and the deformation that accompanies wear. (Young et al., 1998)

Tribology of metal-on-metal prostheses

Cobalts-chrome alloy is a useful metal sliding pair, and has been used several times in hip prosthesis. The high wear resistance and the low coefficient of friction observed in these implants are due to the excellent boundary lubrication characteristics of the proteins present in synovial fluids.(Walker, 1977: 383) In hip replacements, a high friction

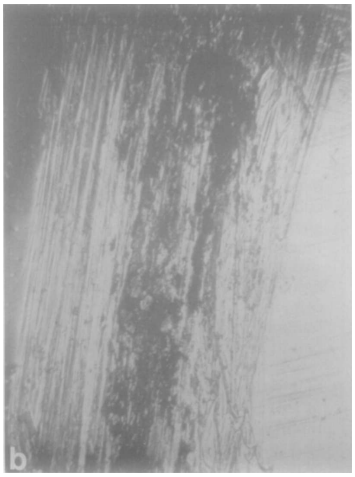

Figure 2.8: Abrasive wear in a metal-on-metal prosthesis as reported by Unsworth (1995).

coefficient is very undesirable, because it facilitates loosening of the prosthesis. Walker (1977: 383) states that most of the cases it is actually the design of the bearing itself with a big ball radius, lack of built-in damping and tendency to impinge that is responsible for loosening. Due to the fact that metal-on-metal has been widely used in replacements, and its uses today and in future, a tribological property study is of great use, although other materials are more commonly used today.

Metallic biomaterials used for artificial joint replacements in vivo shows some signs of degeneration due to the destruction of the protective oxide film due to its reaction with ions and molecules. This corrosive and wear resistance of metals can be improved by surface modification techniques like bone conductivity and ion beam technology. (Hanawa, 1999)

When studying the wear of metal-on-metal sliding pair, three types of wear can occur in artificial joints. They are: (Walker, 1977: 390)

- **Type 1 wear:** Initial scratching of the surfaces
- **Type 2 wear:** Smoothing down of surfaces
- **Type 3 wear:** New smooth surfaces showing signs of degradation, usually pitting

The types 1 and 2 wear are normally due to abrasive wear between the sliding surfaces. Although one would expect adhesive wear between contacting metals, localised hard particles cause the major damage. Type 3 wear is caused by fatigue wear. This is evident from 1μm diameters pits and small fine cracks on the surfaces.

Causes of these wear mechanisms could be due to: (Walker, 1977: 391–393)

- Variations in surface hardness
- Incorrect surface finishes

- Subsurface deformation or porosity due to an incorrect casting process.

In conclusion, metal-on-metal prostheses show favourable low wear rates, but rigid metal systems and poor design can have its drawbacks.

Tribology of metal-on-polymer prostheses

Professor Sir John Charnley introduced metal on plastic joints in the 1950s. (Unsworth, 1995) Metal-on-plastic systems of today come very close to the low friction performance of natural joints. These systems show very low wear rates. This makes it difficult to do accurate wear analysis. Other physical properties of polymers, like polymer creep, pose new challenges in the field of prosthesis. Polymer creep is the gradual movement or deformation of polymer material due to constant loading.

Common polymers that were considered for use in replacements include PTFE, UHMWPE, acetal and polyester. First, PTFE were considered as bearing surface, sliding against a smooth metal surface due to its extremely low frictional resistance. The wear of the polymer was found to be unacceptable high and the wear volume produced could not be tolerated by the human body. (Fisher & Dowson, 1991) (Dowson, 1995a) Polymers like acetal and polyester showed the same amount of wear debris. The emphasis then moved to the use of UHMWPE. Total joint arthroplasty has been conducted successfully for the last thirty years due to the use of UHMWPE as a bearing surface. What distinguishes this material from other polymers is that its molecular chains are extremely long and highly entangled, which makes it very wear resistant. (Wang et al., 1998)

The polymer is used as the hemispherical socket, while a hard material with a highly polished finish is used as the convex femoral ball surface. Typical friction coefficients of metal polymer pairs measured in hip simulators range between 0.03 and 0.1. (Fisher & Dowson, 1991)

Several authors place great emphasis on studying the wear of polymer pairs. Important parameters that should be addressed in any prosthesis laboratory investigation is different material, specimen configuration, lubricant, sliding speed, test duration, and load. Material and configurations used must be applicable for prosthetic joints. The best lubricant will always be synovial fluid, but plasma, Ringer's solution and distilled water is good enough for comparative studies. Sliding speeds and loads should be realistic, preferable with oscillatory motion. Test duration should be long enough to reach steady state conditions.(Walker, 1977) (Dowson, 1995a)

Walker (1977: 396–397) mentions a number of interesting facts about wear rates in polymer joints:

- Wear rate decreases with increase in molecular weight
- Increasing contact stress increases the wear rate

- Increasing the clearance increases the contact stress, but wear particles can escape easier, causing less damage
- Ball 'out-of-roundness' has little effect on the wear rate

Interestingly, Wang et al. (1998) disagree with this. After investigating the wear rate on a contacting convex CoCr surface on a conforming concave UHMWPE surface with bovine serum used as lubricant, they concluded that the wear rate decreased with increasing contact area up to a critical point. The wear rate then increases again. These findings are shown in figure 2.9. Wear analysis shows that below the critical contact area, the surfaces were extremely smooth with very little surface damage. Above this critical value, the worn surfaces showed extensive tearing and rupture damage which is characteristic of adhesive wear. This showed that an increase in femoral head radius decreased the wear resistance of the implant.

Fisher & Dowson (1991) agree that the design and geometry of the prosthesis has an effect on a range of variables including the stress distribution and tribological aspects like friction and wear. According to the authors, a number of factors influencing the wear coefficient of polymer pairs include counterface material, surface roughness, sliding velocity, contact stress, lubrication, and test duration.

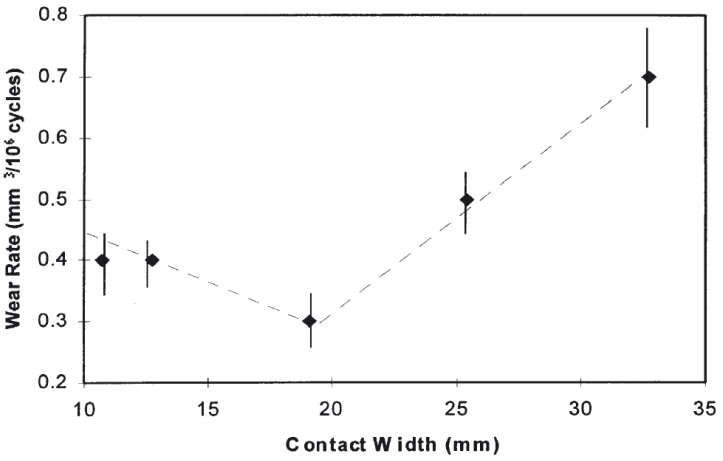

Figure 2.9: Wear rate vs. contact width for conforming contact sliding between CoCr and UHMWPE with serum lubrication as depicted by Wang et al. (1998)

Walker (1977: 397) asks the question: "Is the wear affected by the counterface metal material?" By placing emphasis on making sure that in vivo conditions apply during testing, he assures the reader that different metal types make little difference in joint prosthesis. Next, he asks the question whether polymer materials with higher wear resistance can be found. This answer is simple, "the most promising direction lies in further improvement of polyethylene by optimising its molecular weight, degree of crystallinity and associated processing methods." The different counterface materials used together

with UHMWPE includes stainless steel, titanium alloy, cobalt chrome molybdenum alloy and aluminium oxide ceramics. (Fisher & Dowson, 1991)

Shi et al. (2003) did a preliminary evaluation of the tribological performance of alternative bearing materials for artificial joints. They used a normal pin-on-plat machine with a polished stainless steel disk. The balls were the different materials that were investigated: stainless steel, alumina, zirconia and a diamond-like carbon (DLC) thin film coating on stainless steel. Preliminary results indicate that the DLC thin film coated stainless steel shows the lowest friction characteristics and has the least amount of wear damage. These results need to be verified with more experiments including hip simulations and biocompatibility.

When polymer pairs wear, the surfaces are worn down by three mechanisms. (Dowson, 1995a) They are discussed in order of importance in terms of producing wear particles. (Wang et al., 1998) (Walker, 1977: 404)

1. **Abrasion**

   Already worn plastic particles makes the small surface grooves and release granular fragments. Scratches can occur in the presence of sharp asperities.

2. **Adhesion**

   Adhesive contact between the smooth metal ball and high plastic points leads to the formation of thin sheets, shreds and filaments which can either become part of one of the surfaces or form abrasive wear debris.

3. **Fatigue**

   Fatigue cracks form the site for subsequent adhesive points and may also give rise to abrasive debris.

Wear is increased by fragments harder than polyethylene, like acrylic cement. When they are drawn into the contacting area, they disrupt the plastic surface and generate large adhesive points.

Surface finish play a very important role in the tribological performance of polymer implants. Fisher & Dowson (1991) reports that an increase in surface roughness from 0.01 to 0.1 μm causes a 13 fold increase in the wear rate. Young et al. (1998) monitored UHMWPE bearing surfaces with different surface finishes, sliding against steel in a pin-on-disk type testing machine. They concluded that an undulated surface finish reduced the friction by 42% compared to a non-patterned surface. The authors hypothesise to reflect that patterned surfaces act as a reservoir for the lubricating fluid and also trap wear particles, minimising abrasive third body-type wear. However, patterning of the UHMWPE surface was not effective in reducing wear presumably because the polyethylene surface was plastically deformed by the high contact stresses. (Young et al., 1998)

Surface roughness in Charnley prostheses of the counterface of reciprocating and hip simulators were investigated by Wang et al. (1998) They found a good correlation between the wear factor and the surface roughness. This builds on the work done by Dowson (1995a), where the author determined an expression for the wear coefficient for UHMWPE as a function of surface roughness. This relationship, given as equation (2.3), was determined from a reciprocating pin-on-disk test for UHMWPE sliding on stainless steel in the presence of water.

$$k = 4.0 \times 10^{-5} R_a^{1.2} \tag{2.3}$$

Bigsby et al. (1998) developed a new composite cushion acetabular cup comprising of two layers of graded modulus polyurethane integrally moulded into a metal shell. This builds on the work of previous investigators including Dowson et al. (1991), Medley (1994) and Unsworth (1995). The shell is basically used as an injection mould tool. The first layer of polymer injected into the metal shell is of high modulus. The second layer is only 3 mm thick, with a low modulus. This layer is known as the cushion layer. The low frictional torques recorded on these systems are indicative of fluid film lubrication. Bigsby et al. (1998) tested the cushion cup on a hip simulator and compared the results to a normal UHMWPE cup. They found considerably less creep and wear. Further work needs to be done on the degradation and chemical changes at the interface of the two layers. Nevertheless, the results look promising.

Authors Ingham and Fisher (2000) studied the in vivo biological reaction to wear debris in total joint replacements. The fact that evidence show that prosthesis are prone to failure due to aseptic loosening of the joints creates a need to understand the mechanism of failure and possible solutions for the problem. The authors propose that initial wear testing of possible new materials should include a wear particle analysis and a biological reactivity assessment.

Xiong (2005) tested the tribological properties of carbon fibre reinforced UHMWPE composites. Friction and wear behaviour were evaluated with an MM-200 tester where the reinforced polymer was loaded against stainless steel rings. The author found that increasing the carbon fibre content increased the hardness of the composite and decreased the amount of wear debris formed during experiments. Under dry conditions, the friction coefficient of the composite increased, while it showed a decreasing characteristic under lubricated conditions. SEM scans showed that the dominating wear mechanism for the composite is mainly adhesive and abrasive wear.

Both wear and polymer creep cause penetration of the femoral head into the acetabular cup. Although creep dominates as cause of penetration for the first million cycles, wear plays a constantly important role and is generally the main factor that causes long term penetration. (Dowson, 1995a) Penetration is measured in vivo by radiological means.

Work done by previous investigators show that creep is greater under constant loading than for cyclic loadings of three times that of the body weight. It is dependent on the applied loads and the resulting stress levels.

Tribology of ceramic prostheses

Fisher & Dowson (1991) report on the use of ceramic pairs as bearing surfaces for joint implants. These pairs have extremely low wear rates and a low friction coefficient. They require complex manufacturing procedures to achieve the exact surface finish. The authors report on disappointing clinical results and little clinical use of ceramic pairs. This has changed a lot in the past few years. Ceramics are widely used today in joint replacements due to their excellent material properties. Later, Dowson (1995a) did a comparative study on the performance of metallic and ceramic femoral heads, which included laboratory and clinical observations. He concluded, due to overwhelming clinical proof, that the ceramic femoral heads outperform its metallic counterpart. Alumina ceramic heads in general result in a reduction of approximately 50% in UHMWPE wear compared with the use of metal femoral heads. (Wang et al., 1998) (Dowson, 1995a) An example of abrasive wear of ceramic ball against a steel plate are shown in figure 2.10.

Figure 2.10: SEM micrograph of stainless steel plate tested against zirconia ball showing abrasive wear scratches and grooves (University of Iowa Archives, 2004)

Yttria-stabilized Tetragonal Zirconia Polycrystal ceramics or Y-TZP is a ceramic with excellent mechanical properties that is very often used as a biomaterial for ball heads of total hip replacements. Piconi et al. (1998) investigated the stability of the material properties of Y-TZP. The investigation was launched due to clinical reports of the in vivo degradation of the material. The authors found degradation of the samples under different conditions.

Zhou et al. (1997) measured and compared the start up and steady state friction of four ceramic materials against themselves, lubricated with 1% water solution of carboxymethyl cellulose sodium salt. The experiments were carried out using a pin-on-disk testing machine, with the pin manufactured to have a spherical surface. This was done

to approximate the contact conditions in a hip joint.The four different ceramics under investigation were alumina, zirconia, silicon carbide and silicon nitride. The authors found that the start up and steady state friction of the silicon nitride-on-silicon nitride are the highest of the four ceramics. Silicon carbide-on-silicon carbide yielded the lowest start up and steady state coefficients. (Zhou et al., 1997) These results were obtained under very specific testing conditions which could never replicate the exact hip joint conditions, but could be beneficial to total hip joint replacements. What was quite disturbing was the fact that the surface finishes of the four ceramic samples differed. This makes an accurate comparative study very difficult.

Dowson (1995a) did a range of laboratory studies to investigate the tribological performance of ceramics on polymers. First he conducted a pin-on-disk wear test under dry atmospheric conditions with alumina ceramic and polyethylene. The author found that a polymer surface transfer film of 1 μm readily formed. The steady state friction coefficient were quite high, 0.3-0.4, with a low long term wear factor of about 1.7×10^{-7} $mm^3N^{-1}m^{-1}$. Dowson (1995a) extended the work to investigate the wear effects of ceramic on polymer for dry compared to wet conditions. He used distilled water as lubricant. Under dry conditions, the author noted a gradual increase in wear rate over time. Under wet conditions, a much lower wear rate was observed, with a gradual decline in wear rate throughout the duration of the test.

In order to obtain a better quality artificial joint, the wear resistance of UHMWPE should be increased. Ge et al. (2003) researched the surface treatment of UHMWPE by nitrogen ion implantation. They dosed the polymer surface with 5 - 125 $\times10^{14}$ ions/cm^2. They studied the tribological properties of the surface treated polymer with a ball-slid-on-disk tribometer where the ion implanted polymer was tested against zirconia ceramic under dry and lubricated conditions. They found that the treated polymer showed higher friction coefficients under both dry and lubricated conditions. Surface treatment reduced the wear rates between 10-44% under lubricated conditions, but wear rates increased under dry conditions. Abrasive wear is the dominating wear mechanism found in these systems. A very active topic in biomaterials research is the improvement of cross-linking polyethylene. This strengthens the polymer considerably and reduces wear drastically if compared to normal UHMWPE. (Affatato et al., 2005)

2.4.3 Simulative testing of joint prostheses

New and current developments of replacement prostheses have to be assessed and tested before implantation in human patients. The International Organisation of Standards has a few guidelines on performing such work. One of the standards is the ISO 14242-1:2002 which addresses the loading and displacement parameters for hip joint prosthesis wear-testing machines and the corresponding environmental conditions that have to be adhered

to during these tests. Then there is the technical report of ISO TR 9325:1989 which makes certain recommendations for simulators used for evaluating hip joint prostheses. It is recommended that specimens be weighed, sterilised, and all relevant history be recorded before commencing the test procedure. Together with the test specimen, a reference and control specimen has to be included in the studies. The specimens have to be assembled and submerged in bovine serum maintained at a temperature of 37°C. The specimens are then subjected to oscillatory load cycle with a frequency range 0.5 to 1 Hz, with maximum peak loads of at least 1500 N. The duration of the test is generally 5×10^6 cycles. The wear damage of the articulating surfaces is then assessed. $10,5 \times 10^6$ cycles of the recommended test corresponds approximately to a 4 year period of use in the human body. (International Standard ISO TR 9325:1989)

ISO TR 9325:1989 recommends that load cycles should be developed from in vivo bio-elementary measurements or from predictions from external dynamic measurements. Bergmann et al. (1993) measured the in vivo forces and moments in hip joints during walking and running. He found typical oscillatory behaviour where the measured forces ranged between 40% and 550% that of the body weight. This is a good measure to incorporate into a joint simulator where the specimens will be exposed to actual in vivo conditions. The ISO specification has little standard regulations on the load cycle used for wear testing with joint simulators. Several investigators have expressed the need to standardise the load used in experimental testing. (Baleani et al., 1999) A range of authors have published simulative wear testing of hip joint prostheses based on the guidelines provided by the ISO standards. (Essner et al., 2005) (Affatato et al., 2005) (Cooke et al., 1978)

2.5 Joint tribology modelling

Joint lubrication and joint lubrication modelling is a very actively debated and controversial subject. From as early as 1932, investigators started proposing governing lubrication mechanisms found in human synovial joints. (Sokoloff, 1978: 438) This lead to the establishment of the research area of joint lubrication modelling, where rigorous mathematical analysis could prove the applicability of some of these proposed mechanisms. (Sokoloff, 1978: 460) In this section, an overview of the development of joint lubrication modelling is given.

Torzilli and Mow (1976a) investigated the fundamental transport mechanisms associated with articular cartilage. This was done to understand the bio-mechanical and lubrication processes involved in normal and pathological synovial joints. They viewed the articular cartilage as a mixture of two mechanical interacting phases. The linear elastic solid matrix phase consists of mainly cartilage, and the incompressible liquid phase is composed mainly of water. During articulation, pressure gradients are generated when

the liquid phase moves through the solid matrix phase, and results in a squeeze film mechanism. Squeeze film lubrication is where a thin liquid lubricant film is squeezed between the solid moving surfaces. The pressure gradients, motion of the synovial fluid and the frictional resistance were evaluated by describing the transport of synovial fluid through the articular cartilage tissue using the physical law of Darcy, where the fluid is assumed to be incompressible, Newtonian and fluid flow is a function of the pressure gradient through the cartilage. The authors used a two dimensional layered half-space geometry together with a time-varying loading function stationary over an articulating section. In part two of their paper, authors Torzilli & Mow (1976b) attempted an order of magnitude numerical analysis to solve the problem derived in part one. They found a strong dependency between fluid flow and tissue geometry, frequency of loading and tissue properties. They also successfully characterised the differences between healthy and degenerative cartilage operations. (Torzilli & Mow, 1976a) Torzilli & Mow (1976b)

Next came the in-depth study of the rheological behaviour of synovial fluids by authors Lai, Kuei, and Mow (1978). They developed rheological equations that describes the complex non-Newtonian behaviour of synovial fluids. The models used include integral type, rate type and generalised Newtonian fluid models. They also included parameters for the models derived from literature and experimental work for normal and diseased synovial fluids.

The first real investigation into a possible squeeze film lubrication mechanism was led by Bujurke and Jayaraman (1982). They studied the non-Newtonian flow effects during squeeze film generation in synovial joints. They modelled the synovial fluid as a couple stress fluid as published by Stokes (1966). The reason for this is due to the presence of the polar hyaluronic macromolecule found in synovial fluid. In short, the couple stress model takes into consideration the consequences of one deforming body on that of neighbouring bodies. Stokes (1966) also showed that molecule size and behaviour can have important implications on flow and therefore on lubrication, making the use of couple stress even more applicable. Bujurke & Jayaraman (1982) modelled the synovial joint as a infinitely long rigid cylinder approaching a plane at constant velocity. They showed that couple stress fluid lubricants provide significant load support, coming close to the natural characteristics of the synovial joint. They revealed that squeeze film time was adequate for proper joint lubrication and that the time needed to generate an efficient squeeze film increased dramatically for non-Newtonian fluids compared with Newtonian fluids with an identical viscosity.

Collins (1982) derived a fluid mechanical model for lubricant gelling in synovial joints. A two dimensional, time dependent loading and finite deformation model of cartilage is presented where special attention is devoted to lubricant gel formation in the intra-articular gap. The lubricant gel refers to synovial fluid that is compacted in the narrowing intra-articulating gap during loading. During this event, the concentration of the

hyaluronic acid increases whereby the molecules overlap and the chains intertwine to form a firm and stable gel. The author defines two separate events during lubrication:

- The fluid interchange across the deforming cartilage
- The variation in the hyaluronic acid polysaccharide concentration in the gap of the approaching articulating surfaces

A correlation between the polysaccharide concentration and the fluid film thickness was found. The increase in polysaccharide concentration determines the rate of build-up of the lubricating gel. It was reported that spontaneous gelling should occur above a critical concentration of 1%.

Mabuchi and Sasada (1990) report on the numerical analysis of a total hip prosthesis. The mechanism of lubrication that these authors proposed was elastohydrodynamic squeeze film lubrication. By assuming that the pressures between the conforming ball and cup are axisymetrical, the computational time required to solve the model is minimised. The authors chose an elastohydrodynamic approach, although several authors concluded that the film thicknesses in the elastohydrodynamic regime is insufficient to keep the sliding surface asperities from touching. (Sokoloff, 1978: 455) (Unsworth, 1995). However, a squeeze film mechanism would provide sufficient load bearing capacity for effective lubrication. (Unsworth, 1995) Mabuchi et al. (2004) republished the same work, using only different manufacturing materials for the prosthesis.

Dowson et al. (1991) did a critical design analysis of different materials for a cushion form bearing in artificial joints. Cushion bearings consist of a low elastic modulus lining on the hard bearing surface which promotes a continuous lubricant film between the contacting surfaces. The aim of the study was to investigate and compare the contact and lubrication mechanisms found in normal hard joints, natural joints and cushion bearing joints. They approximated the hip joint with a cushion bearing, ball on plane geometry. This model incorporated a constant angular velocity rotation where the effects of the curvature was neglected. The Reynolds equation was used for lubrication analysis. They found that by increasing the contact area and hence lowering the contact pressures, the lubricating film thickness improves. At a constant contact area, an increase in the cushion layer thickness and radial clearance had a small effect on the lubricant film thickness. By employing the cushion bearing effect, effective lubrication regimes and effects like squeeze films can ensure effective lubrication. The performance of this proposed prosthesis was evaluated by stress analysis. (Jin et al., 1991) The stress distribution analysis revealed the maximum shear stress region to be at the contacting interface, predicting that the mode of failure will be either at the interface under fluid film or mixed lubrication conditions, or complete surface breakdown under dry contact conditions.

Bujurke et al. (1991) continued on their earlier work by publishing a model of porous-elastic slider bearings, referring to synovial joints, lubricated by a couple stress fluid as

defined by Stokes (1966). The system geometry consists of fixed lower porous matrix surface and a rigid long cylinder in motion. By applying Reynolds cavitation boundary conditions, they proved by means of extensive mathematical methods that couple stress fluid has enhanced load carrying capacity compared to viscous fluid. Elasticity increases the load bearing capacity and decreases the frictional resistance. Neglecting the role of cartilage structure and the biomechanical and complex rheological characteristics of synovial fluid have an effect on the accuracies of the results obtained. (Bujurke et al., 1991)

Jin et al. (1992) investigated the effect of articular cartilage porosity in a dynamic squeeze film lubrication model of a normal hip joint. They kept to their previous geometry configuration of sphere on plane. The articular cartilage was modelled as a porous-elastic layer. Synovial fluid was assumed to be Newtonian, isoviscous and incompressible. Lubrication analysis was done by solving the Reynolds equation. They found, in contrast with authors like Torzilli & Mow (1976a), that the cartilage decreases the lubricant film thickness rather than increase it. This occurs especially at very small film thicknesses. The authors assure that, according to the results obtained, normal elastohydrodynamic analysis is sufficient for studying human joints. Furthermore, they concluded that the porosity of the cartilage on the lubrication analysis can be neglected when large fluid film thicknesses prevail. Finally they concluded that boosted lubrication is more likely to be prevalent in synovial joints. Boosted lubrication refers to the transport of non-Newtonian fluid, like synovial fluid, into the cartilage to produce a more viscous layer on the articular cartilage.

Hlaváček (1993a) looked into the effect of synovial filtration through cartilage and the role it plays in lubrication in a multi-part paper. During a typical loading cycle in a human joint, squeeze film actions lead to a concentration of hyaluronic acid-protein complex. This is due to the diffusion of water and other low molecular weight substances through the cartilage surface. In the first part of the paper, the author models the synovial fluid as a mixture of two incompressible fluids. (Hlaváček, 1993a) A simple squeeze film analysis is carried out with the fluid. In part two, Hlaváček (1993b) described the filtration of the synovial fluid squeeze film between two cartilage layers. This ties up with the work of Collins (1982), where the author finds a critical concentration of the high molecular weight complex of 50 mg/ml, which forms a stable gel film of 0.1 μm thickness that protects the articulating surfaces before fluid film lubrication is restored. Although the author uses a geometrically simplified model that idealises the human hip joints and uses only moderate loading conditions, he finds good correlations for normal and inflammatory joints. (Hlaváček & Novák, 1995) Finally the author extends the model to include axially symmetrically high loading conditions. (Hlaváček, 1995)

Jie-min & Jie-hui (1994) published a three dimensional numerical model on human joint squeeze film lubrication. They present the synovial fluid with the Oldroyd four

constant non-linear viscoelastic fluid model. They approximate the joint geometry with a long plate moving on another plate. Here the lower surface is fixed and porous while the upper portion is rigid and moves. Results investigate the viscoelastic behaviour of the synovial fluid and the porosity of the cartilage. Results compared very well with previously published model results.

Medley (1994) developed the theoretical understanding of the cushion bearing concept by means of a numerical solution procedure that analyses the lubrication by using the "column model". He aims to investigate the effects of curvature on the film thickness. He simulated a rigid cylinder in a layered cylinder sleeve with empirical equations for the film thickness.

Jin et al. (1997) modelled the lubrication mechanism and contact mechanics of hard bearing surface pairs, including metal-on-metal and ceramic-on-ceramic total hip joint replacements. The model, based on their ball-on-plane analogy, revealed that the radial clearance between the ball and socket and the effective surface roughness of the bearing surface are the overriding factors that determine the lubrication regime of the implant. Proper fluid film lubrication in joint replacements can be achieved with a good surface finish. Contact mechanics play an important role in achieving fluid film lubrication. (Jin et al., 1997)

Jin et al. (1999) did a complete contact analysis for UHMWPE cups against metallic femoral head for artificial hip joints. They emphasised the importance of contact mechanics in artificial hip joint replacement design. Contact mechanics is the study of load transfer between two contacting solids. They compared experimental findings with results obtained from finite element prediction models. They used the ball-in-cup analogy together with fluid film analysis for joints loaded for a range of loads. The authors found a good agreement between the experimental measured contact radius and that predicted by the model.

Jalali-Vahid et al. (2000) developed an elastohydrodynamic lubrication model for metallic femoral heads articulating against an UHMWPE cup. This paper deals with the numerical solving of the Reynolds equation and other mathematical equations in spherical coordinates by means of the Newton-Raphson method. They critically compared two different approach models, the ball-in-cup and the ball-on-plane model. They modelled a Newtonian fluid in the joint, where the joint rotated in one direction at a constant angular velocity and at a constant load. The investigation revealed that there is a significant increase in the predicted film thickness due to the elastic deformation of the polymer bearing surface. The film thickness for the ball-in-cup model is slightly less than that of the ball-on-plane model, and both are insufficient for effective fluid film lubrication in artificial replacements of this kind. Jalali-Vahid et al. then published a technical note on this same work. (Jalali-Vahid et al., 2001) They monitored the effect of design parameters on the minimum film thickness. They found that an increase in the femoral

head radius, increase in UHMWPE cup thickness, decrease in radial clearance and a decrease in UHMWPE elastic modulus all lead to an increase in the minimum predicted film thickness. This increase, although noticeable, will still be insufficient for complete fluid film lubrication due to the surface roughness of the UHMWPE cups. They concluded that design features would not be able to secure full fluid film lubrication but could be optimised to minimise the wear rate of the implant.

Hlaváček (2002) researched the effects of joint pathology on the synovial fluid squeeze film. This is achieved by the modelling of synovial filtration by the articular cartilage in a step loaded spherical joint. This complicated mathematical model gives insight in the generation of the squeeze film between the articulating surfaces, and the effect that normal and inflammatory cartilage has on this lubrication mechanism.

Pascovici & Cicone (2003) presented in their study of the squeeze film effect for a layered contact joint two cases:

- impermeable and compliant layer for a spherical contact where the squeeze film acts between a rigid and compliant surface
- porous and deformable layer with variable permeability where the porous layer is squeezed and the lubricant in this layer is extracted

The first model for both ball-on-plane and ball-in-cup cases showed excellent agreement with literature data. The authors report an optimum radial clearance for the ball-in-cup case but could not back it with literature data. With the second model, the authors report an optimum porosity of the porous matrix, which is very close to that of articular cartilage, but yet again it could not be backed up by any theoretical studies on optimum porosity of squeezed layers. The authors recommend a future model that combine the two models that they investigated. (Pascovici & Cicone, 2003)

A variety of different lubrication mechanisms in several other human synovial joints are also found in literature. This includes the boundary lubrication model of an artificial wrist implant by Pylios & Shepherd (2004), the microelastohydrodynamic human ankle joint model published by Dowson & Jin (1992) and the human ankle joint lubricated by squeeze film synovial fluid by Hlaváček (2000).

2.6 Lubricant flow equations

In the previous section, most of the authors use the Reynolds equation to describe the flow of lubricant in their tribological models. This section is devoted to equations of flow, their derivations and limitations.

2.6.1 The conservation of mass equation

This equation is derived by writing a mass balance over a stationary volume element of dimensions $\Delta x\ \Delta y\ \Delta z$ shown in figure 2.11 through which a fluid is flowing.

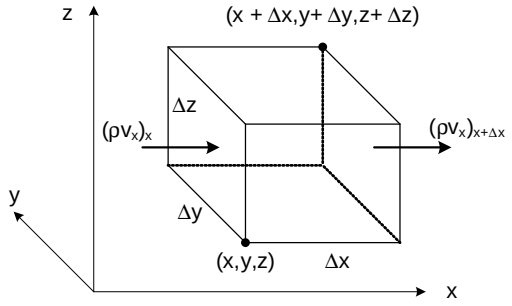

Figure 2.11: A stationary volume element through which a fluid is flowing.

A mass balance over the control volume would be

$$\text{rate of mass accumulated} = \text{mass flow rate in} - \text{mass flow rate out} \tag{2.4}$$

Mass flow in the x-direction in through area $\Delta y \Delta z$ is $(\rho v_x)_x \Delta y \Delta z$. The outflow is then $(\rho v_x)_{x+\Delta x} \Delta y \Delta z$. This can be done for all directions. Mass accumulation is simply $(\Delta x \Delta y \Delta z)\left(\frac{\partial \rho}{\partial t}\right)$ Substitution into equation (2.4) gives

$$\begin{aligned} \Delta x \Delta y \Delta z \frac{\partial \rho}{\partial t} &= \Delta y \Delta z \left[(\rho v_x)_x - (\rho v_x)_{x+\Delta x}\right] + \Delta x \Delta z \left[(\rho v_y)_y - (\rho v_y)_{y+\Delta y}\right] \\ &+ \Delta x \Delta y \left[(\rho v_z)_z - (\rho v_z)_{z+\Delta z}\right] \end{aligned} \tag{2.5}$$

Dividing the whole equation by $(\Delta x \Delta y \Delta z)$ and taking the limit as these dimensions approach zero gives

$$\frac{\partial \rho}{\partial t} = -\left(\frac{\partial}{\partial x}\rho v_x + \frac{\partial}{\partial y}\rho v_y + \frac{\partial}{\partial z}\rho v_z\right) \tag{2.6}$$

2.6.2 The conservation of momentum equations

For the same volume element as presented in section 2.6.1, the momentum balance will be

$$\begin{aligned} \text{rate of momentum accumulation} &= \text{momentum influx} - \text{momentum efflux} \\ &+ \text{sum of forces on the system} \end{aligned} \tag{2.7}$$

Consider the stationary volume element given in figure 2.12. For now, the momentum of fluid flowing through this element in the x-direction will be discussed.

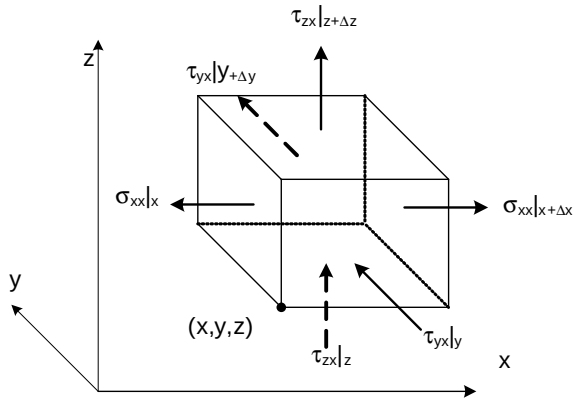

Figure 2.12: A stationary volume element through which a fluid is flowing.

Momentum into the element in the x-direction through area $\Delta y \Delta z$ is $(\rho v_x v_x)_x \, \Delta y \Delta z$. The outflow is then $(\rho v_x v_x)_{x+\Delta x} \, \Delta y \Delta z$. The x momentum entering at y is then $(\rho v_y v_x)_y \, \Delta x \Delta z$ This can be done for all the faces. The net momentum flux in the x-direction through the element is then

$$\begin{aligned} \Delta y \Delta z \left[(\rho v_x v_x)_x - (\rho v_x v_x)_{x+\Delta x} \right] &+ \Delta x \Delta z \left[(\rho v_y v_x)_y - (\rho v_y v_x)_{y+\Delta y} \right] \\ &+ \Delta x \Delta y \left[(\rho v_z v_x)_z - (\rho v_z v_x)_{z+\Delta z} \right] \end{aligned} \tag{2.8}$$

The forces acting on the system will include force due to shear stress and the normal stress. The shear stress , τ_{yx}, refers to a stress in the x-direction at constant y while the normal stress, σ_{xx}, is a normal stress on the x face in the x direction. The forces acting on the element due to stresses are then

$$\begin{aligned} \Delta y \Delta z \left(\sigma_{xx} \mid_x - \sigma_{xx} \mid_{x+\Delta x} \right) &+ \Delta x \Delta z \left(\tau_{yx} \mid_y - \tau_{yx} \mid_{y+\Delta y} \right) \\ &+ \Delta x \Delta y \left(\tau_{zx} \mid_z - \tau_{zx} \mid_{z+\Delta z} \right) \end{aligned} \tag{2.9}$$

The other forces acting on the system include pressure, P, and gravitational force per unit mass g. The resultant in the x-direction will be

$$\Delta y \Delta z \left(P \mid_x - P \mid_{x+\Delta x} \right) + \rho \, g \; \Delta x \Delta y \Delta z \tag{2.10}$$

The rate of x-momentum accumulation is the $\Delta x \Delta y \Delta z \frac{\partial \rho v_x}{\partial t}$. Summing all these terms and dividing by $\Delta x \Delta y \Delta z$ while taking the limit as these dimensions approach zero, gives the x-component of the equation of motion.

$$\begin{aligned}\frac{\partial}{\partial t}\rho v_x = &- \left(\frac{\partial}{\partial x}\rho v_x v_x + \frac{\partial}{\partial y}\rho v_y v_x + \frac{\partial}{\partial z}\rho v_z v_x\right) \\ &- \left(\frac{\partial}{\partial x}\sigma_{xx} + \frac{\partial}{\partial y}\tau_{yx} + \frac{\partial}{\partial z}\tau_{zx}\right) - \frac{\partial P}{\partial x} + \rho g_x\end{aligned} \tag{2.11}$$

Similarly, the y and z components are

$$\begin{aligned}\frac{\partial}{\partial t}\rho v_y = &- \left(\frac{\partial}{\partial x}\rho v_x v_y + \frac{\partial}{\partial y}\rho v_y v_y + \frac{\partial}{\partial z}\rho v_z v_y\right) \\ &- \left(\frac{\partial}{\partial x}\tau_{xy} + \frac{\partial}{\partial y}\sigma_{yy} + \frac{\partial}{\partial z}\tau_{zy}\right) - \frac{\partial P}{\partial y} + \rho g_y\end{aligned} \tag{2.12}$$

$$\begin{aligned}\frac{\partial}{\partial t}\rho v_z = &- \left(\frac{\partial}{\partial x}\rho v_x v_z + \frac{\partial}{\partial y}\rho v_y v_z + \frac{\partial}{\partial z}\rho v_z v_z\right) \\ &- \left(\frac{\partial}{\partial x}\tau_{xz} + \frac{\partial}{\partial y}\tau_{yz} + \frac{\partial}{\partial z}\sigma_{zz}\right) - \frac{\partial P}{\partial z} + \rho g_z\end{aligned} \tag{2.13}$$

The Navier-Stokes equations

The Navier-Stokes derivation published by Welty et al. (2000) is shown in this section. These equations are a simplified case of the momentum balance shown in section 2.6.2.

The nett flux of momentum in the x-direction can be simplified as follows

$$\begin{aligned}\frac{\partial}{\partial x}\rho v_x v_x + \frac{\partial}{\partial y}\rho v_y v_x + \frac{\partial}{\partial z}\rho v_z v_x &= v_x\left[\frac{\partial}{\partial x}\rho v_x + \frac{\partial}{\partial y}\rho v_y + \frac{\partial}{\partial z}\rho v_z\right] \\ &+ \rho\left[v_x\frac{\partial v_x}{\partial x} + v_y\frac{\partial v_x}{\partial y} + v_z\frac{\partial v_x}{\partial z}\right]\end{aligned} \tag{2.14}$$

Simplifying the above equation (2.14) with the continuity equation in section 4.3 equation (2.6) yields

$$\frac{\partial}{\partial x}\rho v_x v_x + \frac{\partial}{\partial y}\rho v_y v_x + \frac{\partial}{\partial z}\rho v_z v_x = -v_x\frac{\partial \rho}{\partial t} + \rho\left[v_x\frac{\partial v_x}{\partial x} + v_y\frac{\partial v_x}{\partial y} + v_z\frac{\partial v_x}{\partial z}\right] \tag{2.15}$$

The accumulation term simplifies to

$$\frac{\partial}{\partial t}\rho v_x = \rho\frac{\partial v_x}{\partial t} + v_x\frac{\partial \rho}{\partial t} \tag{2.16}$$

The x component of the momentum balance upon substitution of the simplifications done in equations (2.16) and (2.14) now becomes

$$\rho\left[\frac{\partial v_x}{\partial t}+v_x\frac{\partial v_x}{\partial x}+v_y\frac{\partial v_x}{\partial y}+v_z\frac{\partial v_x}{\partial z}\right]=\left[\frac{\partial}{\partial x}\sigma_{xx}+\frac{\partial}{\partial y}\tau_{yx}+\frac{\partial}{\partial z}\tau_{zx}\right]-\frac{\partial P}{\partial x}+\rho g_x \tag{2.17}$$

The Stokes viscosity relationship for a Newtonian fluid in laminar flow is

$$\tau_{xy}=\tau_{yx}=\mu\left(\frac{\partial v_x}{\partial y}+\frac{\partial v_y}{\partial x}\right) \tag{2.18}$$

$$\tau_{yz}=\tau_{zy}=\mu\left(\frac{\partial v_y}{\partial z}+\frac{\partial v_z}{\partial y}\right) \tag{2.19}$$

$$\tau_{zx}=\tau_{xz}=\mu\left(\frac{\partial v_z}{\partial x}+\frac{\partial v_x}{\partial z}\right) \tag{2.20}$$

$$\sigma_{xx}=-P-\mu\frac{2}{3}\left(\frac{\partial v_x}{\partial x}+\frac{\partial v_y}{\partial y}+\frac{\partial v_z}{\partial z}\right)+2\mu\frac{\partial v_x}{\partial x} \tag{2.21}$$

$$\sigma_{yy}=-P-\mu\frac{2}{3}\left(\frac{\partial v_x}{\partial x}+\frac{\partial v_y}{\partial y}+\frac{\partial v_z}{\partial z}\right)+2\mu\frac{\partial v_y}{\partial y} \tag{2.22}$$

$$\sigma_{zz}=-P-\mu\frac{2}{3}\left(\frac{\partial v_x}{\partial x}+\frac{\partial v_y}{\partial y}+\frac{\partial v_z}{\partial z}\right)+2\mu\frac{\partial v_z}{\partial z} \tag{2.23}$$

If the fluid is assumed to be incompressible, and equations (2.18) and (2.20) are substituted into equation (2.17), the x-component of the Navier-Stokes equation is

$$\rho\left[\frac{\partial v_x}{\partial t}+v_x\frac{\partial v_x}{\partial x}+v_y\frac{\partial v_x}{\partial y}+v_z\frac{\partial v_x}{\partial z}\right]=-\frac{\partial P}{\partial x}+\rho g_x+\mu\left[\frac{\partial v_x}{\partial x}+\frac{\partial v_x}{\partial y}+\frac{\partial v_x}{\partial z}\right] \tag{2.24}$$

Similarly, the y and z components are

$$\rho\left[\frac{\partial v_y}{\partial t}+v_x\frac{\partial v_y}{\partial x}+v_y\frac{\partial v_y}{\partial y}+v_z\frac{\partial v_y}{\partial z}\right]=-\frac{\partial P}{\partial y}+\rho g_y+\mu\left[\frac{\partial v_y}{\partial x}+\frac{\partial v_y}{\partial y}+\frac{\partial v_y}{\partial z}\right] \tag{2.25}$$

$$\rho\left[\frac{\partial v_z}{\partial t}+v_x\frac{\partial v_z}{\partial x}+v_y\frac{\partial v_z}{\partial y}+v_z\frac{\partial v_z}{\partial z}\right]=-\frac{\partial P}{\partial z}+\rho g_z+\mu\left[\frac{\partial v_z}{\partial x}+\frac{\partial v_z}{\partial y}+\frac{\partial v_z}{\partial z}\right] \tag{2.26}$$

To summarise, the Navier-Stokes equations assume that the fluid is:

- Incompressible
- Newtonian
- Operating under laminar flow conditions

The Reynolds equation

Reynolds (1886) addressed the laws of lubrication for the first time. The author states that when there is a continuous oil film of sufficient thickness to eradicate unknown boundary actions, the flow of this oil can be described by the equations of hydrodynamics.

The Reynolds equation of hydrodynamic lubrication, is a simplified case of the Navier-Stokes equations derived in equations (2.24), (2.25) and (2.26). Reynolds made two assumptions which hold true for lubrication where the spaces between the solid surfaces are small compared to the ratio of the viscosity to the velocity. He disregards the inertia and the weight terms in the Navier-Stokes equations. This is only done when the inertia and weight terms are altogether small compared to the stresses arising from viscosity.

The Reynolds equations are then given by:

$$\frac{\partial P}{\partial x} = \mu \left[\frac{\partial v_x}{\partial x} + \frac{\partial v_x}{\partial y} + \frac{\partial v_x}{\partial z} \right] \tag{2.27}$$

$$\frac{\partial P}{\partial y} = \mu \left[\frac{\partial v_y}{\partial x} + \frac{\partial v_y}{\partial y} + \frac{\partial v_y}{\partial z} \right] \tag{2.28}$$

$$\frac{\partial P}{\partial z} = \mu \left[\frac{\partial v_z}{\partial x} + \frac{\partial v_z}{\partial y} + \frac{\partial v_z}{\partial z} \right] \tag{2.29}$$

To summarise, the Reynolds equations assume that the fluid is:

- Incompressible
- Newtonian
- Operating under laminar flow conditions
- Free from inertia effects
- Free from weight effects

2.7 Summary of literature and motivation of research objectives

From the previous sections it is clear that synovial joints are very complex systems to model, with a whole range of variables affecting their operation. When modelling synovial joints, one would always try to model a system that is comparable to that of an actual joint. Due to the complex nature of joints this is not always possible. An investigator would therefore try to accurately model joints with simplifying assumptions and make the necessary conclusions based on this.

Previous investigators used two-dimensional models to represent a simplified version of a the hip joint. Some geometries that were used include ball-on-plane models (Jin et al., 1997) (Pascovici & Cicone, 2003) and a long cylinder moving on a plane. (Bujurke & Jayaraman, 1982) (Bujurke et al., 1991) (Medley, 1994) Another geometry that is more representative of an actual hip joint is the ball-in-cup geometry. (Jin et al., 1999) (Jalali-Vahid et al., 2000) (Jalali-Vahid et al., 2001) (Pascovici & Cicone, 2003) One way to simplify the joint system is to make certain assumptions about the movements of the joint. Some authors either incorporate a constant rotational movement in one direction (Dowson et al., 1991) (Jalali-Vahid et al., 2000), or an up and down movement of the ball on the cup into the system. (Bujurke & Jayaraman, 1982) Some authors assume that a constant load is applied to the system, while joints operate over a range of dynamic load cycles. (Jalali-Vahid et al., 2000)

Most authors strive to accurately describe the lubrication regimes found in hip joints. From previous sections it is known that lubrication in joints are not limited to a single lubrication regime. Authors propose mechanisms that are likely to predominate in synovial joints. Most of the previous work assume that the lubricant is Newtonian. In this study where the focus lies in the effect of the lubricant properties on the tribological performance of the joint, the lubrication regime will be hydrodynamic with both Newtonian and non-Newtonian fluids as lubricant. Although artificial joints operate in either boundary or mixed lubrication, this regime is an adequate starting point for investigating fluid properties, as none of the properties of the articulating surfaces play an important role in the lubrication. It is also important to emphasise the fact that it is necessary to obtain a thorough understanding of the governing principles of joint simulation. Departing from a hydrodynamic point of view could therefore prove to be valuable in discovering limitations imposed on this model. Lubricating fluids will be modelled with the classical equations of hydrodynamics. The limitations of the Reynolds equation become overwhelming and is entirely unsuitable for modelling non-Newtonian fluids.

In most of the published work that was reviewed in this section, authors compared their findings with that of previously published simulation results. In order to develop a full understanding of the results that are generated from this investigation, the model results will be compared to experimental results. Hopefully such validations would give meaningful insight into the reliability and relevance of this work.

CHAPTER 3

Fluid rheology

This chapter will discuss an important physical property of the liquid lubricant that will be included in the mathematical model of the hip joint, namely Newtonian and non-Newtonian behaviour. Two different non-Newtonian approximations are discussed in this section with a discussion on the transformation of vectors and tensors between coordinate systems.

3.1 Newton's law of viscosity and Newtonian fluids

This section reviews Newton's law of viscosity as presented by Bird et al. (1960: 3–5) Consider the fluid flowing between two large parallel plates with area A and separated by a distance Y shown in figure 3.1. When the bottom plate is is pulled by a constant force F at a velocity $\mathbf{v}$, and the flow is laminar and at steady state, equation (3.1) holds true.

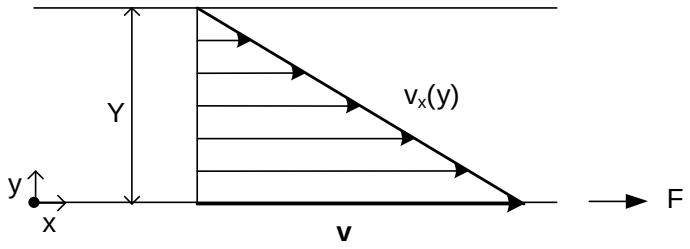

Figure 3.1: Velocity profile for a fluid flowing between two plates.

$$\frac{F}{A} = \mu \frac{\mathbf{v}}{Y} \tag{3.1}$$

In this equation, the proportional constant μ is the viscosity of the fluid. The viscosity is defined as the resistance of a fluid to flow or deform. (Welty et al., 2000: 89)

To generalise this equation, using the coordinates shown in figure 3.1, Newton's law of viscosity is shown in equation (3.2).

$$\tau_{yx} = -\mu \frac{\mathrm{d}v_x}{\mathrm{d}y} \tag{3.2}$$

Here, τ_{yx} is the shear stress exerted in the x-direction on a fluid surface of constant y. Fluids conforming to this relationship are named Newtonian fluids.

For a Newtonian fluid, the components of the shear stress tensor in spherical coordinates are given in the equations below. (Bird et al., 1960: 90)

$$\tau_{rr} = -\mu \left[2 \frac{\partial v_r}{\partial r} - \frac{2}{3} (\nabla \cdot v) \right] \tag{3.3}$$

$$\tau_{\theta\theta} = -\mu \left[2 \left(\frac{1}{r} \frac{\partial v_\theta}{\partial \theta} + \frac{v_r}{r} \right) - \frac{2}{3} (\nabla \cdot v) \right] \tag{3.4}$$

$$\tau_{\phi\phi} = -\mu \left[2 \left(\frac{1}{r \sin\theta} \frac{\partial v_\phi}{\partial \phi} + \frac{v_r}{r} + \frac{v_\theta \cot\theta}{r} \right) - \frac{2}{3} (\nabla \cdot v) \right] \tag{3.5}$$

$$\tau_{r\theta} = \tau_{\theta r} = -\mu \left[r \frac{\partial}{\partial r} \left(\frac{v_\theta}{r} \right) + \frac{1}{r} \frac{\partial v_r}{\partial \theta} \right] \tag{3.6}$$

$$\tau_{\theta\phi} = \tau_{\phi\theta} = -\mu \left[\frac{\sin\theta}{r} \frac{\partial}{\partial \theta} \left(\frac{v_\phi}{\sin\theta} \right) + \frac{1}{r \sin\theta} \frac{\partial v_\theta}{\partial \phi} \right] \tag{3.7}$$

$$\tau_{\phi r} = \tau_{r\phi} = -\mu \left[\frac{1}{r \sin\theta} \frac{\partial v_r}{\partial \phi} + r \frac{\partial}{\partial r} \left(\frac{v_\phi}{r} \right) \right] \tag{3.8}$$

$$(\nabla \cdot v) = \frac{1}{r^2} \frac{\partial}{\partial r} \left(r^2 v_r \right) + \frac{1}{r \sin\theta} \frac{\partial}{\partial \theta} \left(v_\theta \sin\theta \right) + \frac{1}{r \sin\theta} \frac{\partial v_\phi}{\partial \phi} \tag{3.9}$$

3.2 Non-Newtonian fluids

This section describes Non-Newtonian fluids as presented by Bird et al. (1960: 10–15). In the previous section (section 3.1), Newtonian fluids would behave according to Newton's law where the shear stress exerted on the fluid would be linearly proportional to the $-(\mathrm{d}v_x/\mathrm{d}y)$ or the shear rate. There is a range of fluids not adhering to this phenomenon. They are known as Non-Newtonian fluids. In general, the rheological behaviour of these fluids can be expressed by equation (3.10).

$$\tau_{yx} = -\eta \frac{\mathrm{d}v_x}{\mathrm{d}y} \tag{3.10}$$

Here, the non-Newtonian viscosity η is either a function of the shear rate or τ_{yx}. If the viscosity is known at a given shear rate and shear stress, the viscosity is called the

apparent viscosity or μ_{app}. At this given shear rate and τ_{yx} the fluid is assumed to be Newtonian with $\mu = \mu_{app}$.

The relationship between η and shear rate or τ_{yx} can be expressed by means of empirical models published in literature. For the purpose of this study, the synovial fluid is approximated by two different models presented by Lai et al. (1978). These models are discussed in the following sections.

3.2.1 Generalised Maxwell-type fluid

This fluid rheological model exhibits viscoelastic behaviour. If the assumption of simple shearing flow holds true, the approximations are given in equations (3.11) to (3.15).

$$\tau_{xx} = \frac{\eta_0 \gamma^2 \lambda (1-b)}{1 + \gamma^2 \lambda^2 (1-b^2)} \tag{3.11}$$

$$\tau_{yy} = -\frac{\eta_0 \gamma^2 \lambda (1+b)}{1 + \gamma^2 \lambda^2 (1-b^2)} \tag{3.12}$$

$$\tau_{xy} = \frac{\eta_0 \gamma}{1 + \gamma^2 \lambda^2 (1-b^2)} \tag{3.13}$$

$$\tau_{xz} = \tau_{yz} = \tau_{zz} = 0 \tag{3.14}$$

$$\eta_{app} = \frac{\eta_0}{1 + \gamma^2 \lambda^2 (1-b^2)} \tag{3.15}$$

The complete derivation is given by Lai et al. (1978). The constants used to approximate synovial fluid are shown in table 3.1 below.

Table 3.1: Parameters used in the Maxwell equations

	η_0	λ	b
	N.s/m^2	s	-
Synovial fluid	0.0917	0.0191	-0.972

3.2.2 Oldroyd's viscoelastic fluid

This is a four parameter, viscoelastic fluid approximation. The relationships for the shear stresses are given in equation (3.16) to (3.19).

$$\tau_{xx} = \frac{2\eta_0 \gamma^2 (\lambda_1 - \lambda_2)}{1 + \mu_0 \lambda_1 \gamma^2} \tag{3.16}$$

$$\tau_{xy} = \frac{\gamma\eta_0\,(1+\mu_0\lambda_2\gamma^2)}{(1+\mu_0\lambda_1\gamma^2)} \tag{3.17}$$

$$\tau_{xz} = \tau_{yy} = \tau_{yz} = \tau_{zz} = 0 \tag{3.18}$$

$$\eta_{app} = \frac{\eta_0\,(1+\mu_0\lambda_2\gamma^2)}{(1+\mu_0\lambda_1\gamma^2)} \tag{3.19}$$

The complete derivation of these equations are presented by Lai et al. (1978). For the Oldroyd model, the parameters used to approximate different synovial fluids are summarised in table 3.2.

Table 3.2: Parameters used in the Oldroyd equation (3.16) to (3.19)

Synovial Fluid	η_0 N.s/m^2	λ_1 s	λ_2 s	μ_0 s
Osteoarthritic fluid	1.24	1.5×10^{-1}	0.93×10^{-2}	4.03
Rheumatoid arthritic fluid	0.15	0.2×10^{-1}	0.55×10^{-2}	7.92
Bovine fluid	0.175	3.5×10^{-1}	0.58×10^{-1}	0.52

3.3 Transposing vectors and tensors to different coordinates

The mathematical models described in the previous sections give the relationships between the shear stresses in Cartesian coordinates (τ_{xx}) and the shear rates ($\mathrm{d}v_x/\mathrm{d}y$). The hip joint model is in the spherical coordinate system. This section will discuss the transformation of vectors and tensors between different coordinate systems as it is presented by Bird et al. (1960: 737–736). The empirical models will then be transposed to the spherical coordinate system and used in the model. It should however be noted that Bird et al. (1960: 103) commented on the fact that a sound method for transposing vectors and tensors was presented, but that it could not be assured that the empirical constants calculated to approximate the viscous behaviour of the fluids, would be the same for other geometric systems.

3.3.1 Vectors

A vector is a three dimensional number such as velocity shown below.

$$v = \begin{pmatrix} v_x \\ v_y \\ v_z \end{pmatrix} \tag{3.20}$$

By recalling section 4.1, where the definition of the spherical system is given in terms of the cartesian system, the velocity vector can be transposed between coordinate systems with simple geometric relations. The transformation to spherical from cartesian is given in the following equations.

$$v_r = (\sin\theta\ \cos\phi)\, v_x + (\sin\theta\ \sin\phi)\, v_y + (\cos\theta)\, v_z \tag{3.21}$$

$$v_\theta = (\cos\theta\ \cos\phi)\, v_x + (\cos\theta\ \sin\phi)\, v_y + (-\sin\theta)\, v_z \tag{3.22}$$

$$v_\phi = (-\sin\phi)\, v_x + (\cos\phi)\, v_y + (0)\, v_z \tag{3.23}$$

To transpose a velocity vector from spherical to cartesian, the following equations are used.

$$v_x = (\sin\theta\ \cos\phi)\, v_r + (\cos\theta\ \cos\phi)\, v_\theta + (-\sin\phi)\, v_\phi \tag{3.24}$$

$$v_y = (\sin\theta\ \sin\phi)\, v_r + (\cos\theta\ \sin\phi)\, v_\theta + (\cos\phi)\, v_\phi \tag{3.25}$$

$$v_z = (\cos\theta)\, v_r + (-\sin\theta)\, v_\theta + (0)\, v_\phi \tag{3.26}$$

The direction cosine, $l_{i'i}$, is defined as the matrix of the angles between the two vectors in the different coordinate systems between which the transformations are performed. For the direction cosine, the following equations hold true.

$$v_{i'} = l_{i'i} \cdot v_i \tag{3.27}$$

Transposing the velocity vector from the cartesian to the spherical coordinates is shown in equation (3.28).

$$\begin{pmatrix} v_r \\ v_\theta \\ v_\phi \end{pmatrix} = \begin{pmatrix} \sin\theta\ \cos\phi & \sin\theta\ \sin\phi & \cos\theta \\ \cos\theta\ \cos\phi & \cos\theta\ \sin\phi & -\sin\theta \\ -\sin\phi & \cos\phi & 0 \end{pmatrix} \cdot \begin{pmatrix} v_x \\ v_y \\ v_z \end{pmatrix} \tag{3.28}$$

The same can be said for transposing back to the cartesian coordinates with the direction cosine $l_{ii'}$.

$$v_i = l_{ii'} \cdot v_{i'} \tag{3.29}$$

The transposition is shown in matrix algebra, equation (3.30), which corresponds to equation (3.24) to (3.26).

$$\begin{pmatrix} v_x \\ v_y \\ v_z \end{pmatrix} = \begin{pmatrix} \sin\theta\ \cos\phi & \cos\theta\ \cos\phi & -\sin\theta \\ \sin\theta\ \sin\phi & \cos\theta\ \sin\phi & \cos\phi \\ \cos\theta & -\sin\theta & 0 \end{pmatrix} \cdot \begin{pmatrix} v_r \\ v_\theta \\ v_\phi \end{pmatrix} \tag{3.30}$$

3.3.2 Tensors

A tensor is a higher order dimensional number such as shear stress shown below.

$$\tau = \begin{pmatrix} \tau_{xx} & \tau_{xy} & \tau_{xz} \\ \tau_{yx} & \tau_{yy} & \tau_{yz} \\ \tau_{zx} & \tau_{zy} & \tau_{zz} \end{pmatrix} \tag{3.31}$$

A tensor can be transposed from cartesian to spherical coordinates by using both direction cosines defined in equation (3.28) and (3.30). This is shown in equation (3.29) below.

$$\tau_{i'j'} = l_{i'i} \cdot \tau_{ij} \cdot l_{ii'} \tag{3.32}$$

To transform back to the original coordinates, the following matrix algebra is performed.

$$\tau_{ij} = l_{ii'} \cdot \tau_{i'j'} \cdot l_{i'i} \tag{3.33}$$

The rheological models described in this section can now be transposed to the spherical coordinate system.

CHAPTER 4

The hip joint model

This section describes the development of the hip joint model. It gives an overview of:

- The spherical coordinate system
- The simulated hip joint system
- The different hip joint movements
- The fluid velocities in the joint due to its movements

Also included is a brief discussion on the assumptions made during modelling, a degrees of freedom analysis and a numerical solution procedure of the hip model.

4.1 Spherical coordinate system

In many problems, such as the case of modelling a hip joint, it is easier to describe the geometry by using a curvilinear coordinate system like spherical coordinates than using rectangular coordinates. In the spherical coordinate system, let ϕ be the angle between a point and the positive x-axis and θ the angle between the point and the positive z-axis. r is the distance from the origin to the point, shown in figure 4.1.

The spherical coordinates relate to the Cartesian variables in the following equations:

$$x = r\sin\theta\cos\phi \tag{4.1}$$

$$y = r\sin\theta\sin\phi \tag{4.2}$$

$$z = r\cos\theta \tag{4.3}$$

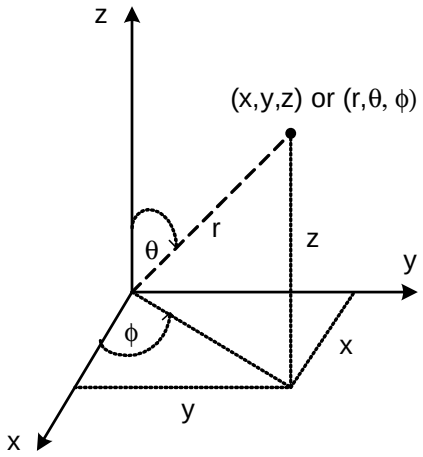

Figure 4.1: The spherical coordinate system as defined by Bird et al. (1960).

$$r = \sqrt{x^2 + y^2 + z^2} \tag{4.4}$$

$$\theta = \tan^{-1} \frac{\sqrt{x^2 + y^2}}{z} \tag{4.5}$$

$$\phi = \tan^{-1} \frac{y}{x} \tag{4.6}$$

4.2 The hip joint system

The hip joint system is shown in figure 4.2. It is a spherical ball-in-cup geometry, published by previous authors. (Mabuchi & Sasada, 1990) (Mabuchi et al., 2004).

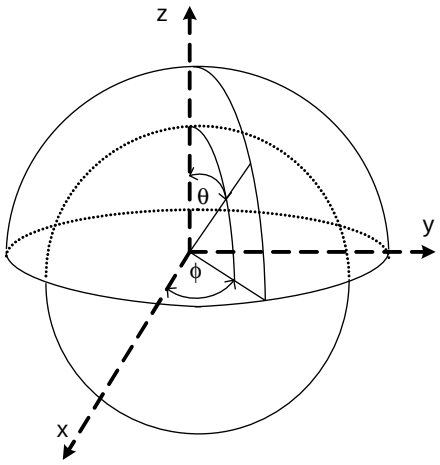

Figure 4.2: The hip joint system.

It is important to note that, for the purpose of this study, the system control volume is the fluid filling the void between the ball and the cup. The simulation models the fluid

in the hip joint during simulated joint actions. To fully describe the fluid system, the spherical coordinate angles, θ and ϕ range between:

- $0 \leq \phi \leq 2\pi$
- $0 \leq \theta \leq \frac{\pi}{2}$

4.3 Governing equations

To describe the fluid system defined in section 4.2 requires solving the general fluid equations of mass and momentum conservation. The general forms of these equations in the spherical coordinate system are given in subsequent sections below. A complete discussion on these equations in the rectangular coordinate system was presented in section 2.6. To transform these equations to spherical coordinates, the relationships given in section 4.1 are used.

The conservation of mass equations

From the mass balance derived in section 4.3, equation (2.6), used with the relationships in equations (4.1) to (4.3), the mass balance over a stationary volume element in spherical coordinates is given below.

$$\frac{\partial \rho}{\partial t} + \frac{1}{r^2}\frac{\partial}{\partial r}\left(\rho\, r^2 v_r\right) + \frac{1}{r\sin\theta}\frac{\partial}{\partial \theta}\left(\rho\, v_\theta \sin\theta\right) + \frac{1}{r\sin\theta}\frac{\partial}{\partial \phi}\left(\rho\, v_\phi\right) = 0 \tag{4.7}$$

The conservation of momentum equations

These equations are derived by writing the momentum balance over a stationary volume element. The r, θ and ϕ components of the motion equation are given in equations (4.8), (4.9) and (4.10) respectively. Here τ_{xy} refers to the shear stress exerted in the x-direction on a fluid surface of constant y.

In the r-direction:

$$\begin{aligned}\rho\Bigg(\frac{\partial v_r}{\partial t} + \; & v_r\frac{\partial v_r}{\partial r} + \frac{v_\theta}{r}\frac{\partial v_r}{\partial \theta} + \frac{v_\phi}{r\sin\theta}\frac{\partial v_r}{\partial \phi} - \frac{v_\theta^2 + v_\phi^2}{r}\Bigg) \\ = \; & -\frac{1}{r}\frac{\partial P}{\partial r} - \left(\frac{1}{r^2}\frac{\partial}{\partial r}\left(r^2\tau_{rr}\right) + \frac{1}{r\sin\theta}\frac{\partial}{\partial \theta}\left(\tau_{r\theta}\sin\theta\right)\right. \\ + \; & \left.\frac{1}{r\sin\theta}\frac{\partial \tau_{r\phi}}{\partial \phi} - \frac{\tau_{\theta\theta} + \tau_{\phi\phi}}{r}\right) + \rho g_r\end{aligned} \tag{4.8}$$

In the θ-direction:

$$\begin{aligned}\rho\Bigg(\frac{\partial v_\theta}{\partial t} + v_r\frac{\partial v_\theta}{\partial r} + \frac{v_\theta}{r}\frac{\partial v_\theta}{\partial \theta} + \frac{v_\phi}{r\sin\theta}\frac{\partial v_\theta}{\partial \phi} + \frac{v_r v_\theta}{r} - \frac{v_\phi^2 \cot\theta}{r}\Bigg) \\ = -\frac{1}{r}\frac{\partial P}{\partial \theta} - \Bigg(\frac{1}{r^2}\frac{\partial}{\partial r}\left(r^2\tau_{r\theta}\right) + \frac{1}{r\sin\theta}\frac{\partial}{\partial \theta}\left(\tau_{\theta\theta}\sin\theta\right) \\ + \frac{1}{r\sin\theta}\frac{\partial \tau_{\theta\phi}}{\partial \phi} + \frac{\tau_{r\theta}}{r} - \frac{\cot\theta}{r}\tau_{\phi\phi}\Bigg) + \rho g_\theta \end{aligned} \tag{4.9}$$

In the ϕ-direction:

$$\begin{aligned}\rho\Bigg(\frac{\partial v_\phi}{\partial t} + v_r\frac{\partial v_\phi}{\partial r} + \frac{v_\theta}{r}\frac{\partial v_\phi}{\partial \theta} + \frac{v_\phi}{r\sin\theta}\frac{\partial v_\phi}{\partial \phi} + \frac{v_\phi v_r}{r} + \frac{v_\theta v_\phi}{r}\cot\theta\Bigg) \\ = -\frac{1}{r\sin\theta}\frac{\partial P}{\partial \phi} - \Bigg(\frac{1}{r^2}\frac{\partial}{\partial r}\left(r^2\tau_{r\phi}\right) + \frac{1}{r}\frac{\partial \tau_{\theta\phi}}{\partial \theta} \\ + \frac{1}{r\sin\theta}\frac{\partial \tau_{\phi\phi}}{\partial \phi} + \frac{\tau_{r\phi}}{r} + \frac{2\cot\theta}{r}\tau_{\theta\phi}\Bigg) + \rho g_\phi \end{aligned} \tag{4.10}$$

4.4 Hip joint movement

The hip joint has a range of complex motions in all three dimensions. Joint movement can be distinguished between flexion-extension and adduction-abduction. These movements are shown in figure 4.3. (Frankel & Nordin, 1980: 149–177)

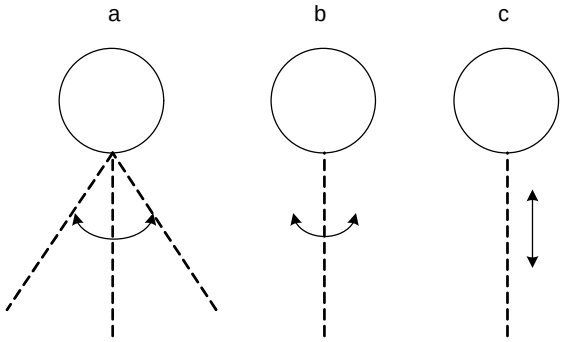

Figure 4.3: Hip joint movements: (a) flexion-extension, (b) adduction-abduction and (c) relative inward ball-into-cup.

Figure 4.3 (a) shows the pendulum motion in the flexion-extension plane, while figure 4.3 (b) shows rotational movement in the adduction-abduction plane. The normal hip joint has flexion of at least 120° and abduction of at least 20°. (Frankel & Nordin, 1980: 175) Figure 4.3 (c) shows the relative inward motion of the ball into the cup.

For the purpose of this study, two specific types of joint movement will be defined and simulated. It should also be mentioned that these two movements only occur in the flexion-extension plane, and no adduction-abduction movement is incorporated in the

model. This is due to the complex nature of the latter, and could be added in future studies. The two movements are defined as follows:

- The relative inward motion of the ball into the cup (Figure 4.3 (c))
- The pendulum ball motion (Figure 4.3 (a))

These motions are described in consecutive sections.

4.4.1 Relative inward ball-into-cup motion

During the loading cycle of the joint, a given load is imposed on the acetabular cup. This would typically be some fraction of the force due to that of the weight of the body that is being supported by the joint. A reaction force, equal magnitude but in the opposite direction, will be experienced by the femoral ball. The fluid in the joint will experience the same magnitude of force, dissipated over the entire articulating surface. There will be a relative motion between the ball and the cup when a load is applied to the joint. This is shown in figure 4.4.

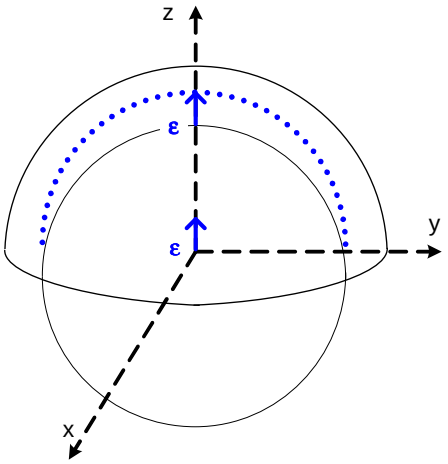

Figure 4.4: The epsilon defined movement of the hip joint system.

As the load increases, the ball will move inward in the positive z-direction, filling the space previously occupied by the fluid. The opposite will apply if the load is lowered again. The value, ε, is defined as the distance between the center of the ball and the center of the cup, in other words, the distance the ball moved inward into the control volume. It is important to note that this movement is of such a nature that the center of the ball moves in a straight line with respect to the center of the cup.

This specific movement leads to a moving boundary problem, where the ball is constantly changing the fluid control volume. It is important to describe the system boundaries accurately at any given time. A section through the joint at a specific time will look similar to figure 4.5. Here R_1 is the radius of the ball, and R_2 the radius of the cup.

The boundaries of the system are defined as follows:

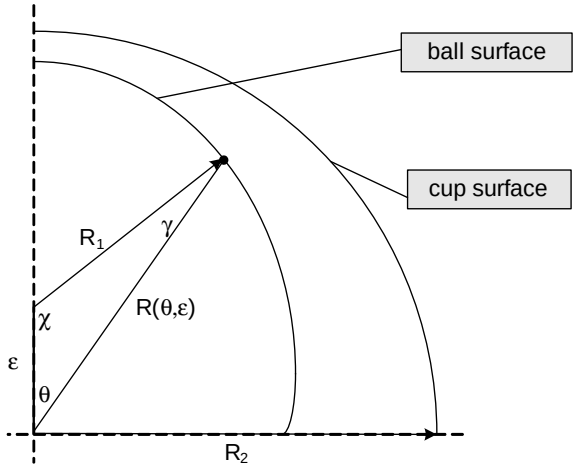

Figure 4.5: Sectional view of the joint as the ball moves inward.

- The cup is the outside stationary boundary, with the center of the cup being the same as the center of the system
- The ball is the inner moving boundary. It is clear from figure 4.5 that the center of the ball is not always the center of the system
- There is a fluid outflow boundary at the edge of the system. It is assumed that the fluid leaving system is contained in an infinite volume reservoir.

The moving boundary can be described in terms of the angle θ and the distance it moved, ε. From the geometry of the system we see that

$$\gamma = sin^{-1}\left(\frac{\varepsilon \sin\theta}{R_1}\right) \tag{4.11}$$

Then

$$\chi = 180 - (\gamma + \theta) \tag{4.12}$$

By implementing the sin rule again we see that

$$\frac{R(\theta,\varepsilon)}{\sin\chi} = \frac{R_1}{\sin\theta} \tag{4.13}$$

Substituting equations (4.11) and (4.12) into equation (4.13) gives an expression of the control volume boundary, $R(\theta,\varepsilon)$.

$$R(\theta,\varepsilon) = \frac{R_1}{\sin\theta}\sin\left[\pi - \sin^{-1}\left(\frac{\varepsilon\sin\theta}{R_1}\right) - \theta\right] \tag{4.14}$$

Fluid flow due to the epsilon movement

Consider a stationary volume element of size $\Delta r\ \Delta r\theta\ \Delta\phi$ shown in figure 4.6 .

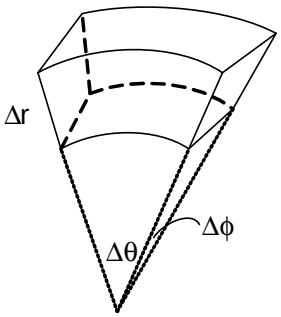

Figure 4.6: A single volume element in spherical coordinates.

At any θ, the distance between the two boundaries, Δr, is simply $R_2 - R(\theta, \varepsilon)$. Integrated over θ gives a fluid area, while integrating further over ϕ will give a fluid volume (equation (4.15)).

$$V = \int_{\phi_1}^{\phi_2} \int_{\theta_1}^{\theta_2} R_2 - R(\theta, \varepsilon) \; \mathrm{d}\theta \, \mathrm{d}\phi \tag{4.15}$$

Flow will occur due to a change in volume of a section, in the θ direction only. The average velocity flowing through the element through the area $\Delta r \; \Delta\phi$ is calculated in equation (4.16).

$$\overline{v}_\theta = \frac{\Delta V}{\Delta r \, \Delta\phi \, \Delta t} \tag{4.16}$$

4.4.2 Pendulum ball movement

In a walking cycle, the hip joint performs a pendulum-like motion, rotating at a certain angular velocity. It is important to clearly define the axis about which this rotation takes place. By following the same analogy as previously, the ball will be oscillating in the yz-plane around the x-axis that goes through the origin of the ball. The ball is moving at a varying angular velocity that is known at a given time. This movement is shown in figure 4.7.

Fluid flow due to the pendulum movement

The magnitude of the linear velocity of the ball surface due to its rotation about the x-axis is calculated from

$$v = \delta \, \omega \tag{4.17}$$

The distance from the ball surface to the axis of rotation is expressed in terms of the y and z components given in equation (4.2) and (4.3).

$$\delta = \sqrt{y^2 + z^2} \tag{4.18}$$

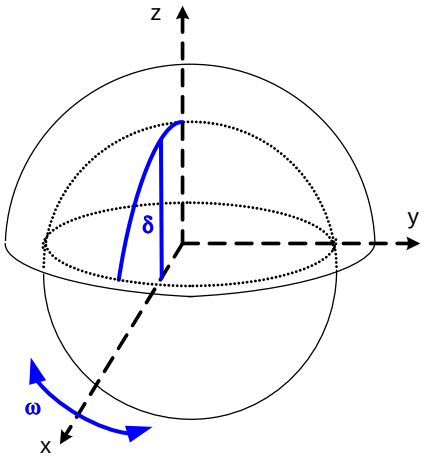

Figure 4.7: The pendulum movement of the ball around the x-axis.

To express the velocity in terms of its directional vectors, a top view of the ball is shown in figure 4.8. Here the z-axis is perpendicular to the page.

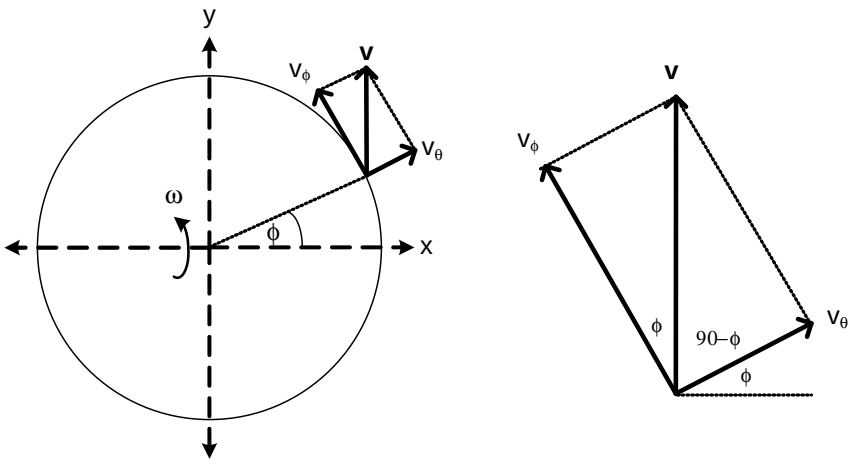

Figure 4.8: A top view of the ball during the pendulum movement.

It is clear that the maximum linear velocity will be near the center of the ball, because the maximum distance from the ball surface to the x-axis is in this region. The linear velocity will decrease toward the edges of the ball due to a decreasing distance to the rotating axis. The velocity vectors will all lie in the same direction as the vector v shown in figure 4.8. The fluid against the ball surface will be moving with the same velocity as the ball at that point. This only holds true if certain simplifying assumptions are made, specifically the no-slip boundary condition. This assumption and others are discussed in detail in the next section. From figure 4.8, the velocity of the liquid at the ball surface can be expressed as

$$v_\theta = v \sin\phi \tag{4.19}$$

$$v_\phi = v\cos\phi \tag{4.20}$$

4.5 Model assumptions

The hip joint model proposed in this section will be solved in the *Matlab* environment. In order to solve the model, some simplifying assumptions have to be addressed:

(I) It was assumed in section 4.4.2, that the no slip condition holds true when calculating the fluid velocity from the angular velocity of the articulating surfaces. The fluid at the ball surface will flow at the same velocity as that of the ball surface.

(II) To simplify the mathematical complexity of the simulation, it is also assumed that there are no wall effects present in the fluid and that no boundary layer exists in the fluid velocity profile.

(III) The fluid velocity profiles are assumed to be linear and completely superimposable. All these assumptions are shown in figure 4.9.

(IV) Finally, the fluid pressure at the edge of the cup was assumed to be atmospheric. This boundary condition is commonly used by most authors (Jalali-Vahid et al., 2001) (Jalali-Vahid et al., 2000) (Mabuchi & Sasada, 1990) (Mabuchi et al., 2004).

Figure 4.9 (a) shows the actual velocity profiles generated between the articulating surfaces due to the different joint movements. In figure 4.9 (b), the velocity profiles are assumed to be linear and average (assumptions (I) and (II)). The combined profile refers to the super imposition of the different velocity profiles into one single profile (assumption (III)).

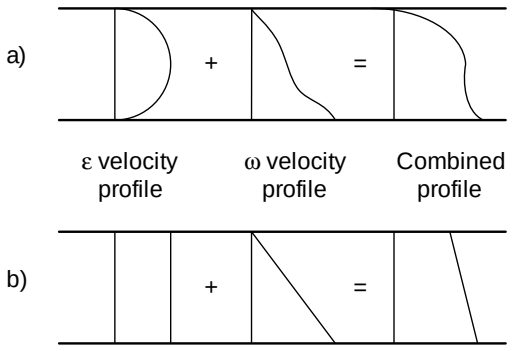

Figure 4.9: The actual fluid velocity profiles (a) and the simplified velocity profiles (b) used in the model after assumptions were made.

4.6 Degrees of freedom analysis

When setting up a mathematical model of any system, it is very important to do a degrees of freedom analysis. This is done to ensure that the problem under investigation is solvable ie. that a solution exists. This analysis becomes very useful when modelling more complex systems, where one easily gets overwhelmed by the amount of information available to solve the equations of the system.

In a degrees of freedom analysis, the number of variables of the system are compared to the number of equations of the system. Three typical scenarios are found: (Stephanopoulos, 1984: 86–89)

- **Exactly specified system:** When the number of variables is equal to the number of equations. There exists a unique solution.
- **Overspecified system:** When there are more equations that variables. No solution for the problem exists.
- **Underspecified system:** When there are more variables than equations. Multiple solutions exist for the model.

With the dynamic hip joint model, the system is treated as a quasi steady state problem. The following argument holds true for every time interval. Consider a solution with M θ increments and N ϕ increments. A complete velocity profile for the entire system is derived from basic geometrical characteristics of the joint. This means that there are MxN values for both v_θ and v_ϕ. Then there are MxN unknown values for the pressure, P. The motion equations can be used to solve the system. The degrees of freedom analysis is shown below.

Number of equations	Origin
$(M-1)\,N$	Equation 4.9 of motion $\frac{\partial P}{\partial \theta}$
M	Boundary conditions $P = 0$
Total $= MN$	

Number of unknowns	Origin
MN	Pressure P
Total $= MN$	

By only utilising the motion equation in the θ direction, together with the boundary conditions, gives a mathematical system with the same number of unknowns as equations. A unique solution to the problem exists. The mathematical problem exists out

of MxN values of v_θ and v_ϕ calculated from firsts principles. Then $(M-1)$ xN partial differential equations for the pressure drop in spherical coordinates is solved together with M boundary conditions for pressure to give MxN pressure values for the system at a given time.

4.7 Numerical solution procedure

Figure 4.10 is a schematic representation of the numerical solution procedure of the model.

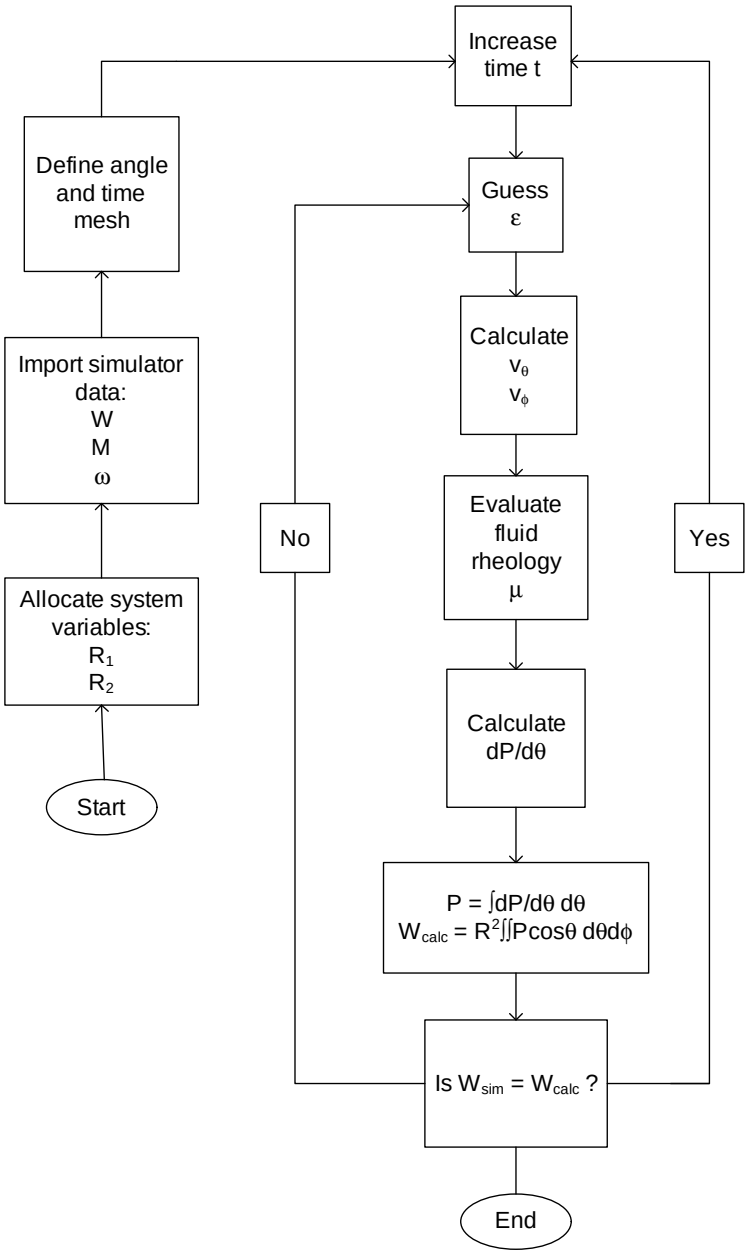

Figure 4.10: Numerical solution procedure.

First, all the system variables are initialised with the values used in the simulator experiment shown in table 5.2. These include the specimen diameters. Then the recorded

simulator variables are imported into the *Matlab* program. These dynamic variables are the weight function, the angular velocity of cyclic movement and the measured torque. The calculation mesh for the time and angles are then initialised. The time interval is then increased to calculate the solution at the first time interval.

An initial guess for ε is used to calculate the fluid velocity profile due to the change in the epsilon value with equations (4.14) to (4.16). The angular velocity of the system is then used in conjunction with equations (4.17) to (4.20) to calculate the fluid velocity due to the pendulum movement. By applying the assumption discussed in section 4.5 and adding the velocity profiles, the entire velocity profile of the system is now known. From the equations of hydrodynamics, the pressure drop in the system is induced by resistance against fluid flow through the system.

The properties of the lubricant are now evaluated. Then the forces in the liquid due to flow is calculated by the appropriate equations depending fluid properties and rheology. All these are then substituted into the motion equation (4.9) to calculate the pressure drop in the theta direction. From there the pressure can be calculated by starting with the atmospheric boundary pressure discussed in section 4.5 and adding the accumulating pressure drop calculated from equation (4.9). The total weight supported by this hydrodynamic pressure distribution is then evaluated with the integral in equation (4.21).

$$W = R_1^2 \int_0^{2\pi} \int_0^{\frac{\pi}{2}} P \cos\theta \, \mathrm{d}\theta \, \mathrm{d}\phi \tag{4.21}$$

The weight supported by the system is then compared to the weight acting on the simulator at that time. If it is not the same, a new value for ε is chosen. This process is repeated until the epsilon value converges and the system is supporting the correct weight.

When the weight is iterated, the next time step is calculated. This procedure continues until an entire weight cycle is completed.

Shear stresses are induced by fluid flow in the system. The shear stress generates a torque around the center of the femoral ball. It is calculated with equation (4.22).

$$M = R_1^2 \int_0^{2\pi} \int_0^{\frac{\pi}{2}} \tau_{\theta\phi} \, \mathrm{d}\theta \, \mathrm{d}\phi \tag{4.22}$$

4.8 Incorporating empirical relationships into the hip model

Section 3.2 discussed two different non-Newtonian fluid models. To use these approximations in the hip model, the empirical models have to be transposed to the spherical coordinate system. Figure 4.11 shows the numerical procedure followed to calculate the

rheological variables in the hip joint model. This sectional procedure replaces the step called "evaluate fluid rheology" in the complete numerical scheme showed in section 4.7, figure 4.10, when the model is used with a non-Newtonian lubricant.

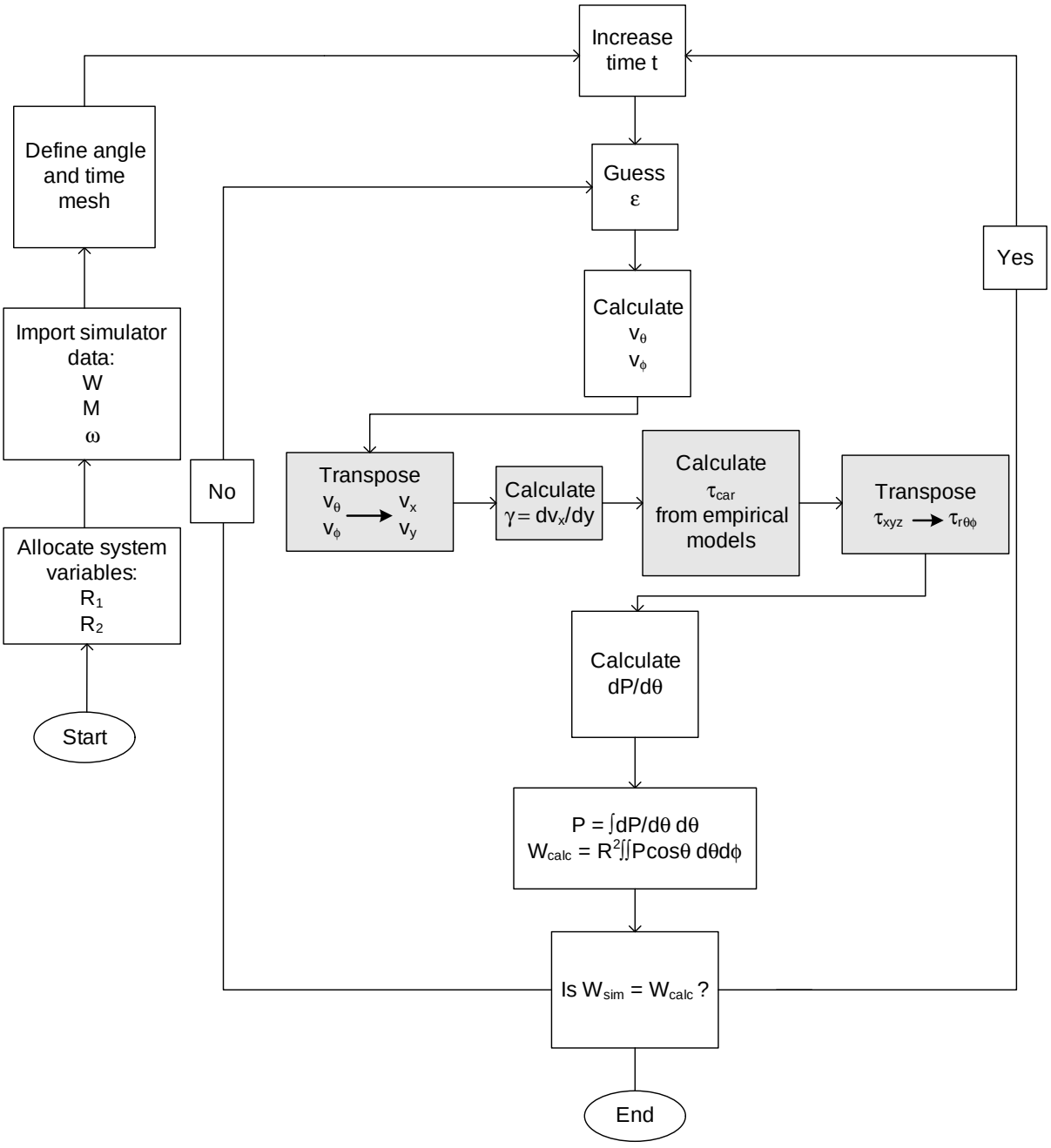

Figure 4.11: Numerical procedure to include non-Newtonian behaviour in the hip model.

CHAPTER 5

Experimental

This section covers the experimental work done to generate results with the hip joint simulator to compare the results obtained from the mathematical model against. It describes the apparatus and the experimental methods used and provides a brief outline of the experimental planning and methodology followed.

5.1 Apparatus and methods

A custom-built, five station hip joint simulator was used for the experimental work. The simulator load is applied mechanically with a swing-over-arm which provides the necessary movement. Load is applied by calibrated springs. Load cycles are similar to that of Bergmann et al. (1993). The simulator is described in a previous publication by Burger et al. (2002) Only one station of the simulator was used for experiments. The hip joint simulator is shown in figure 5.1. A load cycle similar to the Bergman cycle is imposed on the joints. Movements performed by the simulator were restricted to 20° in the flexion-extension plane (pendulum movement), excluding any adduction-abduction planar movement (rotational movement). Refer to chapter 4 section 4.4 for discussion on the joint movements.

The station was fitted with a 28mm zirconia femoral ball. Cross-linked Ultra high molecular weight polyethylene UHMWPE acetabular cups were manufactured out of Chirulen medical grade material, with a radial clearance of 250 μm. The cup was properly run in with the zirconium ball prior to testing to ensure smooth articulating surfaces. The surface roughness of the cup was therefor taken to be the same as that of the zirconium ball, $R_a = 0.1\mu$ m. (Willmann et al., 1996)

Two continuous measurements were taken during each run. Strain gauges were positioned on the femoral stem, which recorded the tensile and compressive forces exerted on

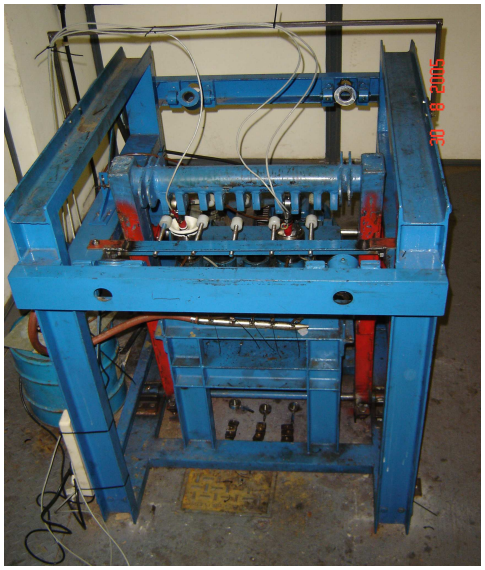

Figure 5.1: The custom-build hip joint simulator used in the investigation.

the ball and cup and the torque experienced by the ball surface. The measuring method corresponds to that previously published by Unsworth et al. (1995). To ensure accurate experimental measurements, the gauges must be positioned with great care and precision. A diagrammatic representation of the stem and the gauges is given in figure 5.2.

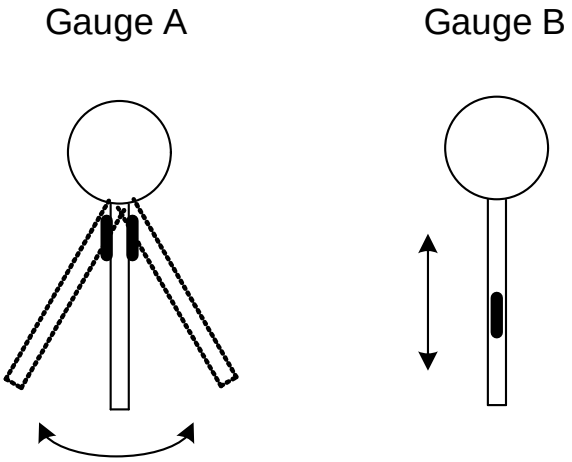

Figure 5.2: The positioning of the strain gauges on the femoral stem.

The gauges marked A in this figure measured the torque. They are positioned as close to the femoral ball as possible on opposing sides. This is to pick up the torque generated by the shear force between the ball and the liquid or the ball and the cup and minimise the possibility of picking up any other moments generated by the bearings of the simulator. The torque gauges are placed on the sides of the stem, in the direction of the stem movement. Gauges marked B in figure 5.2 measure the tensile and compressive forces in the stem. The are placed on both sides, away from the torque gauges and not in the direction of movement. This is to ensure that they do not pick up signals from the

bending of the stem. Both types of gauges were calibrated very accurately for the range in which they measure.

The experimental runtime used was only about ten load cycles. This would provide enough data to use when comparing the results with those generated by the model.

5.2 Lubricants

Two Newtonian lubricants were used in the investigation, namely water and SAE 90 gear oil. The choice of lubricants can be ascribed to the viscosity of the samples. One lubricant had to have almost no load bearing capacity. Water was a good choice, due to the fact that it is readily used as lubricant in hip simulators and other biomaterial studies. (Dowson, 1995a) (Zhou et al., 1997) (Wang et al., 1998) Results of the "poor" lubricant should then be compared to that of a good lubricant. The good load bearing lubricant that was used was Castrol Manual EP 90 oil. It was chosen primarily for its good lubricating ability and high viscosity.

All the runs were done at a constant temperature of 20℃. Temperature was controlled by circulating cooling water. Table 5.1 shows the physical properties of the two lubricants at the test temperature.

Table 5.1: Lubricant physical properties at 20℃

Lubricant	Viscosity Pa.s	Density kg/m^3
Water	0.001	1000
Oil	1.5	880

5.3 Experimental planning

Experimental variables had to be carefully chosen in order to operate the simulator as close to fully hydrodynamically lubricated conditions. By looking at the Stribeck curve in figure 2.5, it is clear that at higher viscosities (μ), higher relative speeds (v) and lower contact pressures (P), the lubrication tends to be hydrodynamic. This was therefore the main objective when selecting experimental parameters for this investigation. The rotational speed of the simulator is fixed from its design and geometry, so this variables was not considered. To obtain as low as possible contact pressures, the spring in the simulator was replaced with a low resistance spring, resulting in a maximum load of 50 kg. The decision to use a proper ran in ball and cup set can be ascribed to the fact that smooth articulating surfaces with small asperities relative to the radial clearance

could ensure good hydrodynamic lubrication, minimising the possibility for solid to solid contact, which in turn would tend to other lubrication regimes. The gear oil used as lubricant, has a high viscosity. This was the main reason for choosing this lubricant. The operating temperature used in the experimental setup, were chosen to be as low as could possible be maintained, to ensure that the highest viscosity of the lubricant could be utilised. Table 5.2 shows a summary of all the important experimental variables.

Table 5.2: Experimental variables summary

Variable	Value
Ball diameter	28 mm
Radial clearance	250 μm
Surface roughness	0.1 μm
Maximum load	50 kg
Maximum angular velocity	3 rad/s
Temperature	20 ℃

CHAPTER 6

Simulation results and discussion

This section discusses the results generated from the model. It investigates the numerical sensitivity of the model and shows the data gathered from the joint simulator. The results obtained from the Newtonian model are discussed, with special attention to the effect of different model parameters and fluid properties. The effect of non-Newtonian behaviour is discussed and the model results are compared to the simulator data.

6.1 Mesh optimisation

An important part of any numerical optimisation problem, is to investigate the sensitivity of the numerical solution and to ensure that its accuracy is independent of the numerical mesh used. In the work published by Jalali-Vahid et al. (2000), the author shows the effect of mesh size and density on the predicted central film thickness. They found that this variable was very sensitive to the numerical mesh, and determined a minimum mesh size from the results.

The incremental variables applicable in this investigations were that of time (Δt), theta ($\Delta\theta$) and phi ($\Delta\phi$). There are only two independent incremental variables, time and theta. Time is totally independent, while θ and ϕ are related by $0 \leq \phi \leq 2\pi$ and $0 \leq \theta \leq \frac{\pi}{2}$. There will therefore always be four times more ϕ nodes in the mesh than θ nodes.

Preliminary results obtained from the model showed that the hydrodynamic model could not support the weight that was imposed on it, whereby a monitoring parameter called the time to touch (t_{touch}) was defined. t_{touch} refers to the time it take for the hydrodynamic film to degenerate, causing the articulating surfaces to touch and shift to the elastohydrodynamic lubricating regime.

A mesh dependence sensitivity analysis was executed with the Newtonian hydrodynamic model. During this analysis, the number of time nodes and the number of angle nodes were increased, while monitoring the time it took for the two articulating surfaces to touch. The optimisation was started with 10 θ nodes (ie 40 ϕ nodes) and 38 time nodes. Results are shown in figure 6.1.

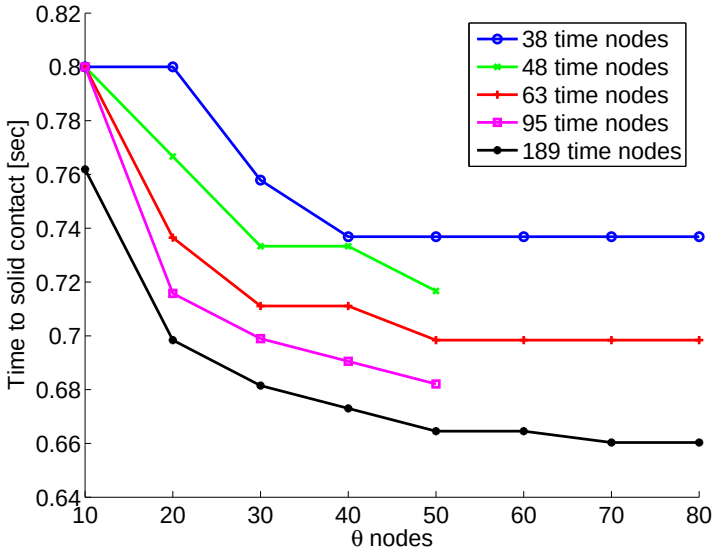

Figure 6.1: Investigating the influence of mesh density on the numerical accuracy of the model.

As the number of time and angle nodes increases, the time to solid contact decreases. Using 189 time nodes, the time to solid contact steadily decreases while increasing the angle nodes up to 70. Increasing the angle nodes over 70, shows no decrease in the contact time. The contact time converges to a value of 0.6603 seconds. The time nodes can not be refined further than 189, due to the limitation of the measuring element used with the experimental setup. Table 6.1 shows in conclusion the optimised incremental variables used in the investigation. It should be mentioned that due to reasons of complexity, a non-uniformal mesh was not investigated.

Table 6.1: Optimised mesh variables

	Time sec	θ rad	ϕ rad
Total	189	70	280
Δ	0.0042	0.0216	0.0113
min	0	0	0
max	0.8	$\pi/2$	2π

6.2 Simulator variables

There are several measured variables that are obtained from the experimental simulator. These measured variables are used to run the hip model and to validate the accuracy of the model. These measured variables include:

- The weight supported by the ball and cup
- The angular velocity of the ball surface relative to the cup surface
- The torque experienced by the articulating surfaces due to either the liquid lubricant or solid contacting surfaces.

Figure 6.2 shows the load cycle performed by the simulator and the angular velocity of the ball in motion.

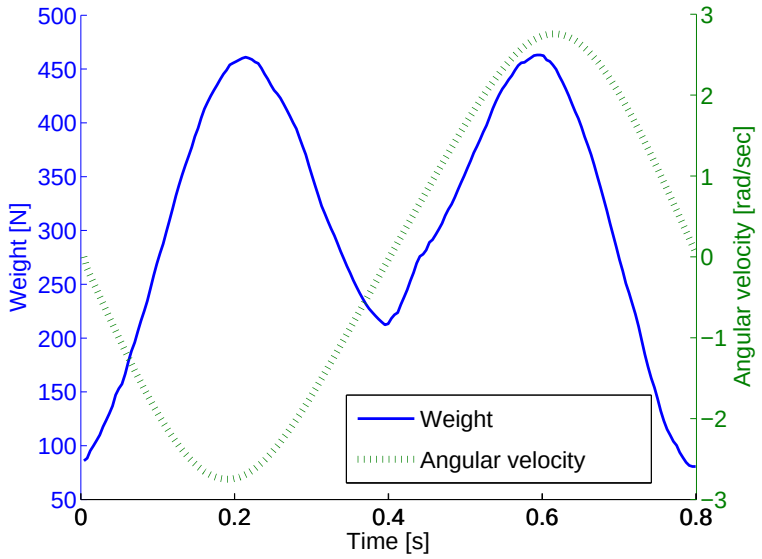

Figure 6.2: The load cycle and angular velocity of the hip joint simulator.

The cyclic load cycle shown in this figure, is a Bergmann type load cycle. The frequency of the cycle is 1.25 Hz with a maximum load of roughly 50 kg and a minimum of 8 kg. These values can vary slightly due to the assembly of the test specimens into the simulator. The angular velocity is set by the test apparatus with maxima occurring at the peaks of the loading cycle. The torque is discussed in section 6.5.

6.3 Newtonian model results

Figures 6.3 and 6.4 show two very important variables of the mathematical model, namely the converged weight and the inward movement of the ball or the ε movement.

Figure 6.3 is a plot of the weight cycle performed by the simulator and the weight that was calculated by the model by iterating the variable ε showed in figure 6.4 (a).

It is clearly seen that the model accurately generates the exact same load cycle of that of the simulator up to t = 0.66 s, where after the model cannot generate a sufficient hydrodynamic pressure distribution to support the needed weight. The cause of this can be seen in the change in ε graph (figure 6.4 (b)). The total void between the two articulating surfaces is represented by the dotted line. This value is calculated from the radial clearance minus the average surface roughness of the articulating surfaces. The ball moves into the control volume as depicted by the ε graph. A big change in ε in turn causes a big flow of fluid through the system which in turn generates a bigger pressure drop. As the change in ε decreases, the opposite holds true. A lower pressure distribution is found in the system, and hence a lower load can be supported. As the ball surface approaches the cup asperities, the change in ε gets smaller and smaller until the two surface eventually touch. At this point ε can no longer change, meaning no fluid can flow and no load can be supported. This is the time defined as t_{touch}. Once the load cycle starts, the system experiences only compressive forces. This means the ball can never move out of the control volume and no flow back into the volume can take place. This characteristic eventually leads to the two surfaces actually touching.

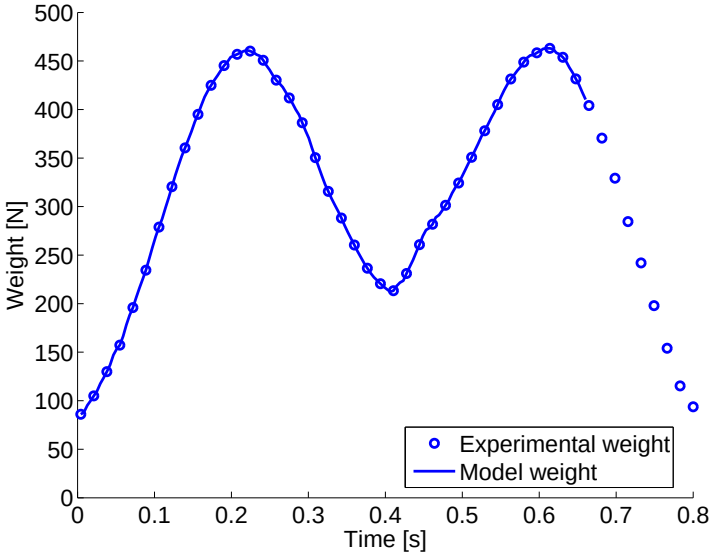

Figure 6.3: Comparing the simulator weight with the weight calculated from the dynamic model.

The velocity profiles (in m/s) at the beginning of the load cycle are shown in figure 6.5. Figure 6.5 (a) is the velocity profile in the θ-direction, calculated from equations (4.16) and (4.19). Figure 6.5 (b) is the ϕ-direction velocity component calculated from equation (4.20). The resultant velocity magnitude scalar is shown in Figure 6.5 (c).

The velocity component in the θ-direction is several orders of magnitude higher than the ϕ velocity. With the resultant velocity magnitude in figure 6.5 (c), the influence of the ϕ-direction velocity is not even visible. This is mainly due to the fact that the inward movement is predominantly more than the pendulum movement. This holds true for the

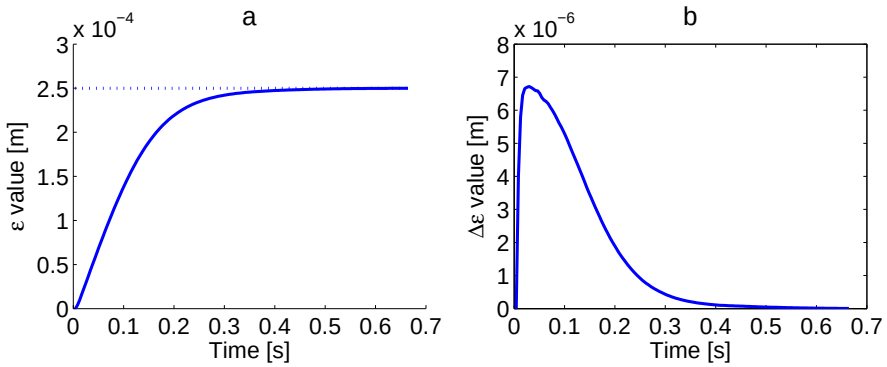

Figure 6.4: The ε factor (a) and the change in ε (b) that induces fluid flow.

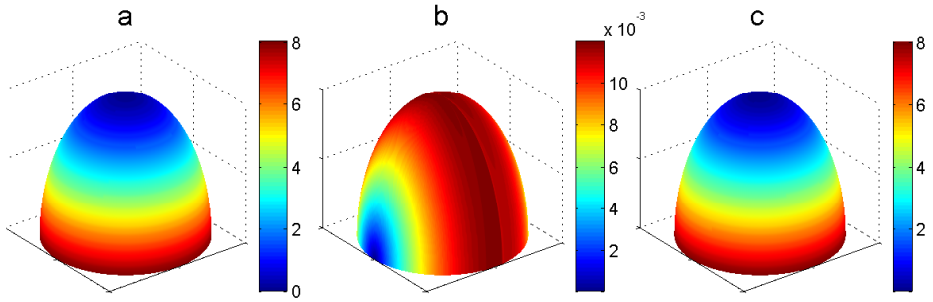

Figure 6.5: The velocity profiles at time t = 0.04 s.

entire duration of the load cycle. The velocity profile due to the pendulum movement only, is mirrored about the axis of rotation, which means it has a cancellation effect, due to the change in velocity direction with equal magnitude. Therefore, this movement does not contribute to the load bearing capacity of the system. Only the inward movement contributes to the load carrying capacity, which makes this velocity effect overwhelmingly large. This will be demonstrated more clearly in figure 6.6.

Figure 6.6 shows sectional views and maximum values of the fluid velocity in the θ-direction (figure 6.6 (a) and (b)) and in the ϕ-direction (figure 6.6 (c) and (d)).

Referring back to the θ-component of the velocity in figure 6.5 (a), the fluid flow is clearly axisymmetrical around the spherical ϕ axis. Figure 6.6 (a) shows the fluid velocity along the θ axis, as the simulation progresses with time. Initially, the flow is widely distributed over the entire θ domain. As the load cycle continues, the region of slower flow increases, and a maximum fluid flow region occurs at the end boundary of the system ($\theta = \pi/2$). The majority of the system then undergoes low flow, increasing until there is insufficient change in ε, and the flow stops when the surfaces touch. Figure 6.6 (b) shows the maximum θ-component of the flow as a function of time. An obvious correlation between this maximum flow and the weight function is apparent. This confirms that the inward movement, which mainly comprises the θ-component of the fluid velocity, supports the weight of the system.

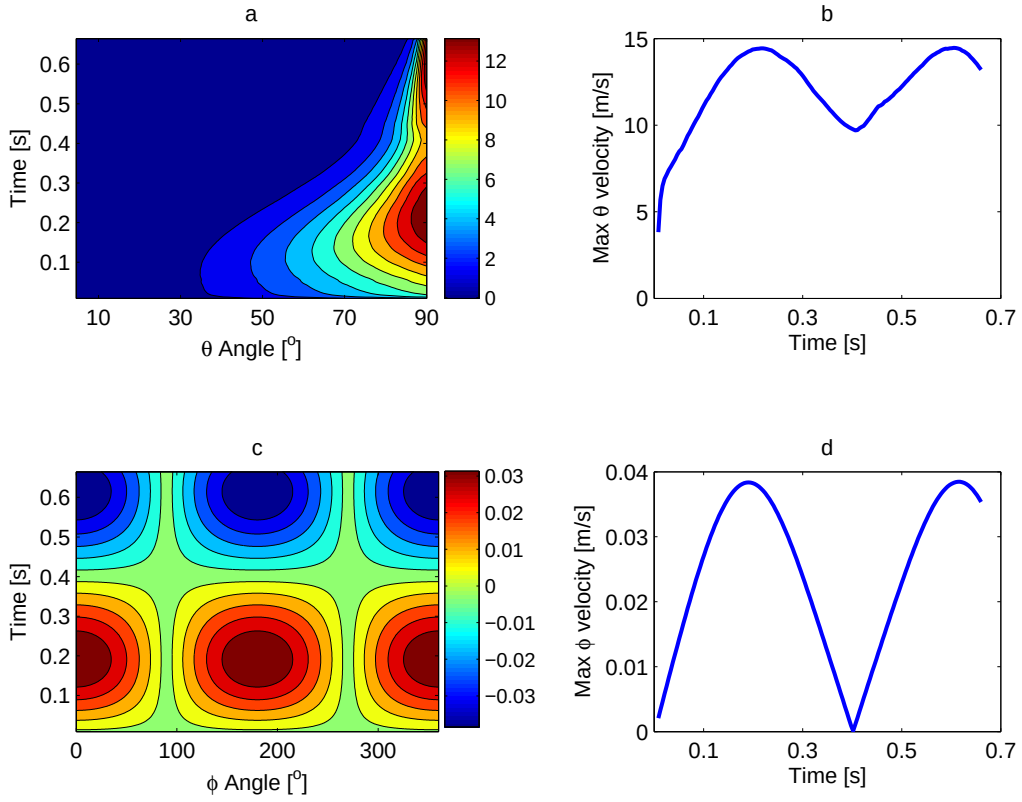

Figure 6.6: Sectional fluid flow and maximum flow (in m/s) in the θ-direction (a) and (b) and in the ϕ-direction (c) and (d).

The velocity in figure 6.5 (b) in the ϕ-direction is not axisymmetrical around either the θ or ϕ axis. Therefore, the ϕ-component of the velocity was plotted at constant $\theta = 50^{\circ}$ over the entire load cycle duration. This plot is shown in figure 6.6 (c). The fluid velocity in this direction is orders smaller than the velocity in the θ direction. The velocity profiles go through a range of peaks and lower values as ϕ is varied. These patterns of flow is due to the pendulum movement of the joint. This is also shown more clearly in figure 6.6 (b). Here, the absolute value of the maximum ϕ-component at each time step was plotted. The trend of the curve follows that of the rotational angular motion shown in figure 6.2.

The pressure distribution (in Pa) at time t = 0.13 s throughout the entire control volume is shown in figure 6.7. Regions of high fluid velocity correspond to lower pressure, as fluid flows in the direction of the pressure drop. The area at the top of the ball experience less fluid flow and therefore the highest pressures. A complete picture of the fluid pressure as it changes with time is given in figure 6.8.

In figure 6.7, the pressure distribution in the fluid is axisymmetrical about the ϕ axis. Therefore, the pressure was plotted only as a function of θ as the simulation progresses. This is given in figure 6.8 (a). As the weight that the system should support increases, so does the pressure distribution throughout the system. Initially at time $0 \leq t \leq 0.4$ s,

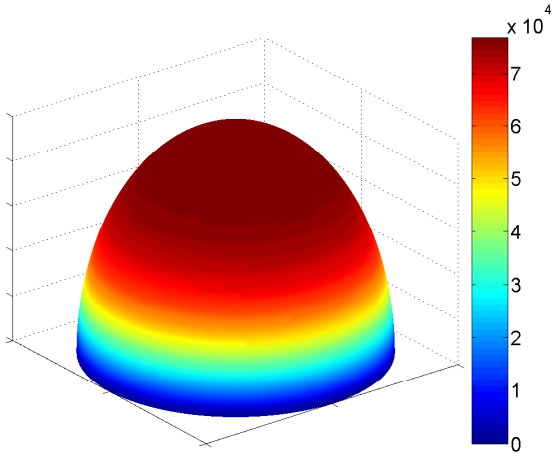

Figure 6.7: The pressure (in Pa) at time t = 0.13 s.

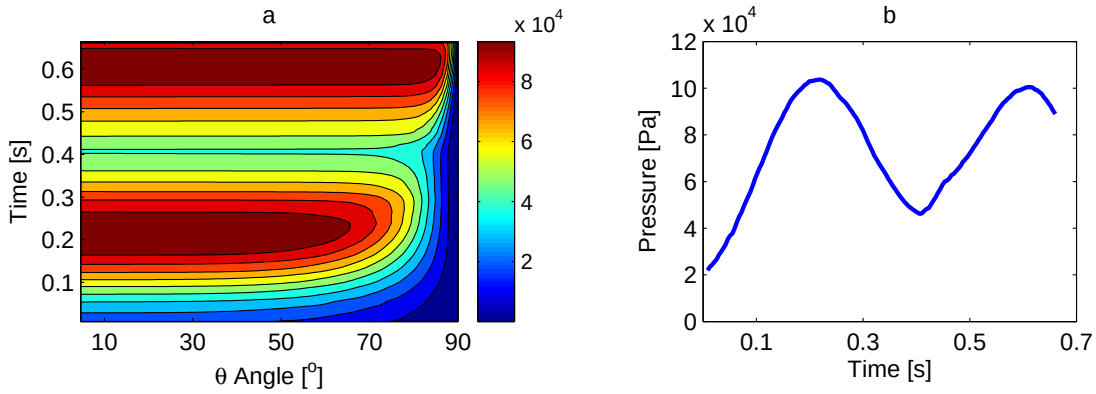

Figure 6.8: Sectional view of the pressure distribution (in Pa) as it varies with θ (a) and the maximum pressure at each time increment (b).

there is a gradual increase in pressure as the weight increases. The maximum pressure is spread over an area that is mapped onto the ball surfaces when $0^o \leq \theta \leq 65^o$. The weight reaches a local minimum at $t = 0.41$ s, where it gradually starts picking up again. The pressure distribution is now different to the previous increase in weight. The large hydrodynamic pressure is distributed over a larger area of θ. This is due to the low fluid velocity in this part of the cycle from the decrease in $\Delta\varepsilon$. At $t_{touch} = 0.66$ s, the pressure is almost equal throughout the entire control volume, as the opposing surfaces touch.

Figure 6.8 (b) is the plot of the maximum pressure throughout the entire loading cycle. It generally looks like the load cycle shown in figure 6.2. The maximum pressures range between 20 and 110 kPa. The pressure is always a minimum of 0 kPa at edges of the system ($\theta = 0$).

Figure 6.9 shows the lubricant film thickness parameter throughout the simulated cycle. Recalling section 4.4.1, the movement of the ball into the control volume was described in detail. It was stated that the ball moves in such a way that the centre of the ball and the centre of the cup are always in a straight line. The film thickness is the difference between the cup radius, R_2, and the corrected radius, $R_{(\theta,\varepsilon)}$, calculated in equation (4.14). This difference in radii is clearly depicted in figure 4.5. With this in mind, it is clear that this variable is also axisymmetrical about the ϕ axis.

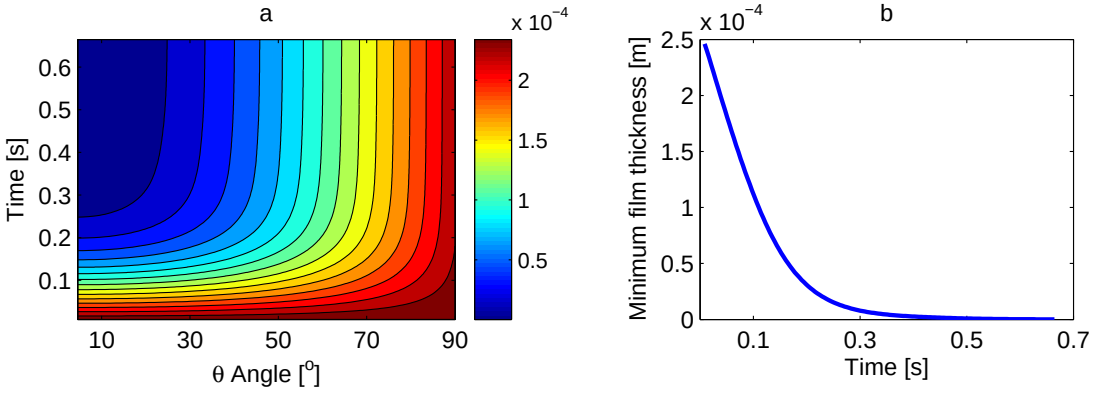

Figure 6.9: The film thickness profile (a) and the minimum film thickness (b).

The film thickness in the region of $50^o \leq \theta \leq 90^o$ compares well to a sufficient hydrodynamic film according to Bhushan (2002). He states that full hydrodynamic lubrication can prevail at film thicknesses between 5 and 500 μm. It is in the area of $0^o \leq \theta \leq 50^o$ where the fluid film becomes alarmingly thin, especially after t = 0.2‘ s. The film thickness is however of adequate magnitude to prevent the surfaces from touching. An important parameter to evaluate is the minimum film thickness given in figure 6.9 (b). Here it is clearer that there is a sufficient fluid film for the system to be in the hydrodynamic lubrication regime. The minimum film thickness only drops very low after t = 0.4 s. The minimum film thickness reaches a critical value at $t_{touch} = 0.66$ s, when the surfaces touch and a new lubrication regime is entered.

Results of the most important model parameters is included as an animated movie. Refer to appendix A for details.

6.3.1 Model parameter investigation

The effect of some of the model parameters on the results of the system was investigated. In particular, the femoral ball diameter and the radial clearance were studied. Results are summarised in figure 6.10.

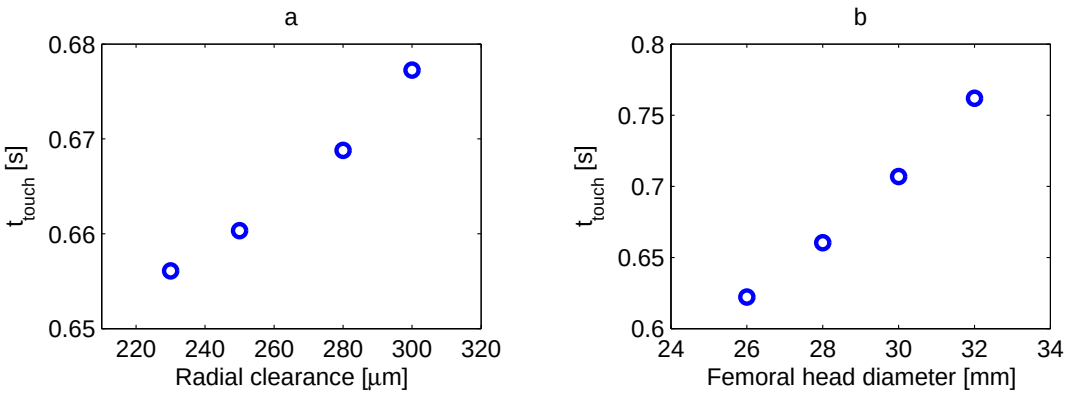

Figure 6.10: The effect of radial clearance (a) at constant femoral head diameter of 28 mm on the touch time and the effect of changing diameter (b) at constant radial clearance of 250 μm on the touch time.

An increase in both off these parameters improves the hydrodynamic lubrication of the system and increases the time it takes for the two surfaces to touch. In figure 6.10 (a), the increasing clearance between the articulating surfaces improves the lubricant fluid film. An increase in clearance of 9% from 230 to 250 μm results in a 1% increase in the surface touch time. The same holds true for radial clearances of 280 and 310 μm, it increases t_{touch} by approximately 1%. An increase in the femoral head diameter (figure 6.10 (b)) has a much larger effect on the hydrodynamic load carrying capability of the system. Increasing the ball diameter by just under 8% from 26 to 28 mm, improves t_{touch} by 6%. By increasing the ball diameter, the area and fluid available to carry the load increases, which in turns mean that lower fluid pressures are present. The effect of the diameter seems almost linear for the range investigated.

6.3.2 Fluid properties investigation

The graph shown in figure 6.11 investigates the effect of two fluid properties on the performance of the Newtonian hip model namely viscosity (a) and density (b).

The change in fluid viscosity at a constant density of 1000 kg/m^3 is shown in figure 6.11 (a). The fluid viscosity seems to have little effect on the performance of the model as it is increased from 0.001 to 2 Pa.s. Such low fluid viscosity is insufficient for

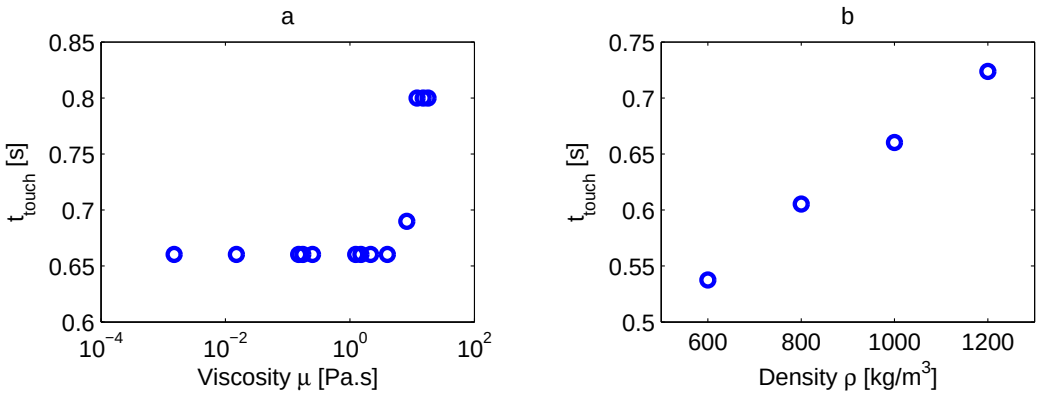

Figure 6.11: The effect of viscosity (a) at constant density of 1000 kg/m^3 on the touch time and the effect of density (b) at constant viscosity of 1.5 Pa.s on the touch time.

the system to support the weight of an entire cycle, and the time it takes for the two opposing surfaces to touch each other stays constant in this viscosity range at 0.66 s. The moment the viscosity increases above 2 Pa.s, the load bearing capacity of the lubricant increases significantly which in turn improves the hydrodynamic lubrication of the system. This is a common phenomenon in tribology and can be verified by using the Sommerfeld number, $S = v\mu/P$, and the Stribeck curve. With a viscosity of about 10 Pa.s and higher, the model is able to complete an entire cycle without touching. The effect of viscosity is shown in more detail in figure 6.12.

Figure 6.11 (b) shows the effect of increasing density on the dynamic model at a constant viscosity of 1.5 Pa.s. As the density increases from 600 to 1200 kg/m^3, the articulating surfaces stay apart for a longer time without touching. The time increases from 0.54 s to just under a full cycle. The effect of density on the system is clearly given in the continuity of motion equation presented in section 4.3. Density is a big contributer to the hydrodynamic pressure drop in the system due to flow. If two different fluids are flowing at the same rate, the pressure drop will be highest for the fluid with the higher density. The opposite also holds true. Therefore, the higher the density of the lubricant in the model, the easier the pressure drop due to flow and hence the easier the weight is supported.

The effect of viscosity is shown in figure 6.12. Here the results were compared for $\mu = 0.0015$ Pa.s and $\mu = 15$ Pa.s. Figure 6.12 (a) shows the difference in the $\Delta\varepsilon$ parameter. The inward movement of the ball into the cup is more dramatic with the higher viscosity. The higher the viscosity, the better the load carrying capacity. The entire weight cycle can be supported by the higher viscosity fluid. This is clear in figure 6.12 (b). Finally, the pressure distributions of the different viscosities are shown in figure 6.12 (c) and (d). The higher viscosity results show that with less movement in ε good pressure distributions were achieved and with little change in ε the fluid can support the load imposed by the system.

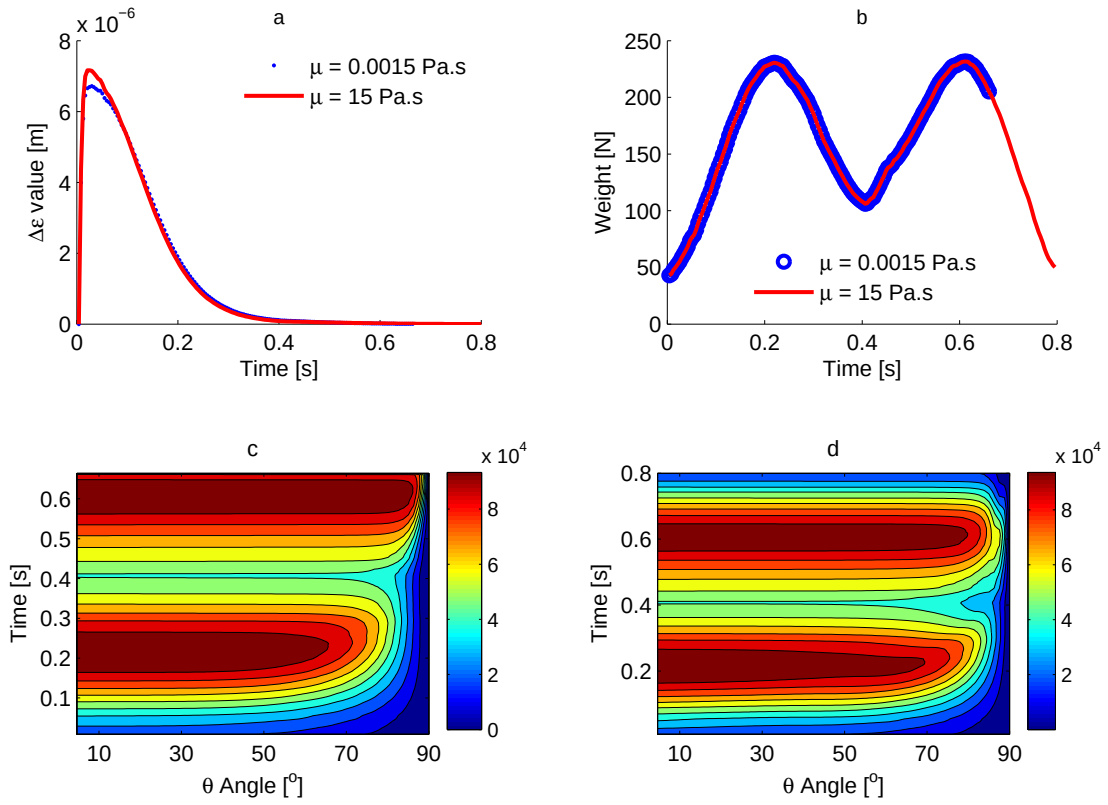

Figure 6.12: The $\Delta\ \varepsilon$ and weight comparison (a) and (b) and the pressure distributions for $\mu = 0.0015$ Pa.s and $\mu = 15$ Pa.s respectively (c) and (d).

6.4 Non-Newtonian model results

Two different empirical non-Newtonian approximations were simulated with the hip joint model. These approximations are briefly discussed in chapter 3. They are:

- Maxwell model
- Oldroyd model
  - Osteoarthritic (OA) fluid
  - Rheumatoid arthritic (RA) fluid
  - Bovine fluid

The results were compared to results obtained as if the fluids were Newtonian. Non-Newtonian fluid will behave like a Newtonian fluid if the shear stresses are independent of the shear rates. In this case, $\mu = \eta_0$. By assuming that the fluid is Newtonian, a constant viscosity of η_0 was used. Results to be compared are given in table 6.2.

From this table it is clear that no differences could be found in the models. The results can be explained by looking at the viscosity investigation in section 6.3.2 and the apparent viscosity, η_0, shown in the table. Figure 6.11 shows the effect of viscosity on the

Table 6.2: Comparison between Newtonian and Non-Newtonian model results

Model	η_0 parameter Pa.s	Newtonian t_{touch} (s)	Non-Newtonian t_{touch} (s)
Maxwell	0.0917	0.6603	0.6603
Oldroyd (OA)	1.24	0.6603	0.6603
Oldroyd (RA)	0.15	0.6603	0.6603
Oldroyd (Bovine)	0.175	0.6603	0.6603

lubrication performance of the model. It was concluded that a lubricant with viscosity below 2 Pa.s has insufficient lubrication ability and the articulating surfaces touch after 0.66 s. Only above 2 Pa.s the lubricant improves the performance and hydrodynamic lubrication. With the non-Newtonian models, the apparent viscosities could only be a maximum of the values reported in table 6.2. As the shear rate increases, the viscosity will be less than the reported apparent viscosity. Now if the model is assumed to be Newtonian with viscosities equal to the apparent viscosity parameter η_0, the model will perform poorly due to the viscosity being lower than 2 Pa.s. The non-Newtonian models will therefore perform just as badly, because the apparent viscosities will be a maximum of η_0 and lower. To summarise, the model would rather operate in the elastohydrodynamic regime if it was lubricated with abnormal synovial fluid like OA, RA and bovine synovial fluid.

It would be interesting to investigate the model with normal synovial fluid which can have apparent viscosities of up to 10 Pa.s. This is well above the critical viscosity of 2 Pa.s, and would produce interesting results. Due to the unavailability of literature data, this could not be included in the current study, but should certainly be investigated in future.

What can be concluded from the previous two sections is that the model behaves like the hip simulator under the specified conditions. With the lubricants used in the model and the simulator, hydrodynamic lubrication is not the prevailing regime and non-Newtonian behaviour have little influence in the results. This will surely not be the case when the current model is adapted to simulate an actual human hip joint. Under these natural conditions, various other lubrication mechanisms play a role and non-Newtonian fluid behaviour contributes to the successful operation of the joint.

6.5 Experimental validation

In order to evaluate the accuracy of the results of the proposed hydrodynamic model, the measured moment from the hip joint simulator is compared to the moment calculated with the hip joint model. The measured moments are shown in figure 6.13. The moments

shown here were filtered to minimise recording noise.

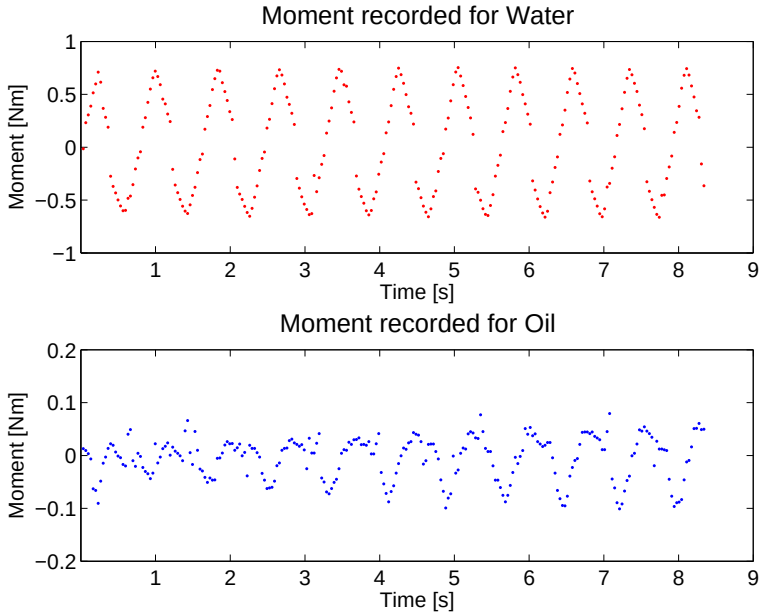

Figure 6.13: The torques or moments measured with the hip simulator for the two lubricants: water (top) and oil (bottom).

In this figure, the torque of water is shown above, while that of the lubricant oil is shown at the bottom. When the simulator ran with water as lubricant, a much higher torque was measured compared to running the simulator with oil as lubricant. This is inherent to the lubricating ability of the lubricant. Water has almost no lubricating ability, therefore the moment measured is basically generated by solid-solid contact. When oil was used as lubricant, the measured torque was drastically lower. This confirms that the oil has much better lubricating and load bearing abilities. The moment recorded with the oil as lubricant is generated due to the liquid lubricant shearing across the articulating surfaces due to the joint movements.

It is important to note that by comparing the two graphs shown in figure 6.13, the torque measuring technique utilised in the simulator is sensitive enough to measure a notable difference in different lubricants used. The moment generated with water has a constant amplitude and looks similar after each cycle, whereas the oil moment seems to increase in amplitude as time progresses. This can be attributed to the fact that the oil is squeezed out of the articulating surfaces. As the oil is squeezed out, the simulator moves into a regime where solid-solid contact predominates. With these observations discussed here, it seems as if the simulator can operate with some order of hydrodynamic lubrication, and that the measuring techniques and devices are able to measure the required variables.

The model results were compared to the measurements gathered from the hip simulator, to investigate the validity of the proposed hydrodynamic hip joint model. After running the model by inputing the simulator weight and angular velocity (section 6.2)

and by iterating the model (section 6.3), the torque from the simulator was compared to the moment calculated with the model by using equation (4.22). The results are graphed in figure 6.14. In this figure, the noise of the torque that was recorded was not filtered.

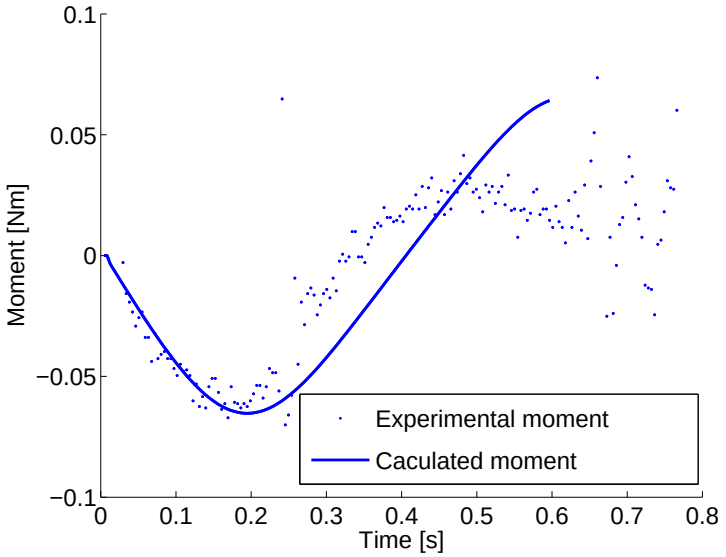

Figure 6.14: Comparing the simulator recorded torque with the torque calculated from the hip model.

Initially, the model moment correlates very well with the experimental moment. This can be due to the fact that there is still proper hydrodynamic lubrication in the system. Then, as the cycle progresses, the prediction of the moment becomes less accurate. It is important to note that at the end of the cycle, a random scattering of data is visible in the experimentally measured moment. This noise may be attributed to a noise found in the weight measurements of the simulator. These noises were filtered out prior to using it in the hip joint model. The noises found in the measurements are from the mechanical movements of the simulator as one of the big shafts rotates around its axis, causing irregular weight pulses and hence scattering in the recorded moment. In figure 6.13, noises are much more pronounced in the oil sample where the torques are small than when compared to that of the water sample.

The dynamic model that was developed from first principles compares well with the results obtained from the joint simulator run with a Newtonian lubricant. The results should be compared in future if it was run with a thick non-Newtonian lubricant. Future research should aim to develop this model further to simulate a human hip joint.

CHAPTER 7

Conclusions and recommended future work

A hydrodynamic model of a dynamic hip joint was developed and simulated using *Matlab*. The model successfully duplicates the joint movements executed by the locally available joint simulator. In future, adduction-abduction movements, which was not included in this study, can be incorporated into the current model. Some simplifying assumptions need to be addressed in future work. This includes the assumption of no wall effects or boundary layers that was used in this model. Using a flow simulation package to accurately describe these effects could be considered. Implementing a boundary layer should have dramatic effects on the model accuracy, because shearing interaction between a flowing liquid and a solid walls is important when evaluating fluids with different rheological properties.

Primary investigation into the results obtained from the dynamic hip joint model showed that the accuracy of the results were very sensitive to the optimisation mesh used in the simulation. The mesh was optimised to give consistent results.

During the mesh optimisation stage it was noted that the lubricating fluid was incapable of carrying the high loads imposed on it by the articulating surfaces. Even at a lowered cyclic load oscillating between 0 and 500 N, the articulating surfaces touched after only 0.66 s, without even completing a single cycle. This finding is validated by the fact that the simulator operates in either the elastohydrodynamic (EHL), mixed or boundary lubrication regime. The next step in this study would be to include other lubrication regimes, starting with EHL. This could prove to be valuable when attempting to correlating higher loads and complete and longer load cycles with the results of the model.

After investigating the effect of different model variables on the performance of the model it was found that an increase in radial clearance and an increase in ball diameter both improved hydrodynamic lubrication.

The influence of different fluid properties on the Newtonian model was also investigated. Results revealed that viscosities below 2 Pa.s were insufficient for hydrodynamic lubrication. Increasing the viscosity above this critical value dramatically improved the models load carrying capability. In future, a higher viscosity Newtonian fluid, $\mu > 5$ Pa.s, can be used as lubricant for the joint simulator. These results aught to compare very well with the dynamic joint model. Results also revealed that increased fluid density, improved the model's load bearing capacity.

Non-Newtonian characteristics were added to the simulation. After investigating the Maxwell and Oldroyd models for shear thinning pathological synovial fluid, results showed that the viscosities were well below the critical viscosity of 2 Pa.s, and therefore could not promote hydrodynamic lubrication. The non-Newtonian results performed as poor as its Newtonian counterparts due to the insufficient viscosities. More focus on the non-Newtonian behaviour and fluid rheology is required in future. It is recommended to incorporating more different correlations into the hip model, including that of normal synovial fluid. Experimental setups can be designed to do own rheological studies on synovial fluid samples. These results can then be used in the current joint model.

The model could predict the torque induced by the fluid shear stresses quite accurately. This model could be used with acceptable accuracy to predict hydrodynamic flow and the point at which solid-solid contact occurs, and the EHL regime is entered. Non-Newtonian fluids can be used in the simulator in future. These results can be compared with model results to investigate the accuracy of the predictions from another angle.

Now that a fundamental hip joint model is available and experimentally validated, future research effort should be aimed at developing an accurate human hip joint with a geometry which includes the femoral head and acetabular cup covered with articular cartilage. Lubrication mechanisms unique to this joint, like synovial fluid filtration by cartilage and weeping lubrication, should be added to this model. Provision could then be made to reintroduce lubricating fluid into the joint cavity via these mechanisms and to investigate lubricant rheology which will then play an increasing role in effective lubrication of the joint. Multi-cycle operation of human joints under various loading conditions like walking and running could then be investigated.

BIBLIOGRAPHY

Affatato, S.; Bersaglia, G.; Rocchi, M.; Taddei, P.; Fagnano, C. and Toni, A. (2005) "Wear behaviour of cross-linked polyethylene assessed in vitro under severe conditions", *Biomaterials, 26*, 3259–3267.

Afify, A. M.; Craig, S.; Paulino, A. F. and Stern, R. (2005) "Expression of hyaluronic acid and its receptors, CD44s and CD44v6, in normal, hyperplastic, and neoplastic endometrium", *Annals of Diagnostic Pathology, 9*, 312–318.

Baleani, M.; Cristofolini, L. and Viceconti, M. (1999) "Endurance testing of hip prostheses: a comparison between the load fixed in iso 7206 standard and the physiological loads", *Clinical Biomechanics, 14*, 339–345.

Bergmann, G.; Graichen, F. and Rohlmann, A. (1993) "Hip joint loading during walking and running- measurement in two patients", *Journal of Biomechanics, 26* (8), 969–990.

Bhushan, B. (2002) *Introduction to tribology*, John Wiley and Sons Inc., New York.

Bigsby, R. J. A.; Auger, D. D.; Jin, Z. M.; Dowson, D.; Hardaker, C. S. and Fisher, J. (1998) "A comparative tribological study of the wear of composite cushion cups in a physiological hip joint simulator", *Journal of Biomechanics, 31*, 363–369.

Bird, R. B.; Steward, W. E. and Lightfoot, E. N. (1960) *Transport phenomena*, John Wiley and Sons Inc., New York.

Bujurke, N. M. and Jayaraman, G. (1982) "The influence of coupled stresses in squeeze films", *International journal of mechanical science, 24* (6), 369–376.

Bujurke, N. M.; Naduvinamani, N. B. and Jayaraman, G. June (1991) "Theoretical modelling of poro-elastic slider bearings lubricated by couple stress fluid with special reference to synovial joints", *Applied mathematical modelling, 15*, 319–324.

Burger, N.; Fourie, E. and von Wielligh, A. "Development of a mechanical hip simulator", Mechanical technology (2002).

College of Engineering, University of California "http://www.coe.berkeley.edu/labnotes/0505/commuter.html", Internet Webpage (2005).

Collins, R. (1982) "A model of lubricant gelling in synovial joints", *Journal of applied mathematics and physics, 33*, 93–123.

Cooke, A. F.; Dowson, D. and Wright, V. (1978) "The rheology of synovial fluid and some potential synthetic lubricants for degenerative synovial joints", *Engineering in medicine, 7* (2), 66–72.

Dowson, D. (1995)a "A comparative study of the performance of metallic and ceramic femoral head components in total replacement hip joints", *Wear, 190*, 171–183.

Dowson, D. (1995)b "Elastohydrodynamic and micro-elastohydrodynamic lubrication", *Wear, 190*, 125–138.

Dowson, D.; Fisher, J.; Jin, Z. M.; Auger, D. and Jobbins, B. (1991) "Design considerations for cushion form bearings in artificial hip joints", *Proceedings of the institution of mechanical engineers, 205*, 59–68.

Dowson, D. and Jin, Z. M. (1992) "A full numerical solution to the problem of microelastohydrodynamic lubrication of a stationary compliant wavy layered surface firmly bonded to a rigid substrate with particular reference to human synovial joints", *Proceedings of the institution of mechanical engineers, 206*, 185–193.

Dowson, D. and Jin, Z. N. (1986) "Micro-elastohydrodynamic lubrication of synovial joints", *Engineering in medicine, 15*, 63–65.

Essner, A.; Schmidig, G. and Wang, A. (2005) "The clinical relevance of hip joint simulator testing- in vitro and in vivo comparisons", *Wear, 259*, 882–886.

Fisher, J. and Dowson, D. (1991) "Tribology of total artificial joints", *Proceedings of the institution of mechanical engineers, 205*, 73–79.

Frankel, V. H. and Nordin, M. (1980) *Basic biomechanics of the skeletal system*, Lea and Febiger, Philadelphia.

Fraser, J.; Laurent, T. and Laurent, U. (1997) "Hyaluronan: its nature, function, distribution and turnover", *Journal of internal medicine, 242*, 27–33.

Fujimura, K.; Segami, N.; Yoshitake, Y.; Tsuruoka, N.; Kaneyama, K. and Sato, J. (2005) "Electrophoretic separation of the synovial fluid proteins in patients with temporomandibular joint disorders", *Oral Surgery, Oral Medicine, Oral Pathology, Oral Radiology, and Endodontology,*.

Gamlin, L. and Brostoff, J. (1997) "Food sensitivity and rheumatoid arthritis", *Environmental toxicology and pharmacology, 4*, 43–49.

Ge, S.; Wang, Q.; Zhang, D.; Xiong, H. Z. D.; Huang, C. and Huang, X. (2003) "Friction and wear behaviour of nitrogen ion implanted UHMWPE against ZrO_2 ceramic", *Wear, 255*, 1069–1075.

Hanawa, T. (1999) "In vivo metallic biomaterials and surface modification", *Materials Science and Engineering, A267*, 260–266.

Hlaváček, M. (1993)a "The role of synovial fluid filtration by cartilage in lubrication of synovial joints-I. Mixture model of synovial fluid", *Journal of Biomechanics, 26* (10), 1145–1150.

Hlaváček, M. (1993)b "The role of synovial fluid filtration by cartilage in lubrication of synovial joints-II. Squeeze-film lubrication: Homogeneous filtration", *Journal of Biomechanics, 26* (10), 1151–1160.

Hlaváček, M. (1995) "The role of synovial fluid filtration by cartilage in lubrication of synovial joints-II. The central film thickness for normal and inflammatory synovial fluids for axial symmetry under high loading conditions", *Journal of Biomechanics, 28* (10), 1199–2105.

Hlaváček, M. (2000) "Squeeze-film lubrication of the human ankle joint with synovial fluid filtrated by articular cartilage with the superficial zone worn out", *Journal of biomechanics, 33*, 1415–1422.

Hlaváček, M. (2002) "The influence of the acetabular labrum seal, intact articular superficial zone and synovial fluid thixotropy on squeeze film lubrication of a spherical joint", *Journal of Biomechanics, 35*, 1325–1335.

Hlaváček, M. and Novák, J. (1995) "The role of synovial fluid filtration by cartilage in lubrication of synovial joints-II. Squeeze-film lubrication: Axial symmetry under low loading conditions", *Journal of Biomechanics, 28* (10), 1193–1198.

Hori, R. Y. and Mockros, L. F. (1976) "Indentation test of human articular cartilage", *Journal of biomechanics, 9*, 259–268.

Ingham, E. and Fisher, J. (2000) "Biological reactions to wear debris in total joint replacements", *Proceedings of the institution of mechanical engineers, 214* (H), 21–37.

International Standard ISO TR 9325:1989 "Implants for surgery- partial and total hip joint prostheses- recommendations for simulators for evaluation of hip joint prosthesis", (1989).

Jalali-Vahid, D.; Jagatia, M.; Jin, Z. M. and Dowson, D. (2000) "Elastohydrodynamic lubrication analysis of UHMWPE hip joint replacements", *Thinning films and tribological interfaces,* pages 329–339.

Jalali-Vahid, D.; Jagatia, M.; Jin, Z. M. and Dowson, D. (2001) "Prediction of lubricating film thickness in UHMWPE hip joint replacements", *Journal of Biomechanics, 34*, 261–266.

Jay, G. D.; Tantravahi, U.; Britt, D. E.; Barrach, H. J. and Cha, C.-J. July (2001) "Homology of lubricin and superficial zone protein (SZP): products of megakaryocyte stimulating factor (MSF) gene expression by human synovial fibroblasts and articular chondrocytes localised to chromosome 1q25", *Journal of Orthopaedic Research, 19* (4), 677–687.

Jie-min, Z. and Jie-hui, Z. (1994) "Three dimensional modelling for lubrication with reference to human joints", *Journal of hydrodynamics, 1*, 103–108.

Jin, Z. M.; Dowson, D. and Fisher, J. (1991) "Stress analysis of cushion form bearings for total hip replacements", *Proceedings of the institution of mechanical engineers, 205*, 219–226.

Jin, Z. M.; Dowson, D. and Fisher, J. (1992) "The effect of porosity of articular cartilage on the lubrication of a normal human hip joint", *Proceedings of the institution of mechanical engineers, 206*, 117–124.

Jin, Z. M.; Dowson, D. and Fisher, J. (1997) "Analysis of fluid film lubrication in artificial hip joint replacements with surfaces of high elastic modulus", *Proceedings of the institution of mechanical engineers. Part H, 211*, 247–256.

Jin, Z. M.; Heng, S. M.; Ng, H. W. and Auger, D. D. (1999) "An axisymmetric contact model of ultra high molecular weight polyethylene cups against metallic femoral heads for artificial hip joint replacements", *Proceedings of the institution of mechanical engineers. Part H, 213*, 317–327.

Lai, W. M.; Kuei, S. C. and Mow, V. C. (1978) "Rheological equations for synovial fluids", *Journal of Biomechanical Engineering, 100*, 169–186.

Mabuchi, K.; Obara, T.; Ikegami, K.; Yamaguchi, T. and Kanayama, T. (1999) "Molecular weight independence of the effect of additive hyaluronic acid on the lubricating characteristics in synovial joints with experimental deterioration", *Clinical Biomechanics, 14*, 352–356.

Mabuchi, K.; Sakai, R.; Ota, M. and Ujihira, M. (2004) "Appropriate radial clearance of ceramic-on-ceramic total hip prostheses to realise squeeze-film lubrication", *Clinical Biomechanics, 19*, 362–369.

Mabuchi, K. and Sasada, T. (1990) "Numerical analysis of elastohydrodynamic squeeze-film lubrication of total hip prostheses", *Wear, 140*, 1–16.

MadSci Network "http://www.madsci.org/posts/archives/apr2001/986571103.bc.1.gif", Internet Webpage (2001).

Mazzucco, D.; McKinley, G.; Scott, R. D. and Spector, M. (2002) "Rheology of joint fluid in total knee arthroplasty patients", *Journal of Orthopaedic Research, 20*, 1157–1163.

Mazzuccoa, D.; Scott, R. and Spector, M. (2004) "Composition of joint fluid in patients undergoing total knee replacement and revision arthroplasty: correlation with flow properties", *Biomaterials,* (25), 4433–4445.

Medley, J. B. (1994) "Some background theory for the cushion bearing concept in joint replacement implants", *Wear, 175*, 9–16.

Momberger, T.; Levick, J. and Mason, R. (2005) "Hyaluronan secretion by synoviocytes is mechanosensitive", *Matrix Biology, 24*, 510–519.

Nonaka, T.; Kikuchi, H.; Shimada, W.; Itagane, H.; Ikeda, T.; Hamanishi, C. and Tanaka, S. (1999) "Effects of sodium hyaluronic acid on fibrinolytic factor in the synovial fluid (in vivo)", *Pathophysiology, 6*, 41–44.

Norkin, C. C. and Levangie, P. K. (1988) *Joint structure and function. A comprehensive analysis*, F.A. Davis Company, Philadelphia.

Opperman, T. "Tribological evaluation of joint fluid and the development of a synthetic lubricant for use in hip joint simulators", Master's dissertation, University of Pretoria (2005).

Pascovici, M. D. and Cicone, T. (2003) "Squeeze-film of unconformal, complaint and layered contacts", *Tribology international, 36*, 791–799.

Pascual, E. and Jovan, V. (2005) "Synovial fluid analysis", *Best Practise and Research Clinical Rheumatology, 19*, 371–386.

Piconi, C.; Burger, W.; Richter, H. G.; Cittadini, A.; Maccauro, G.; Covacci, V.; Bruzzese, N.; Ricci, G. A. and Marmo, E. (1998) "Y-TZP ceramics for artificial joint replacements", *Biomaterials, 19*, 1489–1494.

Praest, B. M.; Greiling, H. and Kock, R. (1997) "Assay of synovial fluid parameters: hyaluronan concentration as a potential marker for joint diseases", *Clinica Chimica Acta, 266*, 117–128.

Pylios, T. and Shepherd, D. E. T. (2004) "Prediction of lubrication regimes in wrist implants with spherical bearing surfaces", *Journal of biomechanics, 37*, 405–411.

Reynolds, O. (1886) "On the theory of lubrication and its applications to Mr Beauchamp Tower's experiments, including an experimental determination of the viscosity of olive oil", *Philosophical transactions of the royal society of London, 117* (1), 157–234.

Saikko, V. and Ahlroos, T. (1997) "Phospholipids as boundary lubricants in wear tests of prosthetic joint materials", *Wear, 207*, 86–91.

Sarma, A. V.; Powell, G. L. and LaBerge, M. (2001) "Phospolipid composition of articular cartilage boundary lubricant", *Journal of orthopaedic research, 19*, 671–676.

Saxena, R. K.; Sahay, K. B. and Guha, S. K. (1991) "Shear properties of articular cartilage of a bovine knee joint subjected to moderate and high loads: An experimental study", *Proceeding of the institute of mechanical engineers, 205*, 89–93.

Scott, D.; Coleman, P. J.; Mason, R. M. and Levick, J. R. (2000) "Concentration dependence of interstitial flow buffering by hyaluronan in synovial joints", *Microvascular Research, 59*, 345–353.

Shi, B.; Ajayi, O. O.; Fenske, G.; Erdemir, A. and Liang, H. (2003) "Tribological performance of some alternative bearing materials for artificial joints", *Wear, 255*, 1015.

Sokoloff, L. (Ed.) (1978) *The joints and synovial fluid. Vol I*, Academic Press, New York.

Stephanopoulos, G. (1984) *Chemical process control. An introduction to theory and practise*, Prentice Hall, New Jersey.

Stokes, V. K. (1966) "Couple stresses in fluids", *The physics of fluids, 9* (9), 1709–1715.

Sugiuchi, H.; Ando, Y.; Manabe, M.; Nakamura, E.; Mizuta, H.; Nagata, S. and Okabe, H. (2005) "Measurement of total and differential white blood cell counts in synovial fluid by means of an automated hematology analyser", *Journal of Laboratory and Clinical Medicine, 146*, 36–42.

Torzilli, P. A. and Mow, V. M. (1976)a "On the fundamental fluid transport mechanisms through normal and pathological articular cartilage during function – I. The formulation", *Journal of biomechanics, 9*, 541–552.

Torzilli, P. A. and Mow, V. M. (1976)b "On the fundamental fluid transport mechanisms through normal and pathological articular cartilage during function – II. The analysis, solution and conclusions", *Journal of biomechanics, 9*, 587–606.

University of Bern- Institute of Anatomy "http://www.ana.unibe.ch/ studer/empact/images/cartilage1.htm", Internet Webpage (2005).

University of Iowa Archives "www.uiowa.edu/.../tempages/ pages/cartilage.htm", Internet Webpage (2004).

Unsworth, A. (1995) "Recent developments in the tribology of artificial joints", *Tribology International, 28* (7), 485–495.

Unsworth, A.; Hall, R. M.; Burgess, I. C.; Wrobleski, B. M.; Streicher, R. M. and Semlitsch, M. (1995) "Frictional resistance of new and explanted artificial hip joints", *Wear,* pages 226–231.

Walker, P. S. (Ed.) (1977) *Human joints and their artificial replacements.*, Charles C Thomas Publishers, Illinois.

Wang, A.; Essner, A.; Polineni, V. K.; Stark, C. and Dumbleton, J. H. (1998) "Lubrication and wear of ultrahigh molecular weight polyethylene in total joint replacements", *Tribology International, 31* (1–3), 17–33.

Wausau Hospital Medical Library "http://www.aspiruslibrary.org/pictures/grey/hipjoint.gif", Internet Webpage (2004).

Welty, J. R.; Wicks, C. E.; Wilson, R. E. and Rorrer, G. (2000) *Fundamentals of Momentum, Heat and Mass Transfer*, John Wiley and Sons, Inc., 4th edition.

Willmann, G.; Fruh, H. J. and Pfaff, H. G. (1996) "Wear characteristics of sliding pairs of zirconia (Y-TZP) for hip endoprostheses", *Biomaterials, 17*, 2157–2162.

Xiong, D. (2005) "Friction and wear properties of UHMWPE composites reinforced with carbon fibre", *Materials Letters, 59*, 175–179.

Young, S. K.; Lotito, M. A. and Keller, T. S. (1998) "Friction reduction in total joint arthroplasty", *Wear, 222*, 29–37.

Zhou, Y. S.; Ikeuchi, K. and Ohashi, M. (1997) "Comparison of the friction properties of four ceramic materials for joint replacements", *Wear, 210*, 171–177.

APPENDIX A

Additional CD material

Accompanying this dissertation is a CD-ROM. Included on the CD is the following:

- **Matlab code**
  All the models discussed in this disseration, Newtonian and non-Newtonian is available in this section. Refer to appendix B for instruction to run the *Matlab* code.
- **Listing documentation**
  This section provides a complete printout of all the program code in pdf format. Appendix C contains a short description of the different mfiles in the program.
- **Simulation results**
  Movies or animations of the model results can be seen in this section. More on this can be seen in appendix D

APPENDIX B

How to run the dynamic hip joint model

The folder *Matlab code* contains two folders namely:

- *Newtonian model*
- *Non-Newtonian models*

Under the *Non-Newtonian models* folder, four different models exists. For more information please refer to section 3.2.

The current directory in *Matlab* needs to be set to the folder of choice. To run the model, simply type the word *model* in the command line. A few points to note:

- This model was programmed on *Matlab* version 7.0.4.365 (R14) Service Pack 2.
- Although only one load cycle is simulated, the simulation takes about 2 hours to complete.

APPENDIX C

Matlab code

This appendix will give a short overview of the different *Matlab* mfiles used to simulate the hip joint. It will also discuss *Matlab* optimisation tools used in the files. The files are discussed in alphabetical order. The program structure with all the mfiles are shown in figure C.1. For a complete printout of the programs, see the listing documentation accompanying this dissertation on CD-ROM.

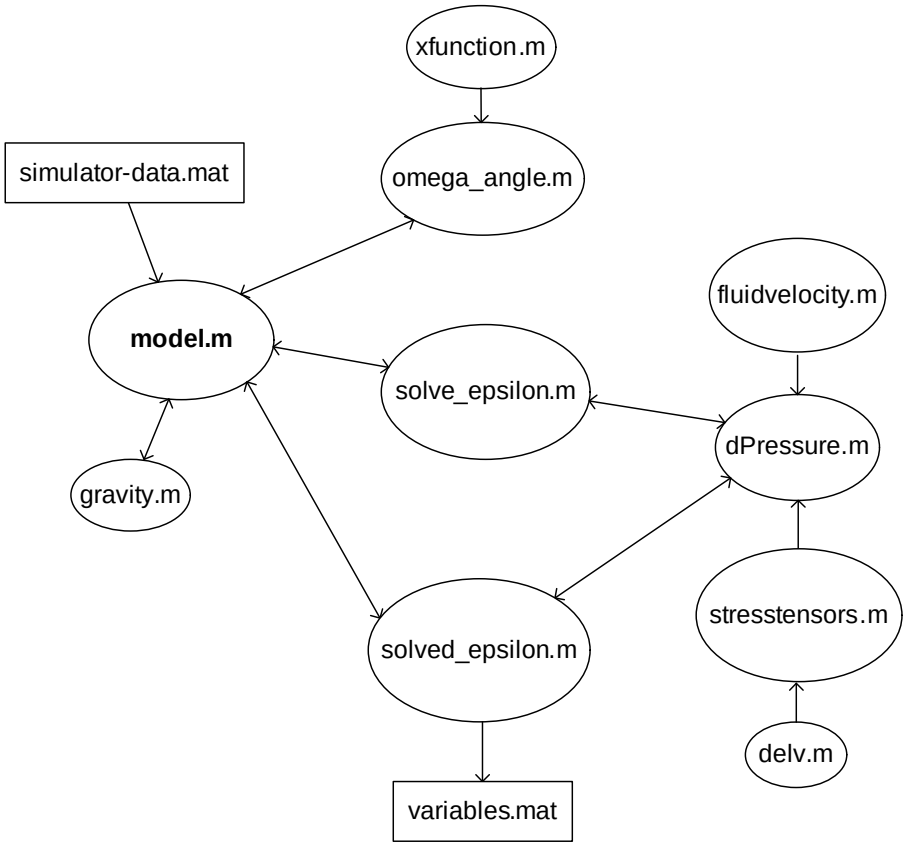

Figure C.1: program structure

deltaR.m

This mfile imports the variables θ, R_1, R_2 and ε, and calculates the new system boundary as described in section 4.4.1. The output of this file is the difference in the two boundary radii, $R_2 - R(\theta, \varepsilon)$, used in equation (4.15) to calculate the fluid volume. This function also detects whether $\theta = 0$, and then assigns $R_2 - R(\theta, \varepsilon) = R_2 - R_1 - \varepsilon$.

delv.m

This function calculates the fluid velocity gradient, $\nabla \cdot v$, for a Newtonian fluid in the spherical coordinate system from the fluid velocities shown in equation (3.9). The velocity gradient is used to simplify the momentum equation.

dPressure.m

In this mfile, all the system variables are calculated to determine $\mathrm{d}P/\mathrm{d}\theta$ by using the momentum balance in the θ-direction (equation (4.9)).

fluidvelocity.m

This file uses the geometry of the system, the angular momentum at any given time and the ε value to determine the fluid velocities in the θ and ϕ-directions. It should be noted that both the velocities are stored in the same variable. The θ-direction velocity is stored as the real part of the velocity vector, while the velocity in the ϕ-direction is stored as the imaginary part of the same vector.

gravity.m

This file is used to determine the gravity experienced by a section of the control volume as a function of theta. This gravity matrix is used in the momentum balance.

model.m

This is the main model mfile which initialises all the system variables, calls the simulator data, solves all important parameters and save all the variables to the disk.

move2endpoints.m

All partial derivatives were calculated analytically. This means that the actual difference of the following data points were subtracted and divided. This is also known as the midpoint rule to determine the gradient or derivative. During this operation, a data point is lost. This function interpolates between the midpoint to give a matrix of the original size.

omegaAngle.m

This file is used to determine the angular velocity of the articulating surfaces at any given time interval. This is done through simple geometry acquired from the actual hip simulator.

simulator-data.mat

This datafile contains the measurements acquired from the simulator namely the:

- Weight
- Bending moment

This data is called up, filtered and used in the model to compare the results of the model to that of the simulator.

solveEpsilon.m

In this mfile, the ε parameter is solved to yield a fluid flow through the system, which in turn generates a pressure drop, which in turn carries the load of the opposing surface. The optimisation is done with a build-in *Matlab* optimisation solver called lsqnonlin. This solver uses the least squares non linear solution method. Due to the highly nonlinearity of this system, using this solver makes good sense, generating results with relative ease and in relative time frames.

solvedEpsilon.m

In the section, the same calculations is repeated as in ***solve_epsilon.m***, but all the variables calculated with the optimised ε is written to the variables datafile.

stresstensors.m

This file calculates all the stress tensors used in the momentum balance. In the case of a Newtonian fluid, it uses the equations summarised in section 3.1 and in the case of a non-Newtonian fluid, the empirical correlations summarised in section 3.2.

Variables.mat

At the end of each time increment, all the variables in the *Matlab* workplace is written to this datafile.

xfunction.m

This function is used in the mfile called ***omega_angle.m*** to calculate the angular velocity of the simulator.

APPENDIX D

Simulation results

Due to the fact that the dynamic hip joint model is programmed in three dimensions, and is changing with time, animated results are included for clarity. Results of the following fluid properties are included in this section:

- Newtonian fluid with a low viscosity ($\mu < 2$ Pa.s)
  NewtonianLowViscosity.avi
- Newtonian fluid with a higher viscosity ($\mu > 5$ Pa.s)
  NewtonianHighViscosity.avi
- Non-Newtonian fluid (Maxwell model)
  NonNewtonian.avi

The results are of type Audio/Video Interleaved files, and contains audio and video data. It can be viewed with Windows Media Player, Winamp or most other media viewers.